creative commons
COMMONS DEED

저작자표시-비영리-변경금지 2.0 대한민국

이용자는 아래의 조건을 따르는 경우에 한하여 자유롭게

- 이 저작물을 복제, 배포, 전송, 전시, 공연 및 방송할 수 있습니다.

다음과 같은 조건을 따라야 합니다:

저작자표시. 귀하는 원저작자를 표시하여야 합니다.

비영리. 귀하는 이 저작물을 영리 목적으로 이용할 수 없습니다.

변경금지. 귀하는 이 저작물을 개작, 변형 또는 가공할 수 없습니다.

- 귀하는, 이 저작물의 재이용이나 배포의 경우, 이 저작물에 적용된 이용허락조건을 명확하게 나타내어야 합니다.
- 저작권자로부터 별도의 허가를 받으면 이러한 조건들은 적용되지 않습니다.

저작권법에 따른 이용자의 권리는 위의 내용에 의하여 영향을 받지 않습니다.

이것은 이용허락규약(Legal Code)을 이해하기 쉽게 요약한 것입니다.

Disclaimer

dCollection

공학석사 학위논문

Effects of Individual Strand Force Deviation in Multi-Strand Post-Tensioning Tendon on Structural Behavior

멀티스트랜드 텐던의 개별강연선 긴장력 편차가 포스트텐션 구조 거동에 미치는 영향

2018 년 2 월

서울대학교 대학원

건축학과

신 형 엽

공학석사 학위논문

Effects of Individual Strand Force Deviation in Multi-Strand Post-Tensioning Tendon on Structural Behavior

멀티스트랜드 텐던의 개별강연선 긴장력 편차가 포스트텐션 구조 거동에 미치는 영향

2018 년 2 월

서울대학교 대학원

건축학과

신 형 엽

Effects of Individual Strand Force Deviation in Multi-Strand Post-Tensioning Tendon on Structural Behavior

지도 교수 강 현 구

이 논문을 공학석사 학위논문으로 제출함
2018 년 2 월

서울대학교 대학원
건축학과
신 형 엽

신형엽의 공학석사 학위논문을 인준함
2018 년 2 월

위 원 장 홍 성 걸 (인)

부위원장 강 현 구 (인)

위 원 이 동 근 (인)

Abstract

Effects of Individual Strand Force Deviation in Multi-Strand Post-Tensioning Tendon on Structural Behavior

Shin, Hyeongyeop
Department of Architecture and Architectural Engineering
College of Engineering
Seoul National University

Multi-strand post-tensioning method is applied to the construction of large-scale building or civil structures. Due to the construction field tolerance and the nature of multi-strand tendons having 'initial slack', there is a deviation of individual strand tensile forces in multi-strand tendons. To the author's knowledge, the effects of tensile force deviation on the structural behavior of post-tensioned structures have not been studied. Some inconsistency issues exist in the code provisions regarding the management of differential post-tensioning forces. In order to provide more reasonable code requirements, it is necessary to understand how the individual strand force deviation affects the structural performance. Thus, in this study, the influence of individual strand force deviation on the behavior of post-tensioned structures is analyzed through theoretical study and numerical analysis.

The effects of initial slack on the tendon stress-strain relationship are identified and investigated in order to apply to numerical analysis along with a new equivalent tendon material model. From the developed equivalent tendon material model, it can be noticed that the equivalent yield stress and tensile strength can be reduced with the deviation of individual strand tensile forces. In addition, it is theoretically verified that the average relaxation loss of tendon can be increased by the individual tensile force deviation. In other words, the material properties of tendon can be changed by the individual strand force deviation.

The numerical analysis results show that the ultimate flexural capacity of post-tensioned beams is fairly reduced when the individual tensile force deviation is excessive. However, the degree of reduction of ultimate strength is found to be limited for most cases. Above all, in the realistic level of tensile force deviation of about 10% C.O.V., the ultimate strength reduction is negligible. Whereas, in the case of partial model of nuclear containment, the effect of individual tensile force deviation on the ultimate pressure capacity reduction is negligible for every case. From the analysis, it is found that the strength reduction caused by individual strand force deviation depends on the tensile stress at ultimate state (f_{ps}). This is because the f_{ps} decreases significantly near the equivalent tendon yield strength (f_{py}) in reference to the f_{ps} of analysis model with no deviation. Therefore, it can be concluded that the strength reduction of structure is perceptible when the f_{ps} reaches to the yield strength region.

This study analyzed the effect of individual strand force deviation on the ultimate strength of post-tensioned structures, and proposed the method to analyze it. The results of this study are expected to be used as basic research data to codify or revise acceptance criteria for the deviation of individual strand tensile force in the code provisions.

Keywords : multi-strand tendon, individual strand tensile force deviation, initial slack, equivalent tendon material model, finite element analysis, post-tensioned beam, nuclear containment building
Student Number : 2016-21074

Contents

List of Tables

List of Figures

Chapter 1. Introduction

1.1 Introduction

1.1.1 Concepts on multi-strand post-tensioning system

Recently, prestressed concrete structures using post-tensioning methods have been actively applied to building and civil structures such as multi-story buildings, long-span bridges, and nuclear containment buildings (PTI, 2006). Prestressed concrete is a method that compensates the nature of concrete, which is strong in compression and weak in tension, by applying pre-compressive force with steel strands or bars. It is an effective way to reduce cracks under service loads and improve the ultimate strength of members.

Post-tensioning method, which is one of the methods of prestressing concrete, is the method that applies tensioning of prestressing steel after concrete curing, via the pre-installed post-tensioning ducts. In the case of a post-tensioning system using prestressing strands, the system can be divided into two categories according to the number of strands in a duct or sheath; single-strand tendon and multi-strand tendon (**Figure 1-1**). The single-strand tendons are used in relatively small structures such as building structures, but the multi-strand tendons are applied in large structures such as bridge girders and nuclear containment structures.

Figure 1-1 Single-strand tendon (left) and multi-strand tendon (right) (VSL, 2015)

The multi-strand tendon systems consist of strands, filling material, duct, and anchorage components (**Figure 1-1**). The filling material may be cement grout, grease or wax, and the strand may be bare-strand or greased-sheathed strand (unbonded single-strand) (**Figure 1-2**). According to the type of filling material, the systems can be classified into bonded tendon, unbonded bare-strand tendon or greased sheathed-strand tendon. The characteristics of each tendon are summarized in **Table 1-1**.

Table 1-1 Characteristics of each post-tensioning method (Kang and Park, 2016)

	Bonded tendon system	**Unbonded bare-strand tendon system**	**Greased sheathed-strand tendon system**
Section	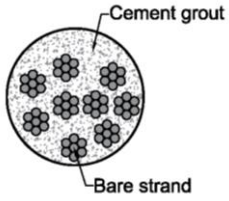	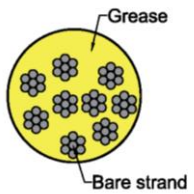	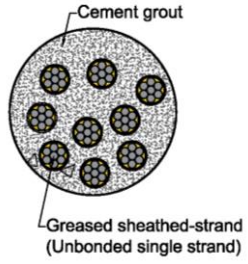
Corrosion protection	Good (cement grout)	Bad (Not good at maintenance of grease)	Best (HDPE sheath + grease + cement grout)
Detensioning	Impossible	Hard (by jacking all strands)	Easy (by individual strands)
Restressing	Impossible	Hard	Easy
Replacement of strands	Impossible	Hard (to replace a strand, all strands should be detensioned)	Easy (to replace a strand, only one strand should be detensioned
Duct size	Small	Small	Larger than other systems
Maintenance	Maintenance free	In-service inspection is possible but hard	In-service inspection is possible and easy
Friction loss	Large	Large	Small

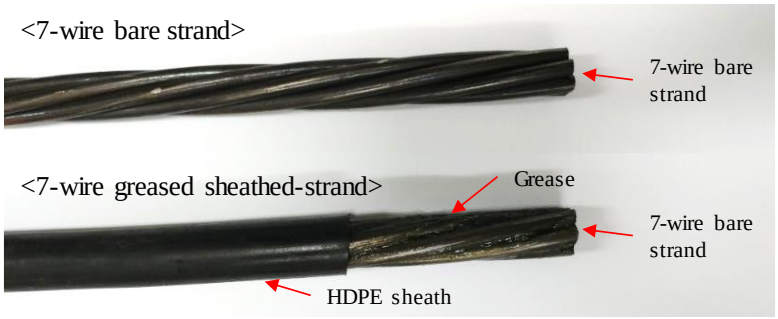

Figure 1-2 7-wire bare-strand (up) and 7-wire greased sheathed-strand (down)

1.1.2 Differential tensile forces of individual strands in the multi-strand post-tensioning tendons

The multi-strand tendons are tensioned using a multi-strand tensioning jack that can simultaneously tension multiple strands (**Figure 1-3**). The multi-strand tensioning jack clamps multiple strands in a temporary wedge plate inside the jack, and moves the plate with the pressure of piston. Then, tensile forces are applied to multiple strands simultaneously. That makes the individual strands of the tendon have the same elongation after post-tensioning. Theoretically, when the material properties of individual strands are the same, the elongations of individual strands are proportional to the applied average tensile force in the tendon. That makes it seem as if the same tensile forces are applied to the individual strands.

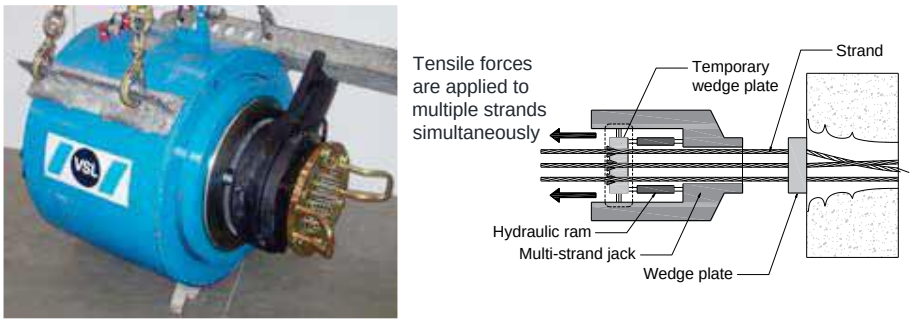

Figure 1-3 Multi-strand tensioning jack (left) (VSL, 2015) and conceptual diagram (right)

However, in the construction field, when tensile forces are applied using a multi-strand tensioning jack, there is a deviation in the tensile forces applied to the individual strands of a multi-strand tendon. The magnitude of the average tensile force applied to the entire tendon can be estimated and controlled quite accurately, if the measured piston pressure of the tensioning jack is available. Yet the tensile forces applied to the individual strands cannot be known without direct measurement using individual load cells. Therefore, it is not easy to control and even monitor the differential tensile forces of individual strands in the field.

The following factors can cause the deviation of tensile forces in the individual strands (KICT, 2015).

- Errors of measurements (load cell or pressure gauge)
- Errors of geometrical and material properties of prestressing steel (cross-sectional area and elastic modulus)
- Errors due to friction in tensioning jack, anchorage, and duct (sheath)
- Initial slack effects

Most of these factors are inevitable errors; however, out of these, tensile force deviations due to the initial slack are affected by the field management method which can be improved. The concept of initial slack in the multi-strand tendon is summarized in **Figure 1-4**. In order to remove this initial slack, an initial arrangement jack which can simultaneously tension multiple strands separately with individual small capacity pistons is used in the field. The use of an initial arrangement jack can significantly reduce the tensile force deviation in individual strands.

However, not all the construction fields utilize the initial arrangement jack, and there is a lack of research on the effect of the adjustment of initial slack on structural behavior. Also, it is necessary to study methods to consider the tensile force deviations of individual strands due to the initial slack effects in

the structural design and analysis of post-tensioned structures.

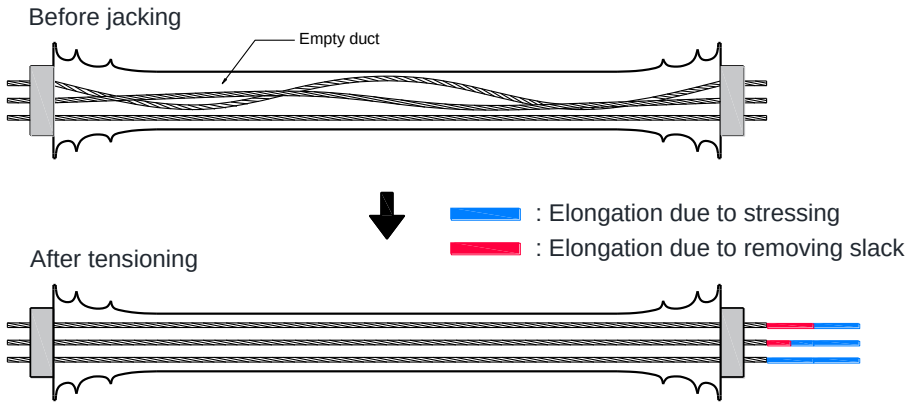

Figure 1-4 Concept of initial slack effect in multi-strand tendon

1.1.3 Relationship with code requirements

Except for the unavoidable errors such as material properties, the deviation of tensile forces in individual strands are mainly affected by the construction field management. Especially, the tensile force deviation due to initial slack effects are affected by the strand installation method and tensioning equipment (e.g., use of initial arrangement jack). Therefore, there are requirements for strand installation method in the codes and specifications, such as AASHTO (2010) or PTI/ASBI (2012) for civil structures and ASME (2015) or AFCEN (2012) for nuclear containment structures (Discussed in **Chapter 2**). In addition, the codes suggest acceptance criteria for the difference between theoretical elongation and measured elongation after jacking, in order to prevent tendons from being tensioned with excessive or insufficient tensile forces. These provisions are specified to ensure the tensile forces applied to tendons closer to design tensile forces and to minimize the tensile force deviation of individual strands. In other words, the purpose is to prevent adverse effects on the structural behavior caused by inaccurate tensile force management.

The requirements for tendon installation methods in the above-mentioned codes are inconsistent to each other. The ASME (2015) requires somewhat unreasonable installation methods, which are difficult to be applied in the construction fields. The elongation tolerances are different for each code. Most of the codes have the acceptance criteria for the average elongation of a tendon (average elongation of strands in a tendon), whereas the elongation tolerance of individual strands is not specified except for MOLIT (2013). Due to the fact that individual tensile forces are not measured in the field, acceptance criteria or guidelines for the allowable standard deviation of individual tensile forces are not presented in the codes, though the installation and elongation are related to the tensile force deviation of individual strands.

1.2 Scope and objectives

As mentioned in the previous section, there is a lack of research on the effect of the individual strand force deviation in a multi-strand tendon on the structural behavior of post-tensioned structures. Accordingly, the codes and specifications do not provide consistent acceptance criteria for the differential tensile force in the individual strands.

The main purpose of this thesis is to analyze the effect of the tensile force deviation of individual strands caused by initial slack on the ultimate capacity of post-tensioned beams and a ring-shaped partial model of nuclear containment buildings, through theoretical and numerical analysis. A theoretical analysis was carried out, with the proposal of equivalent tendon stress-strain relationship considering the tensile force deviation due to the effect of the initial slack. Then, it is analyzed how much the increase of the level of tensile force deviations reduces the ultimate flexural or inner pressure capacity with numerical analysis using finite element analysis software. Also, appropriateness of the requirements for tensile forces (elongation tolerance)

specified in the codes was verified based on the analysis results.

Finally, the purpose of this study includes to provide basic research data for improvement of current code (specification) requirements related to the management of tensile forces and installation operation.

1.3 Organization

This thesis is composed of five main chapters. The research background, purpose and scope of the research are shown briefly in **Chapter 1**. Current codes and specifications related to the tendon installation methods and elongation (tensile force) tolerance are compared and discussed in **Chapter 2**. Also, previous studies related to the field measurement of the tensile force deviations of individual strands are reviewed in **Chapter 2**. **Chapter 3** contains theoretical analysis on the tensile force deviations due to initial slack effects, and an equivalent stress-strain relationship for the tendon was proposed. Numerical analysis for the PT beams and partial model of nuclear containment to study the effect of tensile force deviation is shown in **Chapter 4**. Finally, conclusions are given in **Chapter 5**.

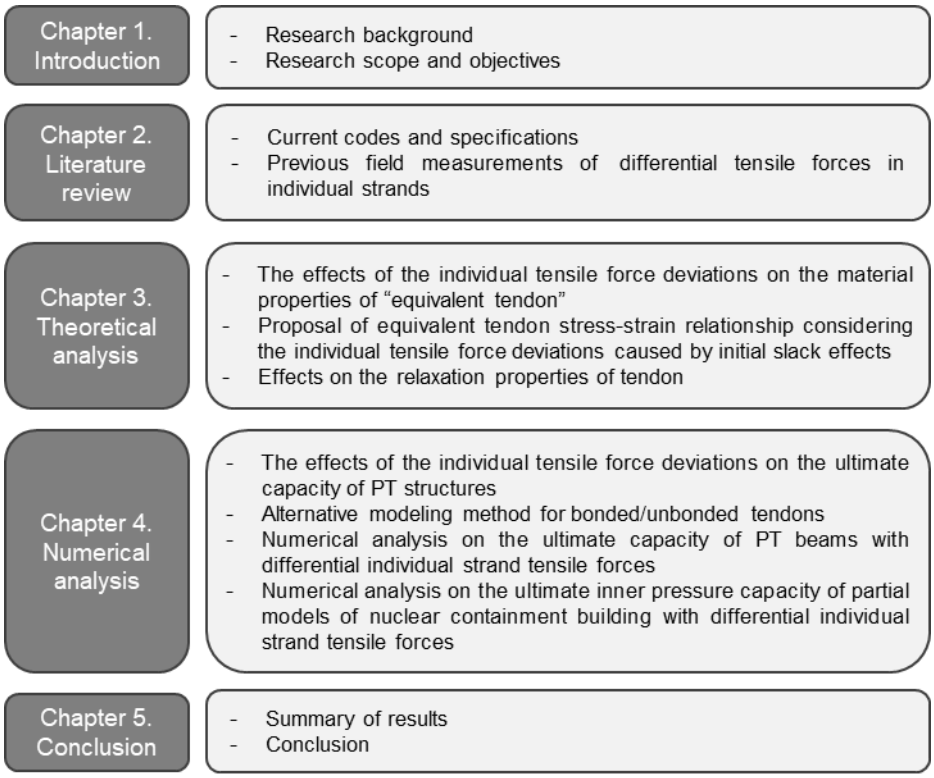

Figure 1-5 Contents of this thesis

Chapter 2. Review of Codes, Specifications and Previous Studies

2.1 Codes and specifications

2.1.1 Requirements for tendon installation methods

In the multi-strand post-tensioning method, the strands are installed by pulling or pushing individual strands one by one or installing bundled strands at once (**Figure 2-1**). Then, the post-tensioning work is done by tensioning the strands at once using hydraulic jacks. Due to the mechanical properties of prestressing steel and the measurement error during tensioning work, there may be a difference between the design tensile forces and the applied tensile forces in real structures (i.e. there may be a difference in tendon elongations). In the field, the tensioning operation is managed to make this difference less than the specified value. ASME (2015), PTI/ASBI (2012), AASHTO (2010), AFCEN (2012) and other related codes and specifications provide guidelines for the tendon installation methods and the acceptance criteria for the error of elongations (tensile forces).

Table 2-1 summarizes the requirements of each code and specification for the tendon installation method. The whole sentences of the code (specification) requirements are shown in **Appendix A-1**.

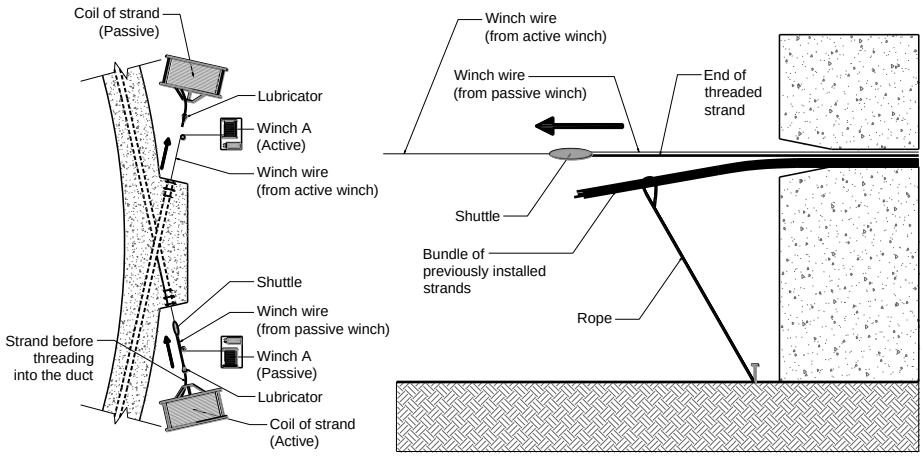

(a) pulling strand 1-by-1 method

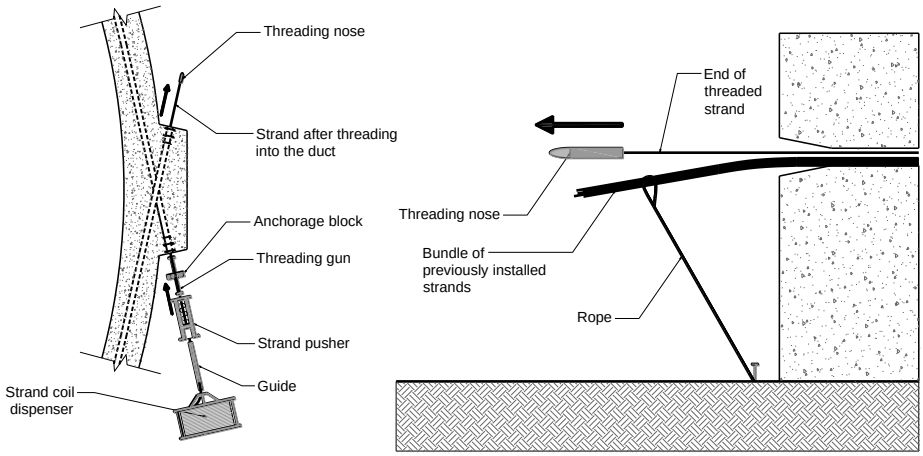

(b) pushing strand 1-by-1 method

Figure 2-1 Tendon (strand) installation methods

Table 2-1 The tendon installation requirements in each code and specification

Code/Specification		Installation methods				Use of initial arrangement jack
		Twisting	**Bundling**	**Pushing strand 1-by-1**	**Pulling strand 1-by-1**	
ASME (2015)	Horizontal tendon	Allowed	Allowed	Not allowed	Not allowed	-
	Vertical tendon	-	-	-	-	-
PTI/ASBI (2012)		-	Allowed	Allowed	Allowed	-
AASHTO (2010)		-	-	Allowed	Allowed	-
AFCEN (2012) (ETC-C)		-	-	Allowed	-	Mandatory
SETRA (2006) (VSL construction specification)		-	Allowed	Allowed	-	-

Note: '-' means 'not mentioned in the code/specification'

As multiple strands are tensioned at the same time and a systematic tensioning operation using a tensioning management sheet is performed, the sum of the tensile forces of the tendon can be adjusted to be close to the target (design) tensile forces. However, the tensile forces of the individual strands in the tendon cannot be adjusted to be same because of the initial slack effects (see **Figure 1-4**), and a deviation of tensile forces between individual strands would occur. If the tensile force deviation is excessive, some strands with excessive tensile forces can be broken, resulting in deteriorated structural performance. This is one of the reasons that the codes, including the CC-4432.5 requirement in ASME (2015) (**Appendix A-1**), restricts some of the tendon installation methods.

In ASME (2015), the reason for the installation restriction only for horizontal tendons is that initial slack occurs in the horizontal (circumferential) tendon, not vertical (inverted-U) tendon, due to geometrical characteristics (**Figure 4-39**). In other words, ASME (2015) includes the installation limitation only for

horizontal tendons, which have a risk of excessive initial slack. On the other hand, in the case of AFCEN (2012), there is no restriction on the installation method of strands, but it requires using an initial arrangement jack to minimize the tensile force deviations of individual strands. Both ASME (2015) and AFCEN (2012) are the codes specifically for the construction of nuclear containment structures. Because nuclear containment structures have circumferential tendons with a high probability of initial slack, some of the installation methods are restricted.

In the codes and specifications other than ASME (2015), the restriction provisions regarding the installation method does not exist, and it is permitted that the strands could be installed individually by pushing or pulling method.

2.1.2 Requirements for tendon elongation tolerances

The acceptance criteria for the elongation (tensile force) discrepancies are indicated in **Table 2-2**, which shows that the codes and specifications suggest similar acceptance criteria.

As indicated in **Table 2-2**, the elongation tolerances are a little different. ASME (2015) and AFCEN (2012) suggest consistent acceptance criteria for all lengths of the tendon because short tendons (less than 15 m) are not applied to nuclear containment buildings. Except for MOLIT (2013), the acceptance criteria for the elongation in individual strands of a tendon is not specified in the codes. Also, no codes require the tolerance of the standard deviation of the individual tensile forces.

Table 2-2 The acceptance criteria for the elongation (tensile force) error for post-tensioning tendons in each code and specification

Code/ Specification	Entire tendon		Individual strand		Tensile force deviations in individual strands
ASME (2015)	7%		-		-
PTI/ASBI (2012)	≤12 m	≥12 m	-		-
	±(7% + 6.35 mm)	±7%			
AASHTO (2010)	≤15 m	≥15 m	-		-
	±7%	±5%			
AFCEN (2012) (ETC-C)	+8%, -5%		-		-
MOLIT (2013)	≤15 m	≥15 m	≤15 m	≥15 m	-
	±7%	±5%	±15%	±10%	

Note: Error means the discrepancy between true (measured) elongation and theoretically calculated elongation; '-' means 'not mentioned in the code and specification'

2.1.3 Discussion on the code requirements

Considering the code requirements for the installation method and the elongation tolerance, the requirements of the ASME code (2015) have the following problems. First, it requires a very large (more than 160 m) working space to twist the strands when applying the CC-4432.5 requirement and requires a large capacity equipment to install a bundled tendon. It is difficult to be applied in actual construction. In the field, without twisting or bundling, it is possible to control the tensile force deviation small enough by using an initial arrangement jack to remove the initial slack, as required by AFCEN (2012). The main tensioning operation is performed after removing the initial slack. Therefore, there is no need to limit the installation methods in order to minimize the strand tensile force variation. In addition, although the twisting

requirement has been included in CC-4432.5 of ASME (2015) for the purpose of minimizing the tensile force deviation, CC-4467.1 specifies only the elongation tolerance for the whole tendon (average elongation of strands), not for the acceptance criteria for the strand tensile force deviation.

Additionally, considering the current trend of applying greased sheathed-strand tendons to large scale civil structures, a more eased tendon installation requirement should be presented. No slack effects are expected for greased sheathed-strand tendons. For unbonded bare-strand tendons, the slack effect can be caused by strand movement from outside to inside of a duct in the jacking process. Whereas, for the greased sheathed-strand tendons, strand movement from outside to inside of a duct is impossible because of hardened cement grout (**Figure 2-13**). Also, the slack effect can occur in the installation process. In both systems, strands can be installed with crooked shape. In the case of the unbonded bare-strands, the crooked shape is straightened in jacking procedure, which causes additional elongation. Whereas greased sheathed-strands cannot be straightened during jacking due to constraint by hardened cement grout. That means the greased sheathed-strand tendons have theoretically low initial slack compared to bare strands. For that reason, in the case of the greased sheathed-strand tendons, the use of initial arrangement jack does need not be utilized to remove the initial slack effects.

Therefore, in order to more reasonably improve the requirements for the tendon installation methods and the tensile force control, it is necessary to consider followings:

- In the case of greased sheathed-strand tendons, there is no need to limit the installation method to reduce individual tensile force deviations. Also, it is not necessary to require specified installation method for different types of tendons (e.g. bonded tendon, unbonded bare-strand tendon), if the initial slack is removed using the initial arrangement jack.

- Acceptance criteria or guidelines for the standard deviation of individual strand tensile forces should be provided. In order to provide the acceptance criteria, it is necessary to analyze the effect of the individual tensile force deviations on the structural behavior of post-tensioned structures.

2.2 Previous studies

2.2.1 Cho et al. (2015) and KICT (2015)

Cho et al. (2015) and KICT (2015) measured and analyzed the tensile force deviations in the individual strands of bare-strand tendons, which were not filled with cement grout or grease. The test specimen used in the measurement is shown in **Figure 2-2**. Total 12 tendons (**Table 2-3**) were installed in the specimen, with different number of strands and tendon curvature (sag ratio).

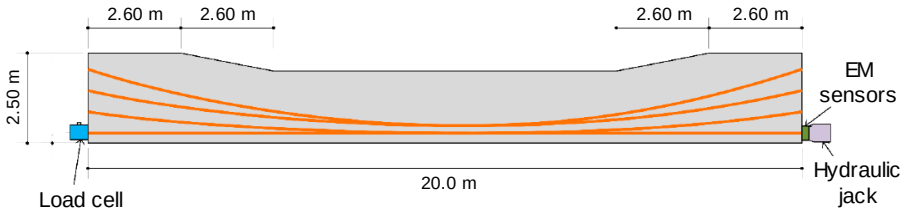

(a) Elevation of the specimen

(b) Whole view of the specimen

Figure 2-2 Shape and tendon layout of the specimen (Cho et al., 2015; KICT, 2015)

The tensile forces in the individual strands were measured by an EM sensor (electromagnetic sensor) attached to a multi-strand tensioning jack. The EM sensor indirectly measures the stresses of strands using the electromagnetic properties of a steel strands. Using the EM sensor, contactless measurement of tensile stress was made, and the tensile forces were measured simultaneously with the tensioning of tendon (strands). The multi-strand tensioning jack and

EM sensor used in the test (**Figure 2-3**) were able to tension and measure up to 19 strands, which were able to measure the individual tensile forces of all the strands in the tested tendon. The tensioning operation was performed with staged jacking as shown in **Figure 2-4**, and individual tensile forces were measured by the EM sensor at each tensioning stage.

Table 2-3 Details of tendons in the specimen (Cho et al., 2015; KICT, 2015)

Cross-section at the end-span	Tendon ID	No. of strands	Curvature (1/m)
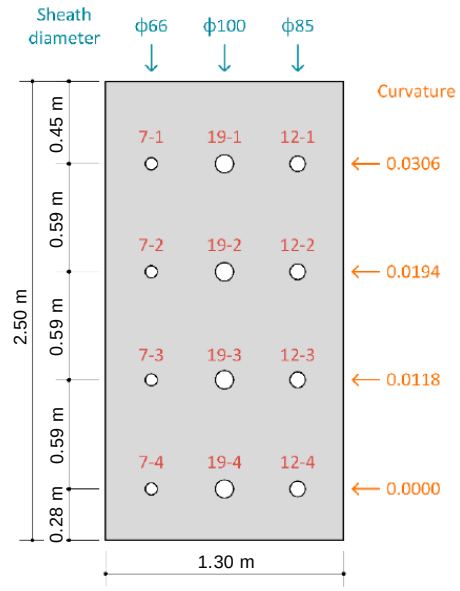	7-1	7	0.0306
	7-2		0.0194
	7-3		0.0118
	7-4		0.0000
	12-1	12	0.0306
	12-2		0.0194
	12-3		0.0118
	12-4		0.0000
	19-1	19	0.0306
	19-2		0.0194
	19-3		0.0118
	19-4		0.0000

(a) EM sensor (b) EM sensor attached to hydraulic jack

Figure 2-3 The tensioning jack and EM sensor (Cho et al., 2015; KICT, 2015)

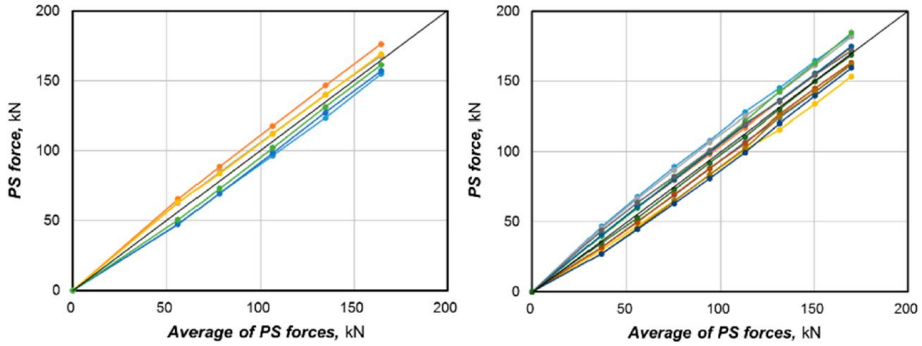

(a) 7-strand tendon (7-1 tendon) (b) 12-strand tendon (12-1 tendon)

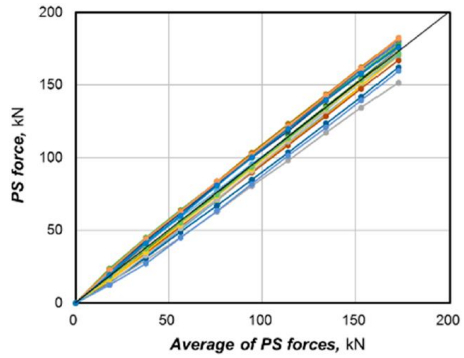

(c) 19-strand tendon (19-1 tendon)

Figure 2-4 Variation of prestress force according to prestress stage (Cho et al., 2015; KICT, 2015)

The measurement results are shown in **Figure 2-5**. The standard deviation of the tensile forces (PS forces in **Figure 2-5**) of individual strands tend to increase gradually as the average tensile force of the tendon increases. However, coefficient of variation (C.O.V.) decreased with increasing average tensile force. The average tensile force – C.O.V. relationship (**Eq. 2-1**) was made with curve fitting. The measured individual tensile forces had C.O.V. of around 5% at 170 kN (= $0.61f_{pu}$), which was at the final tensioning stage. The deviations were not significantly dependent on the tendon curvature and number of strands. The measured individual tensile forces were found to follow normal distributions.

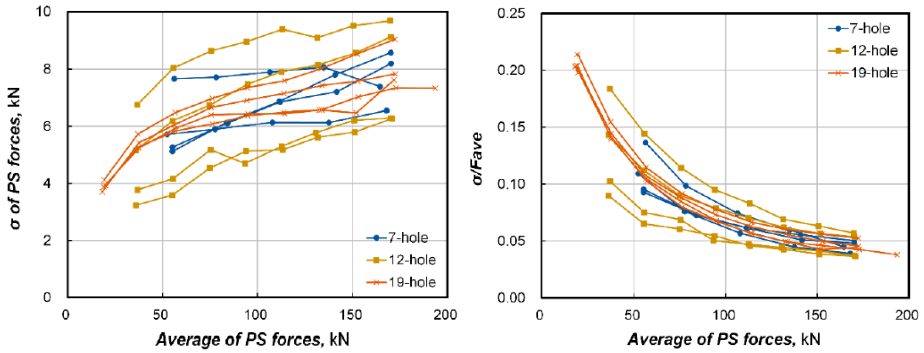

(a) Standard deviation (b) Coefficient of variation

Figure 2-5 Variation of standard deviation and C.O.V. with respect to the average tensile force (Cho et al., 2015; KICT, 2015)

$$\frac{\sigma}{F_{ave}} = \frac{6.9510}{F_{ave} + 16.4042} + 0.0081 \tag{2-1}$$

Where,

σ : Standard deviation of individual tensile forces, kN
F_{ave} : Average tensile force of individual strands in the tendon, kN

For the reason of large C.O.V. in the low average tensile force level measured in the bare-strand tendons (**Figure 2-4**), it can be inferred that the initial slack in the individual strands was removed at the initial jacking stage. It can be seen that the deviation of the tensile forces occurred in the initial jacking stage (below 50 kN average PS force in **Figure 2-4**) was maintained almost similar to the subsequent tensioning stages. This is because the applied tensile forces were used to remove the initial slack at the initial jacking stage, but the initial slack was completely removed at the subsequent tensioning stages. Because the main cause of the individual tensile force deviation was eliminated, the deviation did not significantly increase (Slight increase in the deviations after removing initial slack was due to the errors of measurement or material properties as mentioned in **Section 1.1.2**.). From the results, it can be inferred that individual tensile force deviations are highly dependent on the initial slack effects.

2.2.2 Cho et al. (2016) and KICT (2015)

Cho et al. (2016) and KICT (2015) measured the distribution of individual strand tensile forces in the tendons at three actual prestressed concrete girder construction sites (**Figure 2-6**). The measured tendons were bare-strand tendons before filling cement grout. In the same manner as Cho et al. (2015) and KICT (2015), tensioning and measurements were conducted using a multi-strand tensioning jack with EM sensor.

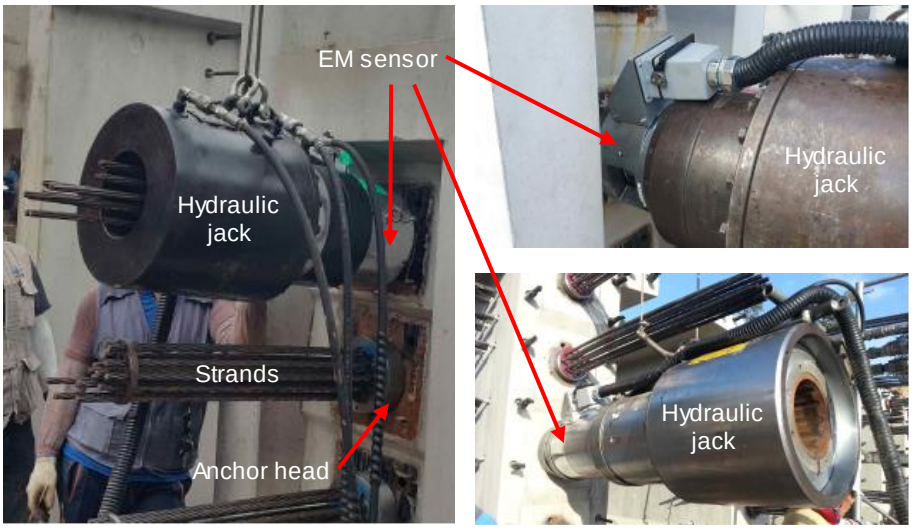

Figure 2-6 Tensioning and measurement with EM sensor attached tensioning jack in three construction sites (Cho et al., 2016; KICT, 2015)

Measurements were made for 49 girders from the three construction sites. A total of 194 tendons with different girder length, tendon curvature (sag ratio), and number of strands were measured. The number of measured strands was 2,761. Information on the measured tendons is summarized in **Table 2-4**.

Table 2-4 Information on the measured tendons in the construction sites (Cho et al., 2016; KICT, 2015)

Type of measured tendons	Length (m)	Sag ratio†	No. of strands in a tendon	No. of measured tendons
1	44.7	0.1082	13	2
2	44.7	0.0868	13	2
3	44.7	0.0546	13	2
4	44.7	0.0224	13	2
5	39.8	0.0974	13	3
6	39.8	0.0614	13	3
7	39.8	0.0252	13	3
8	42.4	0.1392	16	21
9	42.4	0.0966	16	21
10	42.4	0.0542	16	21
11	42.4	0.0118	16	22
12	44.9	0.1314	16	8
13	44.9	0.0914	16	8
14	44.9	0.0512	16	7
15	44.9	0.0112	16	7
16	49.3	0.1420	13	7
17	49.3	0.1144	13	7
18	49.3	0.0868	13	7
19	49.3	0.0592	13	6
20	49.3	0.0186	14	7
21	54.8	0.1278	14	7
22	54.8	0.1030	14	7
23	54.8	0.0782	14	7
24	54.8	0.0532	14	7
Total				194

† Sag ratio = sag/length of a tendon

Figures 2-7(a) ~ (d) show the standard deviations of measured individual strand tensile forces in the tendons with respect to the girder length, sag ratio, number of strands, and average tensile force of tendon. From the measurement, it was found that the standard deviation of individual tensile forces was not correlated with the length of girder (length of tendon), sag ratio, and number of strands. On the other hand, it was found that there was a proportional relationship between the standard deviation and average tensile force of tendon. The standard deviations of individual tensile forces increased

with increasing average tensile force. However, the sensitivity (i.e. the slope of curve fitting line) was not significant. As discussed in the previous section, because of the initial slack effect, the standard deviation did not significantly increased with increasing average tensile force. The relationship between the average tensile force of tendon and C.O.V. of individual tensile forces was obtained from the curve fitting (**Eq. 2-2**).

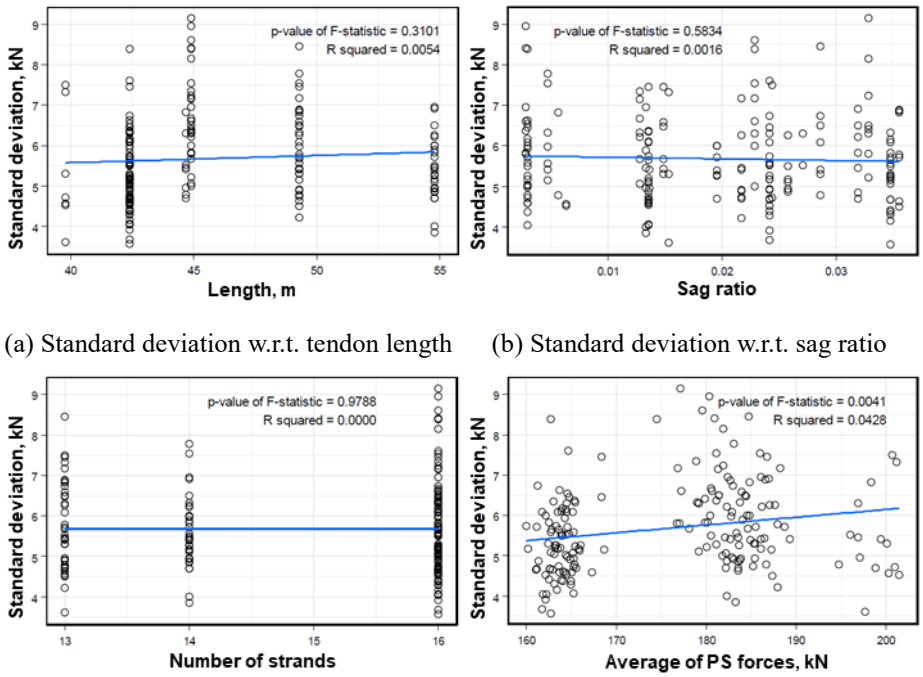

(a) Standard deviation w.r.t. tendon length

(b) Standard deviation w.r.t. sag ratio

(c) Standard deviation w.r.t. number of strands

(d) Standard deviation w.r.t. average tensile force of tendon

Figure 2-7 Standard deviations of measured individual strand tensile forces in each tendon (Cho et al., 2015; KICT, 2015)

$$\frac{\sigma}{F_{ave}} = \frac{2.286}{F_{ave}} + 0.019 \qquad (2\text{-}2)$$

Where,

σ : Standard deviation of individual tensile forces, kN
F_{ave} : Average tensile force of individual strands in the tendon, kN

2.2.3 Domage et al. (2010)

Domage et al. (2010) measured the individual strand tensile force deviations in bare-strand tendons. The tendons were horizontal circumferential tendons of a nuclear containment building. The test specimen was ring-shaped as shown in **Figure 2-8**, which was a part of the nuclear containment building. The effect of the use of initial arrangement jack on the individual tensile force deviation was analyzed. The tested tendon had 55 strands, and the individual strand tensile forces were measured using an EM sensor attached to the multi-strand tensioning jack.

Figure 2-8 Test specimen (Domage et al., 2010)

Figures 2-9(a) and **(c)** show the measured data of tendons of which the initial slack was removed using the initial arrangement jack before the main tensioning operation. **Figure 2-9(b)** and **(d)** show the measured data of tendon without the application of the initial arrangement jack. As seen from the results, the use of the initial arrangement jack could significantly reduce the individual tensile force deviation.

Compared to the results of Cho et al. (2015), Cho et al. (2016), and KICT (2015), the measured individual strand tensile force deviation was relatively large. It can be inferred that the large cumulative angle change (more than 360°) and low level of average tensile force (around $0.45f_{pu}$) made a large deviation. This is because the circumferential horizontal tendons, which had large cumulative angle change (~360°), had the larger degree of initial slack due to curvature. Also, as discussed by Cho et al. (2015) and KICT (2015), the

standard deviation of the individual strand tensile forces did not significantly increase with increasing average tensile force of the tendon. Therefore, in a low level of average tensile force, C.O.V. can be larger.

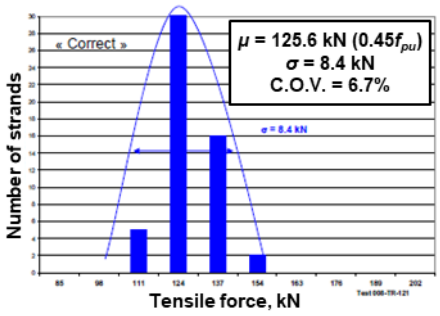

(a) Standard deviation w.r.t. tendon length

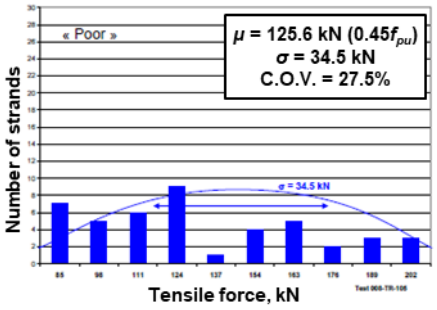

(b) Standard deviation w.r.t. sag ratio

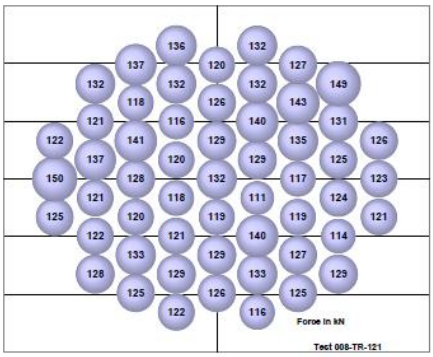

(c) Standard deviation w.r.t. number of strands

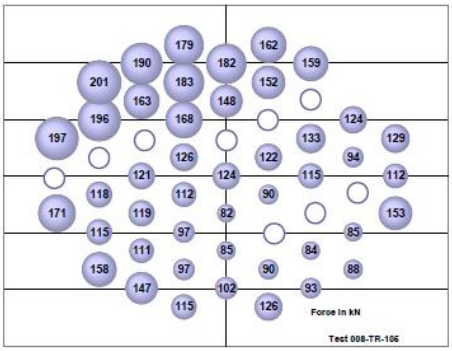

(d) Standard deviation w.r.t. average tensile force of tendon

Figure 2-9 Standard deviations of measured individual strand tensile forces in each tendon (Cho et al., 2015; KICT, 2015)

2.2.4 Chandoga and Jaroševič (2005)

Chandoga and Jaroševič (2005) measured the tensile forces of multi-strand post-tensioning tendons in bridge girders. The structures were segmental bridge girders post-tensioned with bare-strand tendons. Tensile force measurements were performed using a multi-strand tensioning jack (PAUL TENSA M3000kN prestressing jack, 13 holes) with individual EM sensors (PMJS13 sensor) (**Figure 2-10**). Tensioning operation was performed with

staged jacking, and the target jacking stress was set as 1,430 MPa (= 0.79f_{pu}) for all tendons. Total 59 tendons for three structures were measured, and the total number of measured individual strands was 708. The measured jacking stresses of 708 individual strands (59 tendons) are shown in **Figure 2-11**.

Figure 2-10 Multi-strand tensioning jack and EM sensors used in the measurement (Chandoga and Jaroševič, 2005)

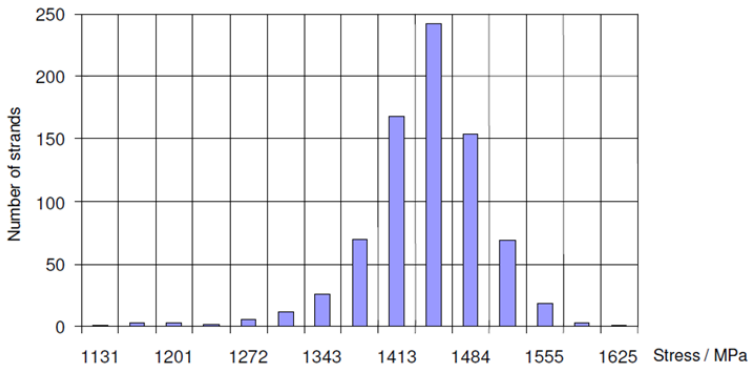

Figure 2-11 Distribution of measured jacking stresses of individual strands (Chandoga and Jaroševič, 2005)

As shown in **Figure 2-11**, there was a deviation in the measured tensile stresses of individual strands. Although the mean value and standard deviation

of measured tensile stresses were not reported in the research paper (Chandoga and Jaroševič, 2005), it can be seen that the measured individual tensile stresses had a wide range from 1,131 MPa (= $0.63f_{pu}$) to 1,625 MPa (= $0.90f_{pu}$).

Chandoga and Jaroševič (2005) also reported that abnormally low tensile stress could be measured on individual strands due to the fracture of strands or anchorage (wedge). **Figure 2-12** shows measured tensile stresses of individual strands at each stage of staged jacking. **Figure 2-12(a)** shows an unusually low measured tensile stress due to sudden failure of the strand during tensioning operation. **Figure 2-12(b)** shows an abnormal strand tensile stress caused by the wedge fracture at fixed end anchorage. Unlike the case of failure of strands, the tensile stress did not decrease to zero due to friction force from the surrounding strands. **Figure 2-12(c)** shows the measurement result of a normally tensioned tendon.

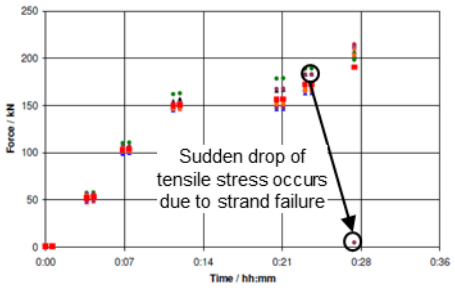

(a) Standard deviation w.r.t. tendon length

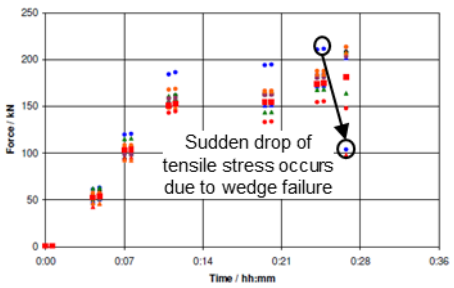

(b) Standard deviation w.r.t. sag ratio

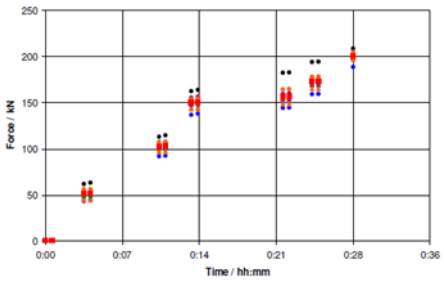

(c) Standard deviation w.r.t. number of strands

Figure 2-12 Measured tensile stresses of individual strands at each stage of staged jacking (Chandoga and Jaroševič, 2005)

2.2.5 Discussion on the previous researches

The measurements of individual strand tensile force deviations occurring in the bare-strand post-tensioning tendons were made in the previous researches. From the results of previous studies, it was found that the design variables such as the length of tendon and number of strands are not significantly related to the deviation of individual tensile forces. Depending on the construction site conditions, the deviations of individual strand tensile forces were measured to be 5 ~ 10% C.O.V. for tendons with $0.6f_{pu}$ or more average tensile stresses. Whereas, it may had a larger C.O.V. of individual tensile forces for tendons with lower average tensile stresses. These tensile force deviations were caused by initial slack and unexpected fracture of strands or wedges.

However, no studies have been conducted on the type of greased sheathed-strand tendons to the author's knowledge. Theoretically, the greased sheathed-strand tendons are tensioned after hardening of cement grout. Due to the independent path created by hardened cement grout and HDPE sheath, there would be no change of individual strand configuration before and after tensioning (**Figure 2-13**). It means that there is negligible initial slack effect, unlike the case of bare-strand tendons. As a part of research to apply greased sheathed-strand tendons, it is necessary to experimentally verify that the individual strand force deviation is lower than that of bare-strand tendons.

Although there have been some prior studies that measured and analyzed the effect of design variables on the individual strand force deviation, no research on the effect of tensile force deviation on the strength and serviceability of post-tensioned structures has been conducted. Therefore, it would be necessary to analyze the effect of individual strand tensile force deviation on the structural behavior, based on the realistic range of tensile force deviation as measured in the previous studies of this chapter. This can be considered as a future study.

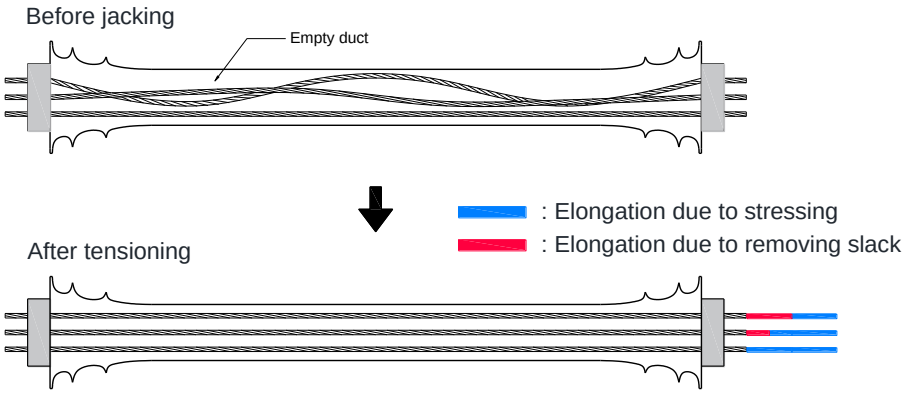

(a) Bare-strand tendon (bonded and unbonded)

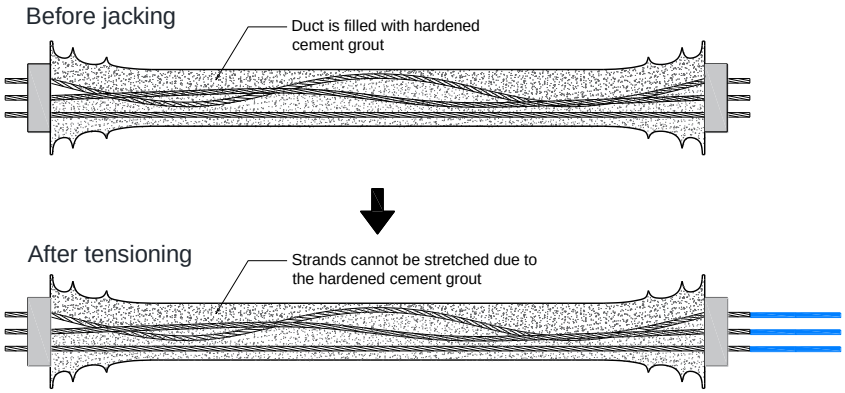

(b) Greased sheathed-strand tendon

Figure 2-13 Comparison of Initial slack effects between bare-strand tendon and greased sheathed-strand tendon

Chapter 3. Theoretical Analysis on the Effect of Individual Strand Force Deviation

In this chapter, prior to numerical analysis, theoretical analysis on the effect of the individual strand force deviation caused by initial slack effect is carried out. In order to intuitively understand the influence of the individual strand force deviation due to initial slack on the stress-strain relationship of the entire tendon, and to easily apply it in the numerical analysis, an equivalent tendon material model and associated Matlab code are proposed.

The factors affecting the stress-strain relationship including the equivalent yield strength and tensile strength of the entire tendon are analyzed using the proposed equivalent tendon material model. In addition, in terms of long-term behavior, the effects of individual strand force deviation on additional relaxation loss are analyzed.

In **Section 3.1**, an equivalent tendon stress-strain curve considering the tensile force deviations is suggested, and the effects on the stress-strain relationship are analyzed. In **Section 3.2**, the effects on the additional relaxation loss are analyzed, and time dependent constitutive relationship is carried out. These contents are concluded in **Section 3.3**.

3.1 Proposal of equivalent tendon material model

3.1.1 Tensile force deviations of individual strands due to initial slack effect

As discussed in **Chapters 2**, tensile force deviations of individual strands inevitably occur in the multi-strand tendons, even if all the strands are tensioned at once by a multi-strand tension jack. This is because there are initial slack effects and other material properties or measurement errors. As shown in **Figure 3-1**, the tensile force deviation due to the initial slack effect is caused by these two phenomena. First, curved strands (e.g. strands in circumferential tendons) tilt inward in the duct during tensioning operation. Second, strands which are not placed in a straight configuration are stretched straightly in the duct during the tensioning operation. Due to these slack effects, although target tensile forces are achieved for the entire tendon consisting of multi-strands, undesirable excessive or insufficient tensile forces in the individual strands may exist. Such tensile force deviations may affect the structural behavior of the entire system. Therefore, it should be considered carefully.

The most intuitive way to properly model this phenomenon and perform a numerical analysis is to model all strands in a tendon(s). All strands constituting a tendon should be individually modeled and analyzed in the same manner as discussed in **Section 4.2**. For example, if one tendon is composed of seven strand, the seven strands should be modeled separately, and different tensile force values (to consider the effect of tensile force deviations) should be input to perform the analysis. However, a large civil structure such as a nuclear containment structure has an excessive amount of information to be input in order to perform the analysis in the same manner. For example, to analyze a nuclear containment building, around 10,000 strands should be modeled. It is very time-consuming and requires significant computational cost. It is necessary to provide a method that can more easily

perform numerical analysis, considering the tensile force deviations of individual strands.

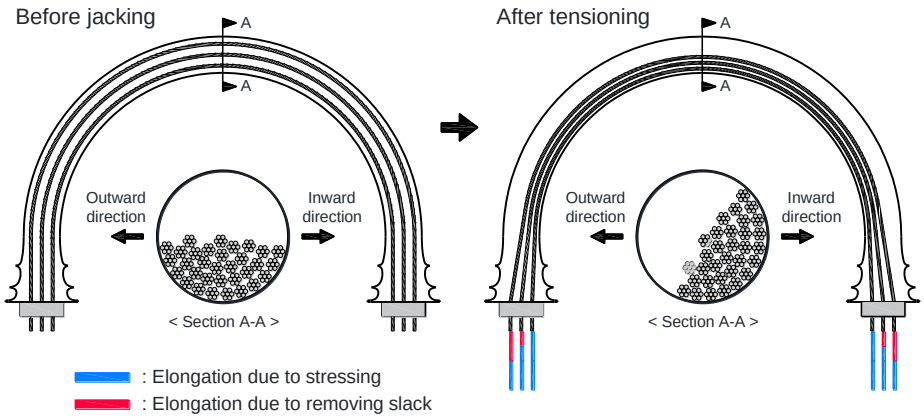

(a) Initial slack effect due to curvature

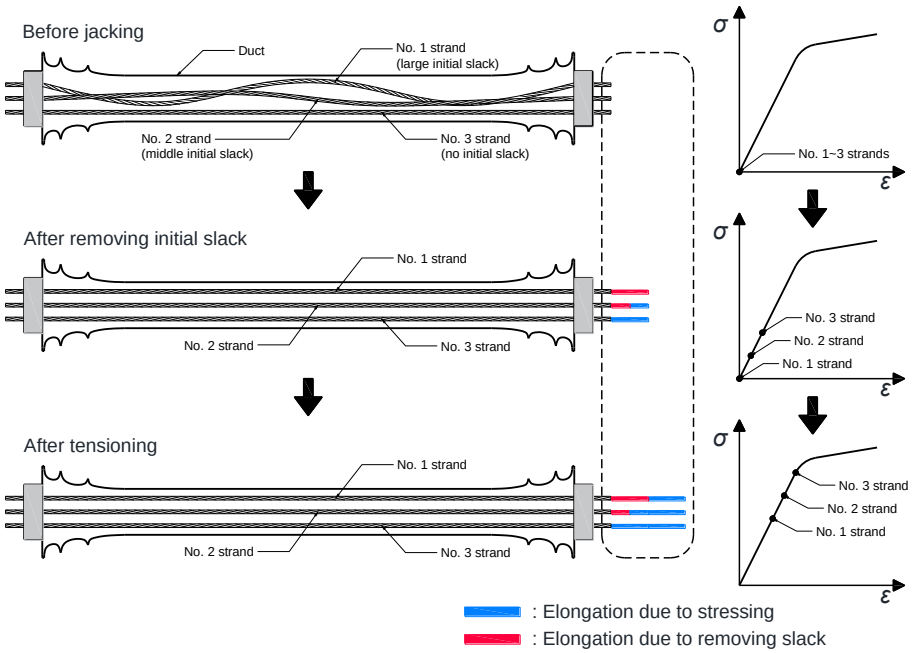

(b) Initial slack due to non-straight placement of the strands

Figure 3-1 Tensile force deviations due to initial slack effects

For that, a method that can simplify the numerical modeling is proposed. The equivalent tendon stress-strain relationship considering the situation that individual strands composing a tendon have a different level of prestressing forces due to the initial slack effect. The concept of the equivalent tendon material model is to create a single stress-strain curve by averaging the individual stress-strain curves of the strands. The equivalent tendon stress-strain curve is used to replace the multi-strands with one equivalent strand with the same cross-sectional area.

The basic assumption in constructing the equivalent tendon material model is that it considers only the tensile force deviations due to the initial slack effect. The tensile force deviation due to the errors in material properties is not taken into account. The deviation of the tensile forces due to the measurement error is also difficult to be considered in the numerical model. Since a tendon is usually composed of strands produced at the same time in the same factory, material properties of the individual strands are assumed not to be different from each other. In addition, as discussed in **Section 2.2.1**, it can be noticed that most of individual strand force deviation occurred in the initial tensioning stages, where the initial slack is being removed. From this result, it can be interpreted that the tensile force deviation of individual strands is dominated by the initial slack effect. Thus, the above basic assumption is reasonable.

The method of constructing the equivalent tendon material model is as follows: As shown in **Figure 3-2**, it is necessary to determine how much stress or strain in the stress-strain curve remains to reach the ultimate strength, f_{pu}, after the strands are tensioned. For example, if three strands (which have bi-linear stress-strain curves with f_{py} = 1,600 MPa, and f_{pu} = 1,860 MPa) compose a tendon and are tensioned with 1,200 MPa, 1,400 MPa, and 1,600 MPa tensile stresses, respectively, then the three strands would have remaining strengths of 680 MPa, 480 MPa, and 280 MPa to reach the ultimate strength. The tendon consisting of these three strands has an average tensile stress of 1,400 MPa, but the states of each strand are on different points on the

same stress-strain curve. In the case of a girder subjected to monotonic loading or a nuclear containment structure with internal pressure, the stress and strain have a tendency to move in an increasing direction when the load is applied. In the numerical analysis, the part of interest is the stress-strain relationship curves after the load is applied to each strand. In other words, the stress-strain relationship curves corresponding to the remaining strengths are the part of interest.

In order to reflect these states on one stress-strain curve, the stress-strain curve corresponding to the tensile force applied to each strand should be translated into the average tensile stress and strain of the tendon as shown in **Figure 3-2**. Then, the average of these translated stress-strain curves should be obtained. To the point corresponding to the average tensile strength of the tendon on the stress-strain curve, it is assumed that all of the strands follow a linear stress-strain relationship. But, after the average tensile force, each strand has a stress-strain curve corresponding to the remaining strength of each strand. Using this method and by modeling only one equivalent tendon (which has the same cross-sectional area as the sum of the multi-strands), it is possible to consider the stress-strain relationship properties of multi-strands with tensile force deviations. As a result, the equivalent tendon stress-strain relationship can be obtained as shown in **Figure 3-2**.

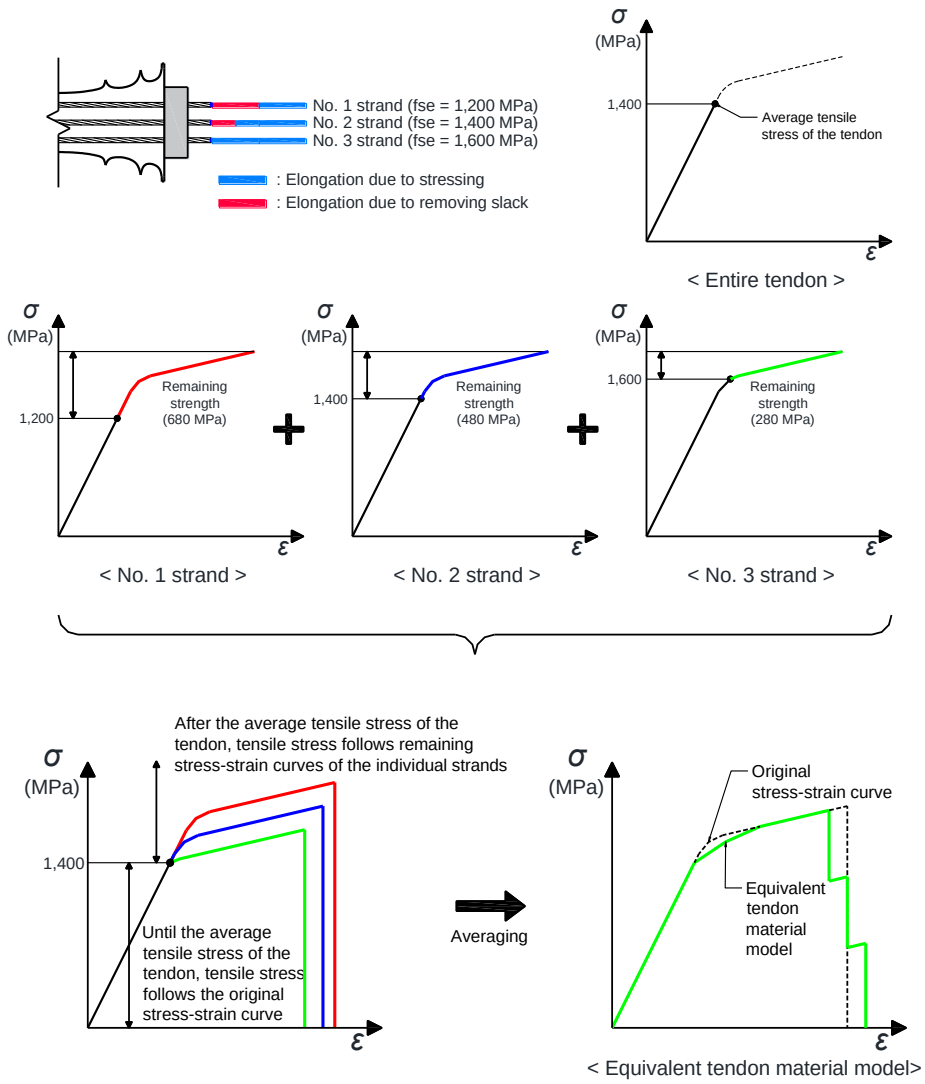

Figure 3-2 The concept of the equivalent tendon material model

Although all of the strands have the same material properties, the stress-strain relationship of the tendon can be changed due to construction conditions such as inherent initial slack. Also, it can be seen that as the tensile force deviations increase, the stress-strain relationship near the yield strength (f_{py}) can be affected, although it has less effect on the tensile strength (f_{pu}). In general, as the deviation increases, the yield strength of the equivalent tendon decreases.

In **Sections 4.2** and **4.3**, applying this method, an analytical study is conducted on the effect of the change of the stress-strain relationship due to tensile force deviations on the structural behavior of post-tensioned beams and partial models of nuclear containment.

With the proposed concept of equivalent tendon stress-strain relationship, the relationship can be expressed as **Eq. (3-1)**. However, because stress-strain relationship of prestressing steel ($g(\varepsilon)$) is usually in form of a complicated formula, hand-calculation of **Eq. (3-1)** may not be effective if the number of strands is large. Therefore, an MATLAB code to automatically calculate the equation is proposed.

$$g_{eq}\left(\varepsilon, f_{avg}, \mathbf{F_d}\right) = \begin{cases} g(\varepsilon) & \text{if } g_{eq}\left(\varepsilon, f_{avg}, \mathbf{F_d}\right) \le f_{avg} \\ \frac{1}{n}\sum_{i=1}^{n}\left\{g\left(\varepsilon + g^{-1}\left(f_{di}\right) - g^{-1}\left(f_{avg}\right)\right) + f_{avg} - f_{di}\right\} & \text{if } f_{avg} \le g_{eq}\left(\varepsilon, f_{avg}, \mathbf{F_d}\right) \end{cases} \quad (3\text{-}1)$$

Where,

n	: number of strands in a tendon
g	: stress-strain relationship function of a strand
g_{eq}	: equivalent tendon stress-strain relationship function of a tendon consisting of n strands
ε	: normal strain of tendon (strand)
$\mathbf{F_d}$	: vector of individual strand tensile stresses of tendon (= $\{f_{d1}, f_{d2}, \ldots, f_{di}, \ldots, f_{dn}\}$)
f_{di}	: tensile stress of i-th individual strand
f_{avg}	: mean value of individual strand tensile stresses ($f_{d1}, f_{d2}, ..., f_{dn}$)

3.1.2 MATLAB code for equivalent tendon material model

A Matlab code which can constitute the equivalent tendon material model is proposed based on the given material model of the prestressing steel and the tensile force measurement data of individual strands. The basic concept of the Matlab code is discussed in the previous section. The schematic diagram of the Matlab code is shown in **Figure 3-3**, and an example of the Matlab code is attached in **Appendix B**.

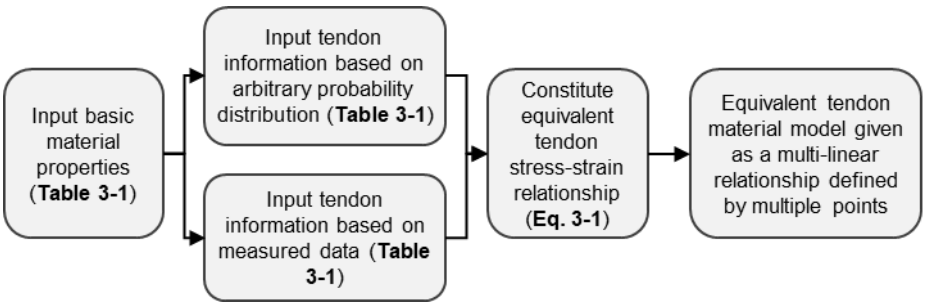

Figure 3-3 Schematic diagram of the Matlab algorithm

In the input section of the Matlab code, the basic information of the tendon, such as material properties of prestressing steel, the number of strands in the tendon, and the measured or assumed tensile forces (stresses) applied to the individual strands, should be specified (**Table 3-1**). The tensile forces or stresses of the individual strands can be directly measured from the experiment, or it can be assumed by using the random number generation function of the Matlab, which follows an arbitrary probability distribution (e.g. Gaussian distribution and uniform distribution). If there are no measured tensile force data from individual strands in the tendon, it can be assumed that the tensile force (stress) distribution follows normal distribution, with a specified mean value and standard deviation, as described in the previous research of **Chapter 2**. Using these assumptions, a reasonable equivalent tendon material model can be obtained.

Table 3-1 Input variables

Basic material properties	• Elastic modulus, E_p • Section area of the prestressing steel, A_p • Yield strength of the prestressing steel, f_{py} • Tensile strength of the prestressing steel, f_{pu} • Stress-strain relationship of the prestressing steel - User-defined multi-linear stress-strain relationship - Mattock (1979)
Tendon information (based on measured data)	• Number of strands in the tendon • Average tensile force or stress of the tendon • Measured tensile forces or stresses of the individual strands
Tendon information (based on arbitrary probability distribution)	• Number of strands in the tendon • Mean and standard deviation (or coefficient of variation) of the tensile forces or stresses of the individual strands • Distribution type - Uniform distribution - Normal distribution

The stress-strain curve of prestressing steel, which is the basis of the equivalent tendon material model, should be specified. For the material model of prestressing steel, pre-defined prestressing steel material models can be used, such as Mattock (1979) (**Eq. 3-2**). Also, the stress-strain curves measured in the experiments, or simplified material models such as bi-linear or multi-linear stress-strain curves are available, but it should be input manually. After specifying the basic properties and material models of prestressing steel, the process is the same as described in the previous section.

$$f_s = \varepsilon E_p \left[Q + \frac{1-Q}{\left\{ 1 + \left(\frac{\varepsilon E_p}{K f_{py}} \right)^R \right\}^{1/R}} \right] \tag{3-2}$$

Where,

$$Q = \frac{f_{pu} - K f_{py}}{\varepsilon_{pu} E_p - K f_{py}} \tag{3-2a}$$

f_s : tensile stress of prestressing steel
ε : strain of prestressing steel

ε_{pu} : strain of prestressing steel at ultimate strength
K : coefficient (a reasonable value for the seven-wire strands is 1.04.)
R : coefficient (can be determined by solving $f_s = f_{py}$ when $\varepsilon = 0.01$.)

3.1.3 Effective parameters of the equivalent tendon material model

It is necessary to identify the variables that affect the equivalent tendon material model, as discussed in the previous section. The equivalent tendon material model only considers the tensile force deviation due to the initial slack of the individual strands in the tendon, with the assumption that all other material properties are the same. The main variables affecting the equivalent tendon material model are related to the distribution of the individual tensile forces in the strands.

Theoretically, the equivalent tendon material model follows an idealized stress-strain relationship of prestressing steel, which has a linear relationship up to the average tensile stress of the tendon, and the modified stress-strain relationship that corresponds to the remaining strength of individual strands beyond the average tensile stress. Therefore, it affects the stress-strain relationship near the yield strength (f_{py}) and ultimate strength (f_{pu}). The variables determine the equivalent tendon material model are indicated in the following subsections.

Standard deviation of the tensile forces of individual strands

The larger the standard deviation of the tensile forces applied to the individual strands, the lower the yield stress of the equivalent tendon material model. If all of the strands have the same tensile forces (the standard deviation is equal to zero), the stress-strain relationship of the entire tendon is the same as the single prestressing steel. However, if there are deviations in the tensile forces, the strand with the largest applied tensile force yields first. Then, the other strands yield sequentially, in order of applied tensile forces. The yield point

becomes lower by the influence of the sequential stiffness reduction due to the sequential yielding of the strands. Conversely, the stress-strain relationship, after all of the strands yield, is the same as the single prestressing steel, with reduction of the ultimate strength and strain. Due to the sequential failure of the strands, there is a softening region, which does not exist in the single prestressing steel material model, and an increase of the strain at failure.

For example, if a tendon with 7 strands is tensioned with the tensile forces as shown in **Table 3-2**, the effect of the standard deviation of the tensile forces on the yield point and the stress-strain relationship of the tendon is shown in **Figure 3-4**.

Table 3-2 Example 1: the effect of the standard deviation of the tensile forces

Tendon	**Tensile stresses in the individual strands (MPa)**							**Mean (MPa)**	**Standard deviation (MPa)**
	No. 1	**No. 2**	**No. 3**	**No. 4**	**No. 5**	**No. 6**	**No. 7**		
Tendon 1	1,250	1,250	1,250	1,250	1,250	1,250	1,250	1,250	0
Tendon 2	950	1,050	1,150	1,250	1,350	1,450	1,550	1,250	200
Tendon 3	650	850	1,050	1,250	1,450	1,650	1,850	1,250	400

Tendon	**Yield stress (MPa)**	**Ultimate strength (MPa)**	**Ultimate strain (mm/mm)**
Tendon 1	1,759	1,930	0.0195
Tendon 2	1,743	1,913	0.0178
Tendon 3	1,702	1,854	0.0132

Note: The yield stresses are defined as the stress at the 1% strain; The yield stress and ultimate strength of the single prestressing steel, f_{py} and f_{pu}, are 1,759 MPa and 1,930 MPa, respectively.

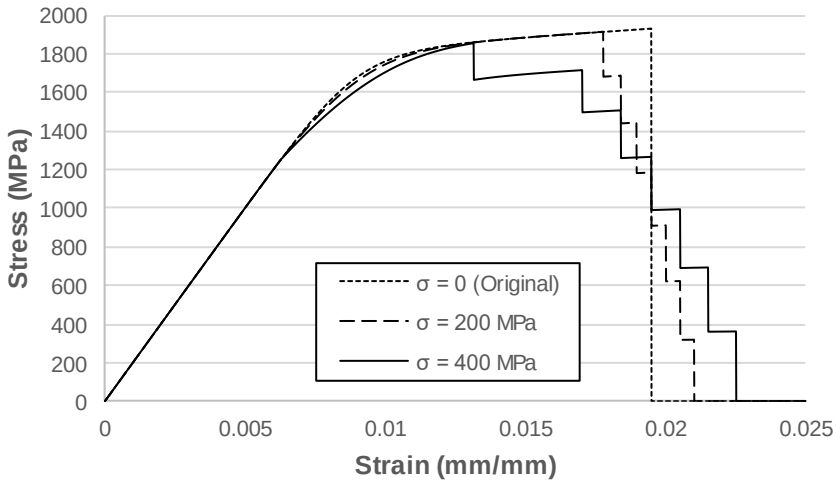

Figure 3-4 The effect of the standard deviation of the tensile forces on the equivalent tendon material model

Distribution type of the tensile forces

Additionally, the distribution type can affect the equivalent tendon material model. Although a tendon has the same standard deviation of the tensile forces, if the distribution types are different, the stress-strain relationship can be different near the ultimate strength and strain.

For example, if a tendon with 7 strands is tensioned with the tensile forces as shown in **Table 3-3**, which has the same standard deviation but different distribution types, it has little difference near the ultimate strength and strain. The higher the maximum applied force (No. 7 strands indicated in **Table 3-3**), the lower ultimate strength and strain. Considered distribution types are uniform distribution, normal distribution, and polarized distribution. However, as summarized in **Table 3-3**, the difference turns out to be insignificant. Therefore, in the numerical analysis, the effect of the distribution type can be neglected. The effect of distribution type of the tensile forces on the equivalent tendon material model is shown in **Figure 3-5**.

Table 3-3 Example 2: the effect of distribution type of the tensile forces

Tendon	Tensile stresses in the individual strands (MPa)							Mean (MPa)	Standard deviation (MPa)
	No. 1	No. 2	No. 3	No. 4	No. 5	No. 6	No. 7		
Tendon 1	740	1,023	1,193	1,250	1,307	1,477	1,760	1,250	300
Tendon 2	800	950	1,100	1,250	1,400	1,550	1,700	1,250	300
Tendon 3	863	906	1,035	1,250	1,465	1,594	1,637	1,250	300

Tendon	Distribution type	Yield stress (MPa)	Ultimate strength (MPa)	Ultimate strain (mm/mm)
Tendon 1	Normal distribution	1,725	1,893	0.0158
Tendon 2	Uniform distribution	1,724	1,901	0.0166
Tendon 3	Polarized distribution	1,724	1,908	0.0172

Note: The yield stresses are defined as the stress at the 1% strain; The yield stress and ultimate strength of the single prestressing steel, f_{py} and f_{pu}, are 1,759 MPa and 1,930 MPa, respectively.

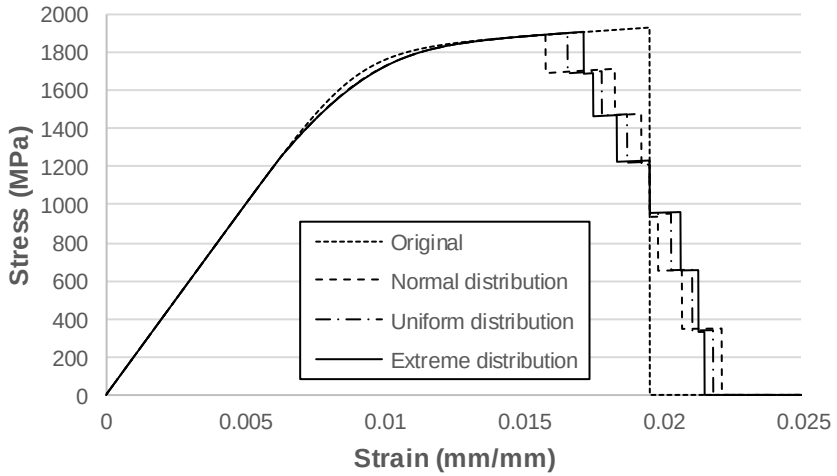

Figure 3-5 The effect of the distribution type of the tensile forces on the equivalent tendon material model

Excessive maximum tensile stress in the strand at jacking

As mentioned above, even though the tensile forces of the individual strands have the same average and standard deviation, the distribution type may affect the ultimate capacity of the tendon. This is because the maximum applied stress in the strands can be different. If the average value or standard deviation of the tensile forces applied to individual strands is large during tensioning operation, the maximum applied stress may be excessively large. If this is the case, the ultimate capacity of the tendon can be significantly reduced, particularly the ultimate strain and ductility.

For example, if a tendon with 7 strands is tensioned with the tensile forces as shown in **Table 3-4**, the effect of the maximum tensile stress in the strand on the stress-strain relationship of the tendon is significant as shown in **Figure 3-6**.

Table 3-4 Example 3: the effect of the maximum tensile stress in the strand

Tendon	Tensile stresses in the individual strands (MPa)							Mean (MPa)	Standard deviation (MPa)
	No. 1	No. 2	No. 3	No. 4	No. 5	No. 6	No. 7		
Tendon 1	1,075	1,311	1,453	1,500	1,547	1,689	1,925	1,500	250
Tendon 2	1,125	1,250	1,375	1,500	1,625	1,750	1,875	1,500	250
Tendon 3	1,177	1,213	1,321	1,500	1,679	1,787	1,823	1,500	250

Tendon	Distribution type	Stress at 1% strain (MPa)	Ultimate strength (MPa)	Ultimate strain (mm/mm)
Tendon 1	Normal distribution	1,528	1,699	0.0181
Tendon 2	Uniform distribution	1,740	1,856	0.0129
Tendon 3	Polarized distribution	1,737	1,895	0.0157

Note: The yield stress and ultimate strength of the single prestressing steel, f_{py} and f_{pu}, are 1,759 MPa and 1,930 MPa, respectively.

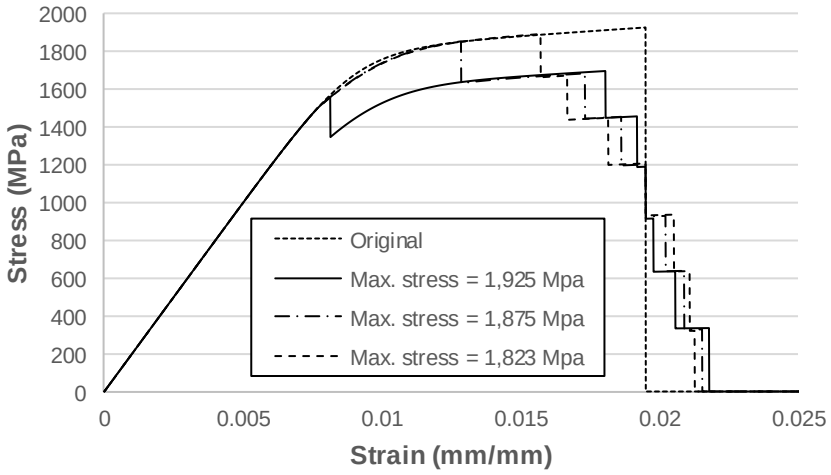

Figure 3-6 The effect of the maximum tensile stress in the strand on the equivalent tendon material model

3.2 Effects of tensile force deviations of individual strands on the relaxation of tendon

3.2.1 Additional relaxation loss due to the tensile force deviations

The tensile force deviations of the individual strands can affect the long-term behavior of post-tensioned structures due to the relaxation of prestressing steel. When the standard deviation of tensile forces is large, some strands are subjected to low stress or excessive stress. The relaxation is a phenomenon in which the stress decreases over time even at a constant strain due to the viscoelastoplastic behavior of the stressed solid. In the case of prestressing steel, the prestress loss due to relaxation depends on the time and the level of prestressing stress. As time goes, the greater the magnitude of applied stress, the greater the loss due to relaxation. At any time, t, and under normal temperature conditions, the stress in the steel tensioned initially to f_{pi} can be estimated by **Eq. (3-3)** (Namman, 2004). **Figure 3-7** shows the prestress loss due to relaxation of prestressing steel.

$$f_p(t) = f_{pi}\left[1 - \frac{\log_{10}(t)}{K}\left(\frac{f_{pi}}{f_{py}} - 0.55\right)\right] \tag{3-3}$$

Where,

$f_p(t)$: stress in the prestressing steel at time t
f_{pi} : initial stress applied in the prestressing steel (at $t = 0$)
f_{py} : yield stress of the prestressing steel
t : time, hours (not less than one hour)
K : constant, which depends on the type of the prestressing steel

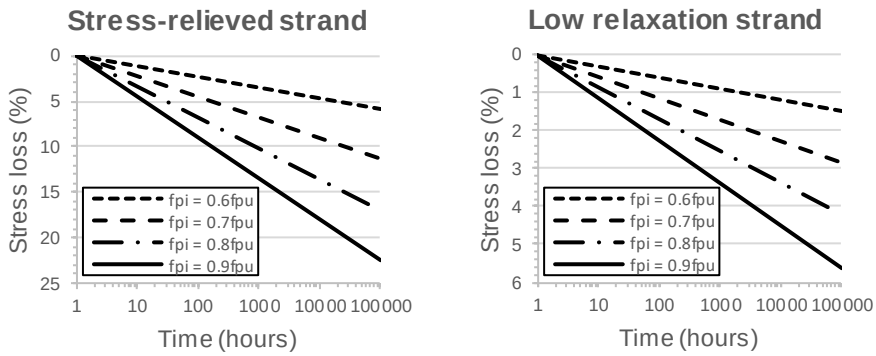

Figure 3-7 Typical effects of initial stress on relaxation loss

The value of the coefficient K is determined by material properties of prestressing steel. For typical stress-relieved strands, the value of K is generally taken equal to 10. For low relaxation strands, the value of K is taken equal to 40 ~ 45 (AASHTO, 2012; PCI, 2010). In ASTM A416 (2016), low relaxation strands require less than 2.5% relaxation at 1000 hours when the initial stress (f_{pi}) is $0.7f_{pu}$. At 1000 hours, the K value for 2.5% relaxation loss is equal to 18.

The relaxation loss is dependent on the initial stress of prestressing steel, and their relationship is not linear. Thus, there is a difference in the average relaxation loss, depending on the level of tensile force deviations, even though tendons have the same average initial tensile stresses. As the standard deviation of the initial stresses in the individual strands becomes larger, the strand subjected to the maximum tensile force has a larger relaxation loss due to the excessive stress. From the quadratic relationship (**Eq. 3-3**) between the initial stress and relaxation loss, the average relaxation loss of the tendon would increase. In other words, there is additional relaxation loss due to the deviation of the initial tensile forces in individual strands. If there is a large additional relaxation loss caused by the deviation, this additional loss must be considered as it appears to affect the long-term performance of a structure.

For example, if a tendon with 7 strands has the initial tensile stresses as shown in **Table 3-5**, the effect of the standard deviation of the initial tensile forces on the average relaxation loss of the tendon is shown in **Figure 3-8**. The effect varies greatly depending on the *K* value. For low relaxation prestressing steel, additional relaxation loss is very small, which can be neglected. However, additional relaxation loss needs to be taken into account in stress-relieved strands.

Table 3-5 The effect of the standard deviation of the initial tensile forces in the individual strands on the average relaxation loss of the tendon

K value	Average initial tensile stress of the tendon	Standard deviation of the initial tensile forces	Relaxation loss at 1000 hours† (%)	Additional loss due to the deviation† (%)
10 (Stress-relived strand)	$0.6f_{pu}$	0	3.50	0
		$0.05f_{pu}$	3.64	0.14
		$0.10f_{pu}$	4.22	0.72
		$0.15f_{pu}$	5.27	1.77
		$0.20f_{pu}$	6.49	2.99
		$0.25f_{pu}$	7.93	4.43
	$0.7f_{pu}$	0	6.83	0
		$0.05f_{pu}$	6.95	0.12
		$0.10f_{pu}$	7.31	0.48
		$0.15f_{pu}$	7.97	1.14
	$0.8f_{pu}$	0	10.17	0
		$0.05f_{pu}$	10.27	0.10
		$0.10f_{pu}$	10.58	0.42
40 (Low relaxation strand)	$0.6f_{pu}$	0	0.87	0
		$0.05f_{pu}$	0.91	0.03
		$0.10f_{pu}$	1.05	0.18
		$0.15f_{pu}$	1.32	0.44
		$0.20f_{pu}$	1.62	0.75
		$0.25f_{pu}$	1.98	1.11
	$0.7f_{pu}$	0	1.71	0
		$0.05f_{pu}$	1.74	0.03
		$0.10f_{pu}$	1.83	0.12
		$0.15f_{pu}$	1.99	0.28
	$0.8f_{pu}$	0	2.54	0
		$0.05f_{pu}$	2.57	0.03
		$0.10f_{pu}$	2.65	0.10

Note: The initial tensile stresses applied in the 7 strands are assumed following uniform distribution.; f_{pu} is tensile strength of the prestressing steel.

† The percentages are calculated with respect to the average initial tensile stress, f_{pi}.

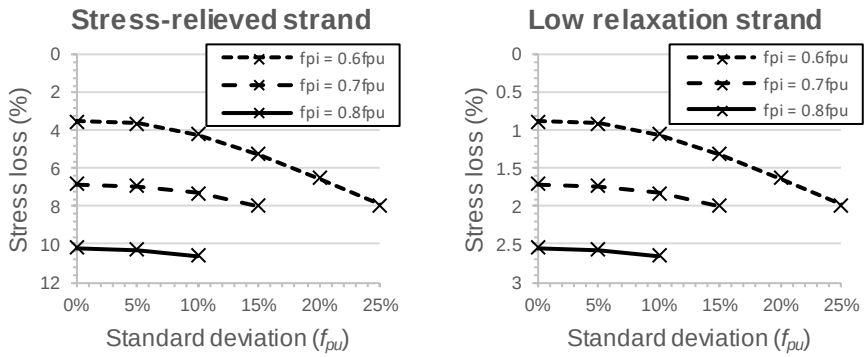

Figure 3-8 The effect of the standard deviation of the initial tensile forces in the individual strands on the average relaxation loss of the tendon

3.3 Discussion

In this chapter, an equivalent tendon material model is proposed to analyze the effect of individual strand force deviation on the tendon stress-strain relationship and to simplify the numerical modeling of a tendon with tensile force deviation. The concept of the proposed equivalent tendon material model is to average the stress-strain curves considering remaining capacity prior to the tensile strength (f_{pu}) of individual strands. This concept is valid for monotonic loadings discussed in **Chapter 4**. However, it will be necessary to propose an improved equivalent tendon material model that enables to implement the hysteresis behavior under cyclic loading. This is not in the scope of this thesis.

From the analysis using the proposed equivalent tendon material model, it is found that the equivalent yield strength of a tendon tends to decrease slightly and the tensile strength and strain (f_{pu} and ε_{pu}) tend to decrease significantly as the standard deviation of individual tensile stresses increases. This is because the remaining strength of individual strands is different from each other, and therefore the yielding and fracture of individual strands occur differently. Also, even though the standard deviations are the same, the equivalent tendon

stress-strain relationship can be different, if the distribution type of individual tensile stresses or the maximum tensile stress of individual strand are different.

In addition, it is theoretically confirmed that an additional relaxation loss in the tendon can occur and affect the long-term structural behavior in the presence of tensile force deviation. In this chapter, it is derived using the theoretical relaxation loss equation, but it is necessary to verify experimentally to observe this phenomenon in the actual tendon. As further studies, in addition to the relaxation loss, the influence from the other types of long-term prestress loss needs to be investigated. Finally, time-dependent constitutive laws need to be induced to apply such long-term losses in numerical analysis.

Chapter 4. Influence of Tensile Force Deviations of Individual Strands on Structural Behavior

Although ASME code (2015) states the purpose that reduces the tensile force deviation in individual strands in the requirement of the tendon installation method, there are no acceptance criteria or related information. As discussed in **Chapter 2**, the tensile force deviation in a tendon itself has been studied by some researchers. However, the influence of tensile force deviations of individual strands on structural behavior has not been studied thoroughly.

To provide basic research data on the effect of tensile force deviations on structural behavior, previous research can be used as a basis for the preliminary acceptance criteria for tensile force deviation in a multi-strand tendon. In this study, a numerical study was conducted for better understanding. In **Section 4.1**, a numerical analysis technique for unbonded post-tensioned members is discussed. In **Sections 4.2** and **4.3**, a numerical study on the ultimate behavior of PT beams and partial models of nuclear containment is conducted. The effect of the variation of tensile forces in a multi-strand tendon on the structural behavior is analyzed. Finally, all of these contents are concluded in **Section 4.4**.

4.1 Numerical modeling method for unbonded post-tensioned concrete members

4.1.1 Previous experimental research on post-tensioned beams

To verify the numerical modeling method which is discussed in the next sections, one of the previous experimental research on post-tensioned beams was reviewed and used in this thesis. Mattock et al. (1971) conducted flexural strength tests of three post-tensioned rectangular beams which were simply supported with a span of 8.53 m. The three tested specimens were named RB1, RB2, and RU2, respectively. The RB1 specimen was a post-tensioned beam using bonded tendons with cement grout in the post-tensioning duct. While the RU1 and RU2 specimens were post-tensioned beams using unbonded tendons with greased sheathed-strands. The only difference between the RU1 and RU2 specimens is the arrangement of bottom reinforcement.

All of the beam specimens were prestressed using two 12.7 mm diameter, Grade 270 seven-wire strands. The tendons were installed parabolically with an effective depth of 254 mm at mid-span and a sag of 160 mm. All of the beam specimens had longitudinal reinforcements in the upper and lower parts of the beam, and the stirrups were placed. **Figure 4-1** shows the geometry of each specimen and the information about the reinforcement arrangement. Also, the geometrical properties of the specimens are summarized in **Table 4-1** (Note: In **Figure 4-1** and **Table 4-1**, #2 = 6.35 mm diameter, #3 = 9.5 mm diameter, and #4 = 12.7 mm diameter).

The mechanical properties of the materials used in the specimen are shown in **Tables 4-2** and **4-3**. Especially for prestressing steel, the measured ultimate strength of the strands was 1,930 MPa, and the stress at 1% elongation, which is defined as the yield strength, was 1,785 MPa. Each beam was subjected to four point external loads which were set as equal forces applied at 0.46 and 1.68 m away from the mid-span on both sides, respectively. The loads were applied monotonically until the failure of the specimen.

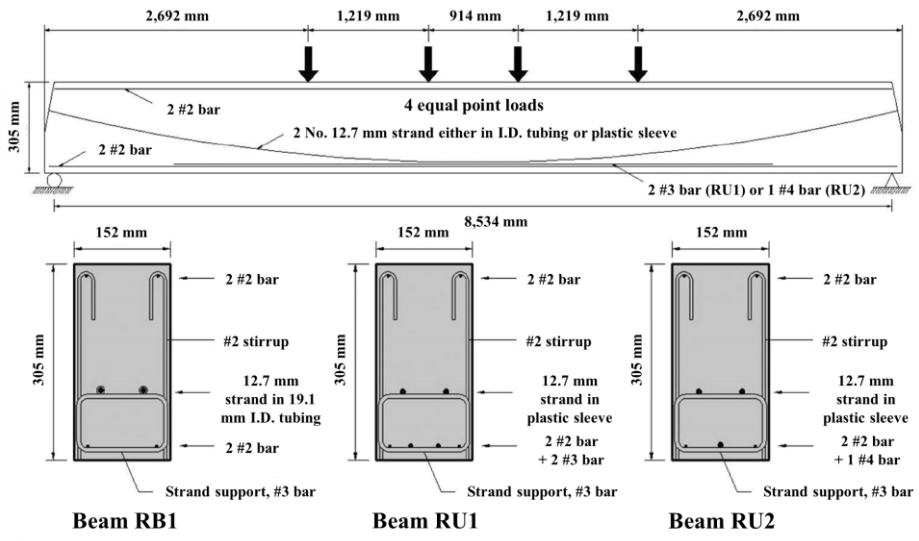

Figure 4-1 Post-tensioned beams tested by Mattock et al. (1971) (adapted from Kang et al., 2015)

Table 4-1 The geometrical properties used in the experiment (Mattock et al., 1971) and numerical modeling

Specimen	Sectional properties			Reinforcement				
	b, mm	h, mm	l_c, mm	A_p, mm^2	A_s', mm^2	A_s, mm^2	d_p, mm	s_p, mm
RB1	152	305	8,534	197.4	63.3	63.3	254	160
RU1	152	305	8,534	197.4	63.3	205.1	254	160
RU2	152	305	8,534	197.4	63.3	190.0	254	160

Note: b is beam width; h is beam depth; l_c is beam length; A_p is tendon area; A_s' is compression reinforcing bar area; A_s is tension reinforcing bar area; d_p is effective depth for the tendon; and s_p is sag of tendons.

Table 4-2 The material properties used in the experiment (Mattock et al., 1971) and numerical modeling: prestressing steel

Specimen	Concrete			Reinforcement			
	f_c', MPa	f_t, MPa	E_c, MPa	$f_{y,\#2}$, MPa	$f_{y,\#3}$, MPa	$f_{y,\#4}$, MPa	E_s, MPa
RB1	31.4	3.49	26,510	377	-	-	199,950
RU1	34.2	3.64	27,680	377	345	-	199,950
RU2	29.3	3.37	25,620	377	-	322	199,950

Note: f_c' is concrete compressive strength; f_t is concrete tensile strength; E_c is elastic modulus of concrete; $f_{y,\#2}$ is yield strength of No. 2 reinforcing bars; $f_{y,\#3}$ is yield strength of No. 3 reinforcing bars; $f_{y,\#4}$ is yield strength of No. 4 reinforcing bars; and E_s is elastic modulus of reinforcement.

Table 4-3 The material properties used in the experiment (Mattock et al., 1971) and numerical modeling: prestressing steel

Specimen	Prestressing steel				
	f_{py}, MPa	f_{pu}, MPa	f_{se}, MPa	E_p, MPa	Stress-strain relationship
RB1	1,760	1,930	1,296	195,470	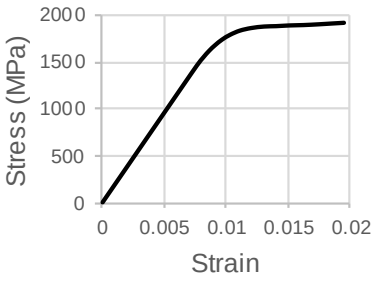
RU1	1,760	1,930	1,262	195,470	
RU2	1,760	1,930	1,282	195,470	

Note: f_{py} is yield strength of prestressing steel, which is defined as the stress at 1% elongation; f_{pu} is ultimate tensile strength of prestressing steel; f_{se} is effective stresses applied to the tendon of each specimen; and E_p is elastic modulus of prestressing steel.

From the experiment, load-deflection curves and tensile stress increment curves were obtained. The results are shown in **Figure 4-2**. From the load-deflection curves, it is noticed that the RB1 specimen with bonded tendons had the largest ultimate flexural strength, even though all of the specimens had similar sections and tendon arrangement. Two unbonded post-tensioned

beam specimens had similar values of ultimate strength. The difference between the bonded and unbonded post-tensioned specimens was due to the different tensile stress in the prestressing steel under ultimate loads. In general, the tensile stress at ultimate strength (f_{ps}) is larger in bonded tendons. The f_{ps} and ultimate capacity have a positive correlation.

The tensile stress increment curves are obtained from the measurement of the tensile forces in the prestressing steel. However, the tensile force increment curve could not be obtained from the bonded tendon (RB1 specimen), because the bonded tendons had tensile stress distribution that varies along its length. The maximum value of tensile stress appeared to occur near mid-span, and direct measurement was not made. On the other hand, unbonded tendons were directly measured at ends using load cells, because the stress distribution did not change much along its length and the maximum tensile stress appeared at the end of the beams.

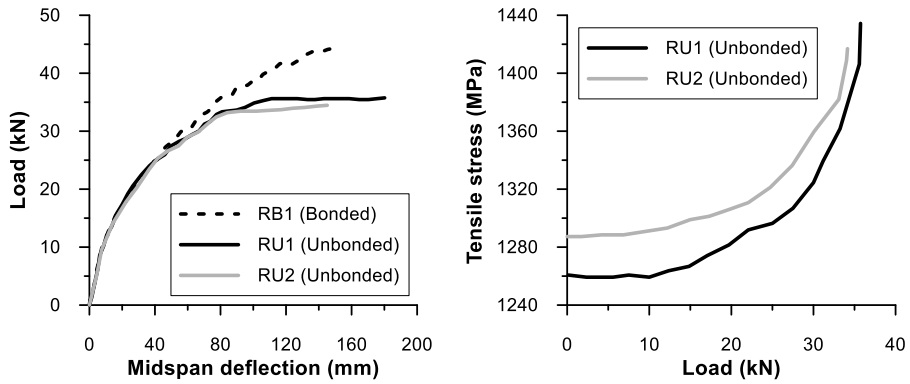

(a) Load-midspan deflection curves (b) Tensile stress increment curves

Figure 4-2 The results of the previous experimental research (Mattock et al., 1971)

4.1.2 Modeling concept

For numerical analysis of the post-tensioned beams, finite element analysis software DIANA FEA is used. The geometrical shapes of the numerical

models for the post-tensioned beams are the same as the specimens tested by Mattock et al. (1971), except shear reinforcements.

In the finite element analysis, 3D quadratic solid elements are used for the beam, load plates, support plates, and anchorages; 1D truss elements are used for prestressing steels; and embedded reinforcement elements are used for non-prestressing reinforcements. Structural interface elements are used to define the contact interface between the plate (loading plate and support plate) and concrete beam. Default mesh size was set as 50.8 mm (2 in.) for the concrete beam, and 25.4 mm (1 in.) for anchorages, which have stress concentration region. For bonded tendons (RB1 specimen), built-in "CEB-FIP (1990) post-tensioning schema" is used to define post-tensioning forces in the tendons. For unbonded tendons (RU1 and RU2 specimens), alternative approaches are taken using "Bond-slip reinforcement" in DIANA FEA (2016). The alternative approaches are discussed in the next section. For numerical iteration method, Quasi-Newton (Secant) method is used.

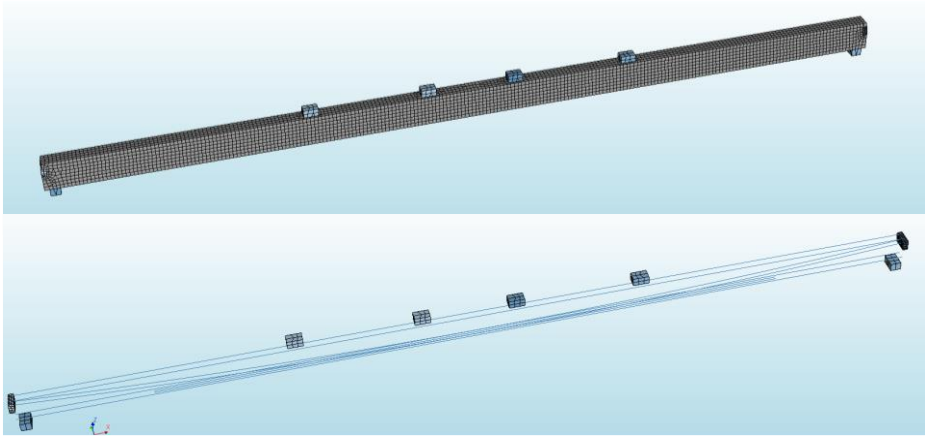

Figure 4-3 Numerical modeling with DIANA FEA, beam (up) and reinforcements (down)

To define mechanical properties of the materials, built-in material models in DIANA FEA (2016) were used. For concrete, the total strain based crack

model is used. Stress-strain relationship for compressive behavior is defined with the parabolic model, and tensile behavior is defined with linear-ultimate crack strain model. The curves for the concrete material models are shown in **Figure 4-4**. For the compressive and tensile curves, the residual stress is set as 20% of the strength.

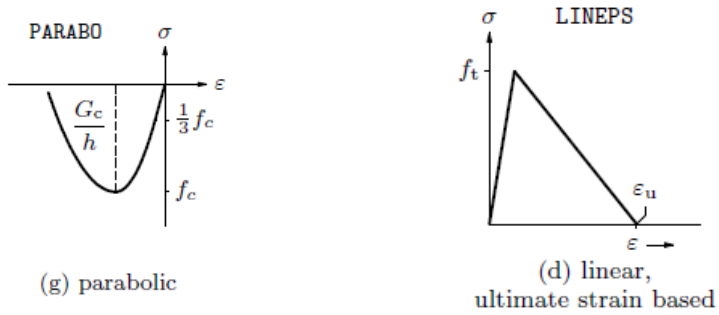

Figure 4-4 Compressive behavior (left) and tensile behavior (right) for the concrete (DIANA FEA, 2016)

For non-prestressed reinforcement, elasto-perfectly plastic stress-strain relationship is applied, which is called "ideal" in DIANA FEA (2016). In this model, the strain hardening effect of steel is not considered. For steel plates and anchorages, elastic stress-strain relationship is applied. The curves for the applied steel material models are shown in **Figure 4-5**.

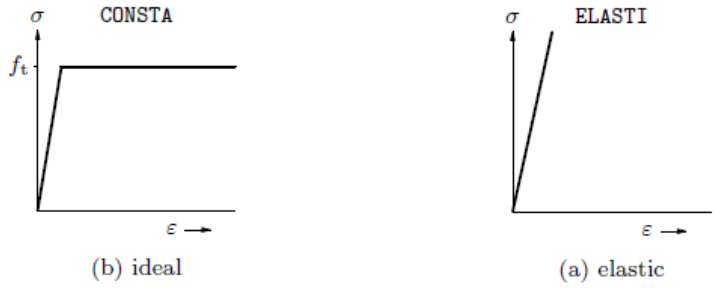

Figure 4-5 Stress-strain relationships for the reinforcement (left) and steel plates and anchorages (right) (DIANA FEA, 2016)

For the prestressing steel, user-defined multi-linear stress-strain relationship is used. The multi-linear relationship is set based on the stress-strain relationship of prestressing steel proposed by Mattock (1979) (**Eq. 3-2**) and experiment data of the prestressing steel (Mattock et al., 1971) (**Table 4-3**). The material model of the prestressing steel used in the numerical analysis is shown in **Figure 4-6**.

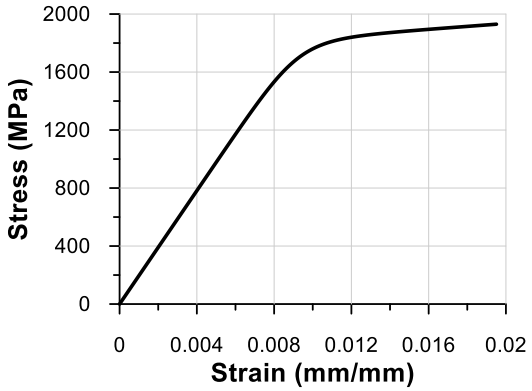

Figure 4-6 Stress-strain relationship for prestressing steel

4.1.3 Tendon modeling using bond-slip reinforcement

The slip behavior and prestressing loss due to friction between the strand and sheath (or duct) should be considered in numerical modeling of the unbonded tendons. In addition, in the bonded tendons before grouting, the friction between the strands and duct should be understood. However, most commercial software does not have such features that automatically defines post-tensioning forces and takes into account the prestress loss of tendons in unbonded states. For that, Kang et al. (2015) studied the finite element modeling method of unbonded post-tensioned members, but still difficult to directly apply to commercial FEA software used in practice. Therefore, modeling of unbonded tendons and their post-tensioning forces is attempted by using an alternative method, i.e., the use of so-called bond-slip reinforcement (DIANA FEA, 2016).

In DIANA FEA (2016), the bond-slip reinforcement is defined using 1D-truss elements with structural interface and used to describe the interaction between the reinforcement and surrounding material (concrete). The slip behavior can be described with normal and shear traction on the boundary between the reinforcement and surrounding material (**Figure 4-7**). In the bond-slip reinforcement, the relationship between the normal traction and normal relative displacement is assumed to be a linear function, whereas the relationship between the shear traction and the slip of reinforcement is assumed to be a linear or nonlinear function (**Eq. 4-1**).

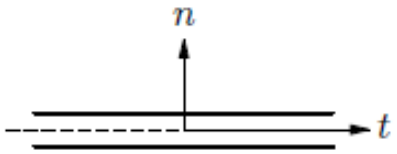

Figure 4-7 Bond-slip reinforcement

$$\mathbf{t} = \begin{Bmatrix} t_n \\ t_t \end{Bmatrix} \qquad \begin{cases} t_n = k_n \Delta u_n & \text{normal traction} \\ \begin{cases} t_t = k_t dt & \text{shear traction (linear)} \\ t_t = f(dt) & \text{shear traction (nonlinear)} \end{cases} \end{cases} \tag{4-1}$$

Where,

t_n : normal traction, kN/m^2
t_t : shear traction, kN/m^2
k_n : normal stiffness modulus, kN/m^3
k_t : shear stiffness modulus, kN/m^3
Δu_n : normal relative displacement, m
dt : shear slip, m

If the shear traction-slip relationship is defined as a linear function, normal stiffness modulus and shear stiffness modulus are the two parameters needed to define the friction behavior of prestressing steel. However, if the shear traction-slip relationship is defined as a nonlinear function, nonlinear function to define the relationship is needed.

Prestress loss due to friction is expressed by **Eq. (4-2)** (PTI, 2006). The curvature friction loss is caused by the curvature of the tendon, and the wobble friction loss is caused by the local irregularity and curvature of the tendon.

$$P_x = P_0 e^{-(\mu\alpha + kx)} \tag{4-2}$$

Where,

P_x : tensile force in the prestressing steel at the location of x, kN
P_0 : tensile force in the prestressing steel at the jacking end, kN
μ : curvature friction coefficient, /rad
k : wobble friction coefficient, /m
α : change in angle between the forces at the anchorage and x, rad
x : curvilinear length of tendon from anchorage to section x, m

Physically, the curvature friction is related to the normal traction of the bond-slip reinforcement. This is because the curvature friction is proportional to the normal force between the prestressing steel and surrounding material, which is induced by tendon curvature. Thus, the level of the curvature friction force can be set by adjusting the normal stiffness modulus value. Although the deterministic relationship between the curvature friction coefficient and the normal stiffness modulus has not been defined yet, it has been empirically found that there is a proportional relationship between the curvature friction coefficient and the normal stiffness modulus as in the following **Eq. (4-3).**

$$k_n = C_n \pi d \mu \tag{4-3}$$

Where,

k_n : normal stiffness modulus, kN/m^3
C_n : proportional coefficient (empirically obtained, recommended value is 7.85×10^8 kN/m^4), kN/m^4
μ : curvature friction coefficient, /rad
d : diameter of the prestressing steel, m

On the other hand, wobble friction can be defined by applying a constant value of shear traction to the unit length of prestressing steel, because the friction force per unit length is applied as a constant value with respect to the longitudinal direction, regardless of the amount of slip. Therefore, constant shear traction can be applied by defining a nonlinear shear traction-slip relationship as a constant function. Using the bond-slip model suggested by Dörr (1980), which is built-in in DIANA FEA (2016) (**Figure 4-8** and **Eq. 4-4**), a constant shear traction can be applied if any slip occurs. Here, dt^0 is the shear slip at start plateau and f_t is the bond-slip parameter. The value of $1.9f_t$ is applied as shear traction when the slip exceeds the value of dt^0. Therefore, the dt^0 should be defined as a very small value (near zero), and f_t may be defined as a value to induce an intended wobble friction loss.

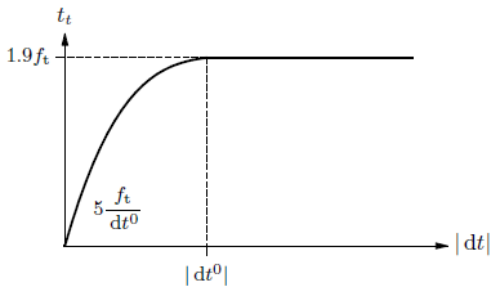

Figure 4-8 Bond-slip model suggested by Dörr (1980) (DIANA FEA, 2016)

$$t_t = \begin{cases} f_t\left(5\left(\frac{dt}{dt^0}\right) - 4.5\left(\frac{dt}{dt^0}\right)^2 + \left(\frac{dt}{dt^0}\right)^3\right) & \text{if } 0 \le dt < dt^0 \\ 1.9\,f_t & \text{if } dt \ge dt^0 \end{cases} \quad (4\text{-}4)$$

Where,

t_t : shear traction, kN/m^2
dt : shear slip, m
f_t : bond-slip parameter, kN/m^2
dt^0 : shear slip at start plateau, m

Theoretically, integration of shear traction on the prestressing steel in the longitudinal direction should be exactly the same as the loss due to wobble friction calculated by **Eq. (4-2)** (See **Eq. 4-5a**). From that, the value of the bond-slip parameter (f_t) can be obtained from **Eq. (4-5b)**.

$$P_o - P_i = 1.9 f_t \pi d l \tag{4-5a}$$

$$f_t = \frac{P_0 - P_l}{1.9\pi d l} = \frac{P_0\left(1 - e^{-kl}\right)}{1.9\pi d l} \tag{4-5b}$$

Where,

f_t : bond-slip parameter, kN/m^2
P_l : tensile force in the prestressing steel at the location of l, kN
P_0 : tensile force in the prestressing steel at the jacking end, kN
k : wobble friction coefficient, /m
l : curvilinear length of tendon from anchorage to section l, m
d : diameter of the prestressing steel, m

By setting of the parameters of the bond-slip reinforcement (DIANA FEA, 2016), prestressing steel can be modeled as a sliding element with the appropriate level of friction. The values of the bond-slip interface parameters are set as shown in **Table 4-4**, so that the initial tensile force distribution applied to the numerical model is close to the initial tensile force distribution following the measured effective stress (f_{se}) and **Eq. (4-2)**. The initial tensile force distributions in the numerical models of the RU1 and RU2 specimens are shown in **Figure 4-9**. For unbonded tendons, the curvature friction coefficient is 0.05/rad and the wobble friction coefficient is 0.00164/m. Using the bond-slip reinforcements, the distribution of the tensile force could be set similar to the theoretical distribution calculated by **Eq. (4-2)**.

Table 4-4 The bond-slip interface parameters in the numerical models

Specimen	k_n, kN/m^3	k_t, kN/m^3	Bond-slip parameters (Dörr, 1980)	
			f_t, kN/m^2	dt^0, m
RU1 (unbonded)	1.57×10^6	-	27.02	1×10^{-7}
RU2 (unbonded)	1.57×10^6	-	27.45	1×10^{-7}

Note: k_n is the normal stiffness modulus; k_t is the shear stiffness modulus; f_t is the bond-slip parameter and dt^0 is the shear slip at start plateau in the bond slip model (Dörr, 1980); the values of the f_t are calculated based on the f_{se} in **Table 4-3**.

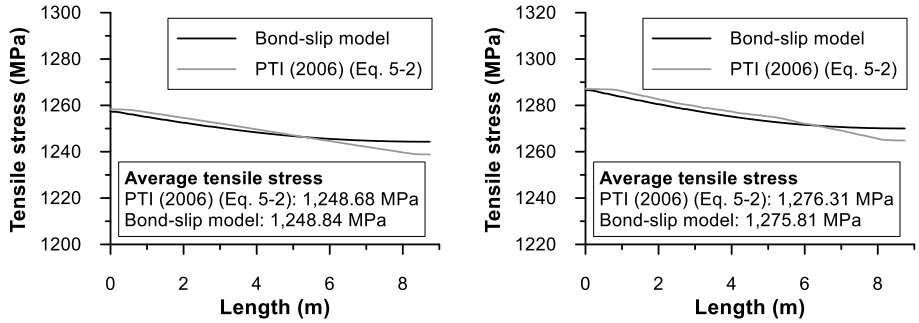

(a) RU1 specimen (b) RU2 specimen

Figure 4-9 Tensile force distributions of the tendons in longitudinal direction

4.1.4 Numerical analysis results of the PT beams

For all numerical models (RB1, RU1, and RU2), nonlinear finite element analysis is conducted and corresponding results are obtained. The results are compared with the measured data from the experiment (Mattock et al., 1971).

First, the load-deflection curves and ultimate flexural capacities are compared. For all of the analysis models, the load-deflection curves have good agreements with the experimental data. The deflection was measured at midspan of the beam. The load-deflection curves are shown in **Figure 4-10**. The ultimate loads, bending moments, and discrepancies are summarized in

Table 4-5. For all of the numerical models, the ultimate loads and bending moments are slightly overestimated, but the discrepancies are less than 5%.

Table 4-5 Comparison of the ultimate capacities: experiment and numerical analysis

Specimen	Ultimate load			Ultimate bending moment		
	$P_{u,exp}$, kN	$P_{u,FEA}$, kN	Error, %	$M_{u,exp}$, kN-m	$M_{u,FEA}$, kN-m	Error, %
RB1	44.3	46.5	4.9	93.4	94.8	1.5
RU1	35.7	37.6	5.3	79.9	80.5	0.8
RU2	34.5	37.2	7.8	77.8	81.1	4.2

Note: $P_{u,exp}$ is the ultimate load measured in the experiment (Mattock et al., 1971).; $P_{u,FEA}$ is the ultimate load obtained from the numerical analysis.; $M_{u,exp}$ is the ultimate bending moment measured in the experiment (Mattock et al., 1971).; $M_{u,FEA}$ is the ultimate bending moment obtained from the numerical analysis.; and P_u is the ultimate load which is the sum of the 4 equal point loads.

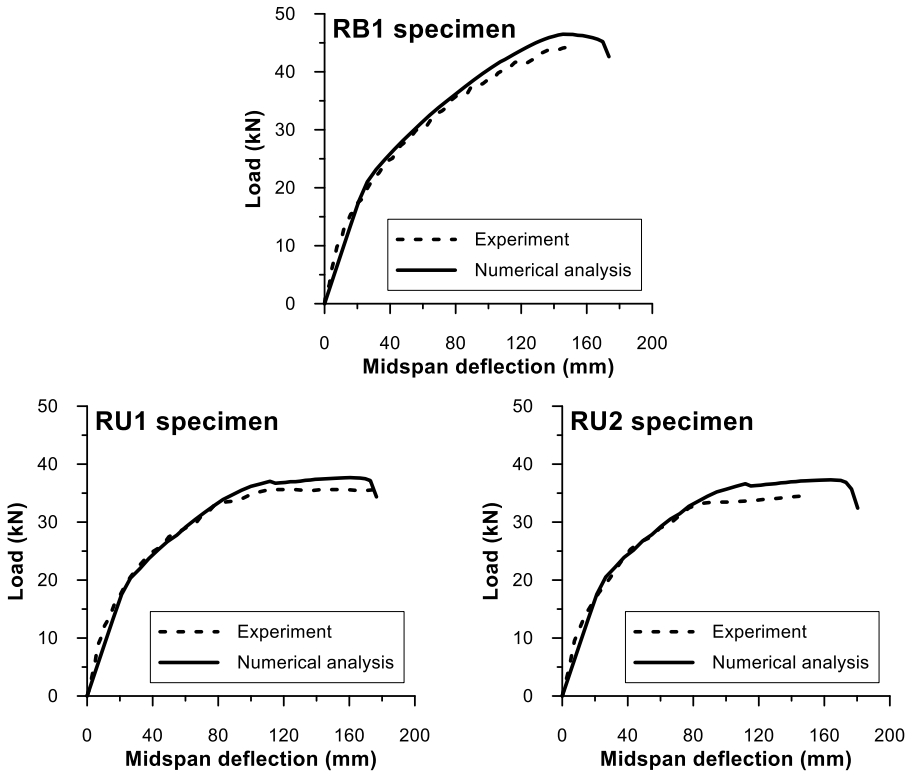

Figure 4-10 Comparison of the load-deflection curves: experiment and numerical analysis

The change of the tensile stress in the prestressing steel can be obtained from the numerical analysis, and the comparable experimental data are available in the paper by Mattock et al. (1971), except the RB1 specimen. In all numerical models (RB1, RU1, and RU2), tensile stress tends to increase rapidly, as the plastic deformation is caused by applying loads to the beam. The tendency of the tensile stress increment is similar to the load-deflection curves. The tensile stress increment is proportional to the deflection. Compared with the experiment data (Mattock et al., 1971), the tensile stress increments are somewhat overestimated in the numerical analysis (**Figure 4-11** and **Table 4-6**). The cause of the discrepancy is speculated to be the use of lower stiffness of concrete in the numerical model. Due to the overestimated tensile stress increment, the ultimate capacity is also overestimated. The discrepancy is larger in the RU2 model, likely due to the overestimated maximum deflection.

Table 4-6 Comparison of the tensile stress at ultimate strength

Specimen	$f_{se,exp}$**, MPa**	$f_{ps,ACI}$**, MPa**	$f_{ps,exp}$**, MPa**	$f_{ps,FEA}$**, MPa**
RB1 (Bonded)	1,298	1,703	N.A.	1,737
RU1 (Unbonded)	1,262	1,385	1,435	1,541
RU2 (Unbonded)	1,287	1,409	1,415	1,569

Note: $f_{se,exp}$ is experimentally measured effective tendon stress; $f_{ps,ACI}$ is tendon stress at nominal flexural strength determined by ACI 318-14 (2014); $f_{ps,exp}$ is tendon stress at nominal flexural strength which was experimentally measured; and $f_{ps,FEA}$ is tendon stress at nominal flexural strength which is analytically monitored.

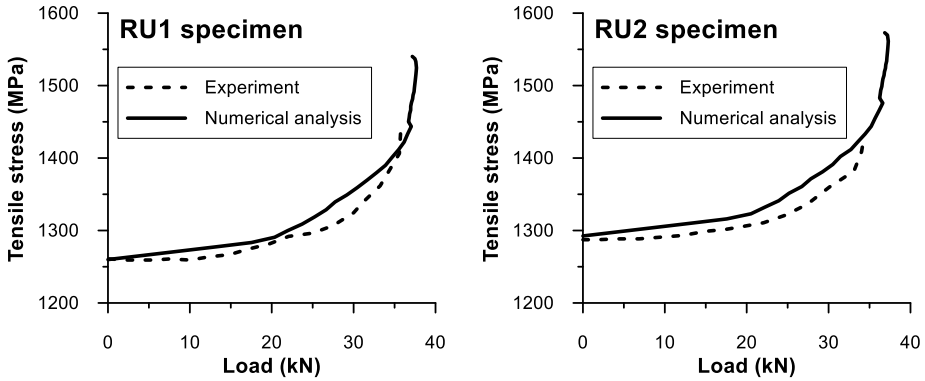

Figure 4-11 Comparison of the tensile stress increment of the tendons: experiment and numerical analysis

Tensile stress distributions at the initial and ultimate states are obtained (**Figure 4-12**). It is found that the tensile stress of bonded tendons (RB1) significantly increases near the locations under the loading points. At the ultimate strength, the distribution of the tensile stress varies in the longitudinal direction. The variation occurs because the strain compatibility is valid in the bonded tendons. On the other hand, even at the ultimate strength, the unbonded tendons have parallel shifted tensile stress distribution of the initial state. The strain increase of the tendon by the overall deformation of the beam is generally uniform over the entire length of the tendon as a result of the unbonded condition.

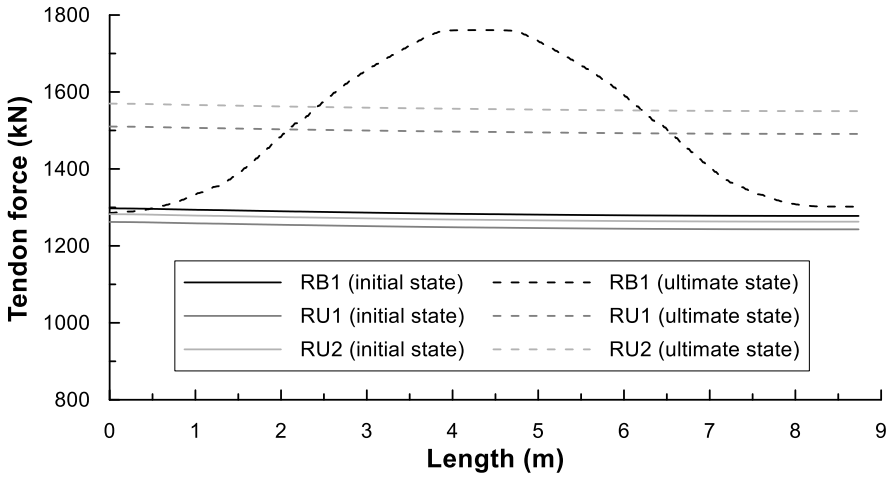

Figure 4-12 Tensile stress distributions of the tendons at the initial and ultimate states

Based on the numerical analysis results, the analysis is quite accurate and corresponds reasonably to the actual data. It means that the alternative modeling technique using the bond-slip reinforcement adequately describes the interaction between prestressing steel and concrete, and the analysis procedure developed in this study is reliable. Therefore, the indirect method of using the bond-slip reinforcement can be a viable alternative to describe the structural behavior of unbonded post-tensioned members with friction. Using this method, an analytical study of multi-strand tendons is carried out, which is discussed in the following sections.

4.2 Effects of tensile force deviations of the individual strands on the structural behavior of PT beams

4.2.1 Analysis concept

The tensile force deviation existing in individual strands affects the stress-strain relationship of the whole tendon. In this section, the effect of the changed material properties of the tendon on the structural behavior of post-tensioned beams is investigated. The analyzed post-tensioned beams are single-span beams, as discussed in **Section 4.1**, which were tested by Mattock et al. (1971). The behavior is analyzed for both bonded and unbonded PT beams (RB1 and RU1, respectively). The basic geometrical shape and material properties used for the analysis are the same as those of the tested RB1 and RU1 specimens, respectively (**Tables 4-1**, **4-2**, and **4-3**).

In order to analyze the effect on the structural behavior due to the tensile force deviations in individual strands, different tensile forces are applied to the individual strands. In the case of a multi-strand tendon, it is necessary to model all individual strands and input different tensile forces in the strands. Since the tensile force deviation is the main variable in the analysis, the average tensile force of the tendon should be controlled to be constant.

Alternatively, the tendon may be modeled as an equivalent large strand having the same cross-sectional area, with the application of the equivalent tendon material model proposed in **Section 3.1**. Using this method, the tensile force should be input only at once, and tensile force deviation can then be considered by setting the tendon material model. However, since it is necessary to verify whether the equivalent tendon material model can adequately simulate tensile force deviation, the equivalent tendon material model is applied in the analysis only for the verification purpose. The basic modeling approach is applied to all the strands for the rest of the study as described above.

Since two tendons consisting of only one strand for each were installed in the RB1 and RU1 specimens, it is not possible to make a deviation of tensile forces. Therefore, in the numerical model, the method dividing into seven equivalent strands is applied. The seven equivalent strands with 1/7 of the cross-sectional area of the original strands are modeled as shown in **Figures 4-13** and **4-14**. If the strand of the original specimen is subjected to a tensile force of P_i, then in this analytical model, tensile forces of '$1/7P_i \pm$ deviation' are input to seven equivalent strands, resulting in the same tendon force of P_i.

Using **Eqs. (4-3)** and **(4-5)** in **Section 4.1**, normal stiffness modulus and bond-slip parameters were input such that the equivalent strands would have the same curvature and wobble friction coefficients as the original analysis model (**Table 4-7**). The resulting friction losses in the numerical model are the same as those from the original RB1 and RU1 numerical models in **Section 4.1**. In other words, all properties are the same except that one strand is divided into seven equivalent strands.

Table 4-7 The bond-slip interface parameters applied in the seven equivalent strands

Specimen		k_n, kN/m^3	k_t, kN/m^3	**Bond-slip parameters (Dörr, 1980)**	
				f_t, kN/m^2	dt^0, m
RB1 (bonded)	At jacking (unbonded state)	2.24×10^5	-	27.02	1×10^{-7}
	After grouting (bonded state)	2.24×10^5	2.24×10^5	-	-
RU1 (unbonded)		2.24×10^5	-	27.45	1×10^{-7}

Note: k_n is the normal stiffness modulus; k_t is the shear stiffness modulus; f_t is the bond-slip parameter; and dt^0 is the shear slip at start plateau in the bond slip model (Dörr, 1980).

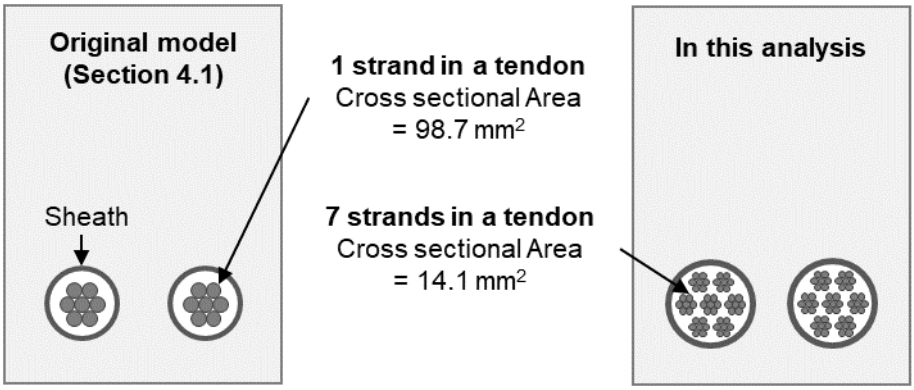

Figure 4-13 The modeling concept of seven equivalent strands

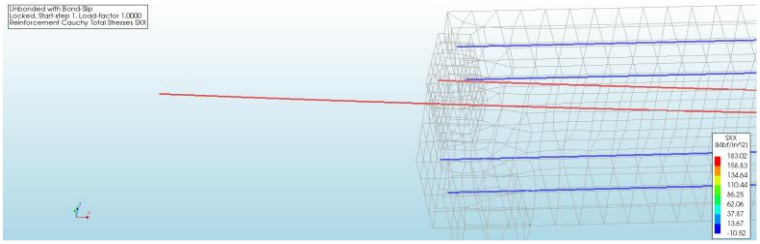

(a) Original model (**Section 4.1**)

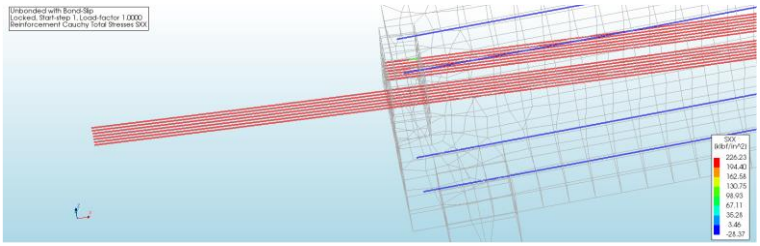

(b) In this analysis (no tensile force deviation)

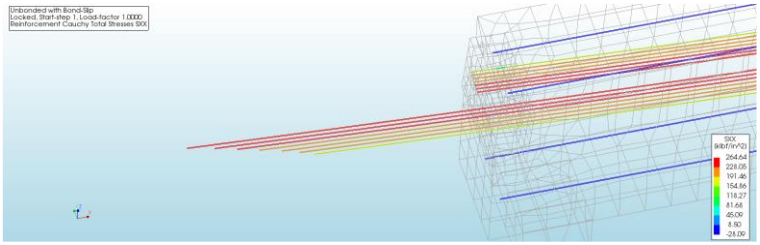

(c) In this analysis (deviation of tensile force and elongation exists)

Figure 4-14 Seven equivalent strands in the numerical model

4.2.2 Analysis parameters

To understand the effects of tensile force deviations on the structural behavior of PT beams, several effective variables are considered in analysis. Including effective variables of the equivalent tendon material model, the analysis parameters are selected as follows:

Bonded/unbonded tendon

There is a difference in tensile stress increment between bonded and unbonded tendons, as shown in **Figure 4-12**. The tensile stress increase is relatively uniform over the entire length of unbonded tendons. Therefore, the difference in tensile stresses between initial and ultimate states is relatively small, and the total tensile stress increment is quite small. For bonded tendons, tensile stress increment is concentrated near the mid-span. Therefore, the stress increment at the beam end is very small. As there is a difference in tensile stress increment between the bonded and unbonded tendons, it is considered as an analysis parameter.

Standard deviation of tensile forces in individual strands

As discussed in **Section 3.1**, the standard deviation of the individual strand forces can affect material properties of a tendon, so it should be the most important parameter in this analysis to assess the effect of tensile force deviation on the strength reduction of a PT beam. In the analysis, the individual tensile forces are set based on the coefficient of variation (C.O.V.). The level of the tensile force deviation is set from 0% C.O.V. to 40% C.O.V.

Average tensile stress of tendon

As the average tensile stress increases, individual strands are subjected to large tensile stresses perhaps exceeding the yield stress, even if the standard deviation is not very high. In order to consider these effects, two average tensile stress levels of $0.65f_{pu}$ (low tensile stress level) and $0.8f_{pu}$ (high tensile

stress level) are analyzed. Actually, the average tensile stress level of $0.8f_{pu}$ is not used in the construction field. It is used just for assessment of the effect of high tensile stress (In ACI committee 318 (2014), the upper limits on jacking stress and initial stress are specified as the smaller of $0.8f_{pu}$ or $0.94f_{py}$ and $0.7f_{pu}$, respectively).

Distribution type of individual tensile stresses

As discussed in **Chapters 2**, the measured tensile force deviations in the construction fields follow normal distribution, and it may not be practical to consider other distribution types such as uniform and polarized distributions. However, as discussed in **Section 3.1**, distribution types can affect the equivalent tendon material model. Because the maximum tensile stress of individual strands can be different even with a constant C.O.V. or standard deviation, it is considered as a variable. The considered distribution types are the normal distribution, uniform distribution, and polarized distribution (**Figure 4-15**).

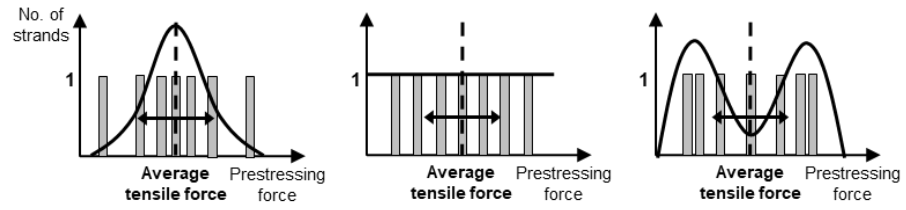

(a) Normal distribution (b) Uniform distribution (c) Polarized distribution

Figure 4-15 Considered distribution types of the individual tensile stresses

Table 4-8 shows the tensile stresses applied to the seven equivalent strands in the numerical analysis, for a given distribution type, and the standard deviation (σ) and mean value (μ) of the tensile stresses in the individual strands.

Table 4-8 The tensile stresses applied to the individual strands in the analysis

Distribution type	Tensile stresses applied to the individual strands						
	No. 1	No. 2	No. 3	No. 4	No. 5	No. 6	No. 7
Normal distribution	μ - 1.70σ	μ – 0.76σ	μ – 0.19σ	μ	μ + 0.19σ	μ + 0.76σ	μ + 1.70σ
Uniform distribution	μ - 1.50σ	μ – 1.00σ	μ – 0.50σ	μ	μ + 0.50σ	μ + 1.00σ	μ + 1.50σ
Polarized distribution	μ - 1.29σ	μ – 1.15σ	μ – 0.72σ	μ	μ + 0.72σ	μ + 1.15σ	μ + 1.29σ

Note: μ is the mean value of tensile stresses in the individual strands; and σ is the standard deviation of tensile stresses in the individual strands.

Application of the equivalent tendon material model

It is considered to verify the validity of the equivalent tendon material model proposed in **Section 3.1**. The analysis results for the method using seven equivalent strands and the method using one strand with the equivalent tendon material model are compared.

Prestressing reinforcement ratio

The prestressing reinforcement ratio of the RB1 and RU1 specimens was 0.43% (Mattock et al., 1971). It is not very large compared to large scale civil structures such as a nuclear containment structure. The higher the prestressing reinforcement ratio, the greater degree the tensile force deviation affects the structural behavior. Two levels of the prestressing reinforcement ratio are applied, 0.43% (Original specimen) and 0.70% (High prestressing reinforcement ratio).

In this study, total 71 analyses are conducted with the aforementioned analysis parameters. The analysis parameters applied to each numerical model are summarized in **Table 4-9**. The name of each numerical model is designated by the rules in **Figure 4-16**.

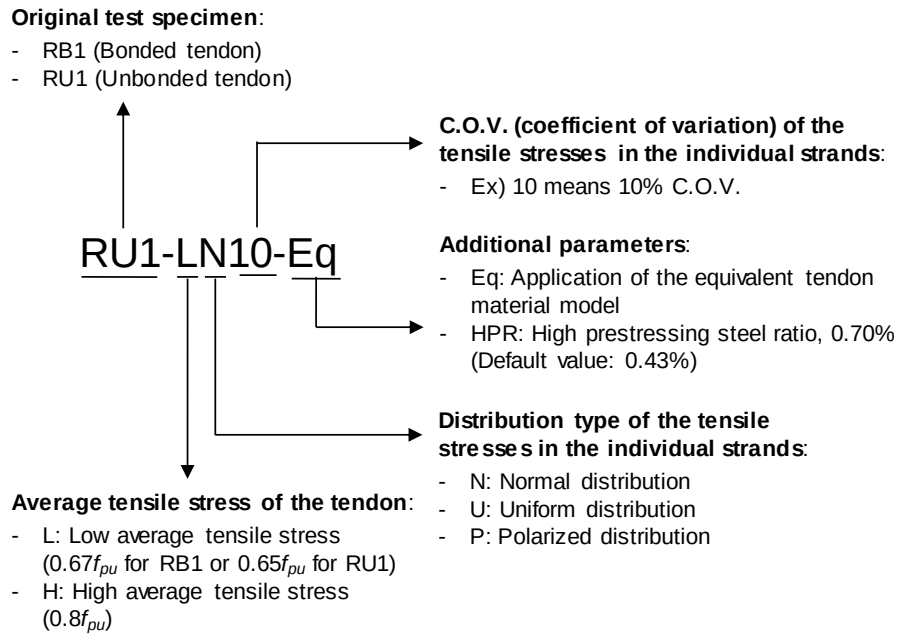

Figure 4-16 Naming rules of the PT beam numerical models

Table 4-9 Analysis parameters of the PT beam analysis

Numerical model	Original test specimen	Average tensile stress of tendon	Dist. type	C.O.V. (%)	Standard deviation (MPa)	Remarks
RB1 (Section 5.1)	RB1 (Bonded tendon)	$0.67f_{pu}$ (=1,296 MPa)	-	0	0	Original numerical model
RB1-L0			-	0	0	
RB1-LN1.0			Normal dist.	1.0	13.0	
RB1-LN2.5				2.5	32.4	
RB1-LN5.0				5.0	64.8	
RB1-LN10				10	129.6	
RB1-LN15				15	194.4	
RB1-LN20				20	259.2	
RB1-LN25				25	324.0	
RB1-LU5.0			Uniform dist.	5.0	64.8	
RB1-LU10				10	129.6	
RB1-LU20				20	259.2	
RB1-LU30				30	388.8	
RB1-LP5.0			Polarized dist.	5.0	64.8	
RB1-LP10				10	129.6	
RB1-LP20				20	259.2	
RB1-LP30				30	388.8	
RB1-H0		$0.8f_{pu}$ (=1,544 MPa)	-	0	0	
RB1-HN1.0			Normal dist.	1.0	15.4	
RB1-HN2.5				2.5	38.6	
RB1-HN5.0				5.0	77.2	
RB1-HN10				10	154.4	
RB1-HN12.5				12.5	193.0	
RB1-HU5.0			Uniform dist.	5.0	77.2	
RB1-HU10				10	154.4	
RB1-HU15				15	231.6	
RB1-HP5.0			Polarized dist.	5.0	77.2	
RB1-HP10				10	154.4	
RB1-HP15				15	231.6	
RB1-LN0-HPR		$0.67f_{pu}$ (=1,296 MPa)	Normal dist.	0	0	
RB1-LN5.0-HPR				5.0	64.8	
RB1-LN10-HPR				10	129.6	
RB1-LN20-HPR				20	259.2	

Table 4-9 Analysis parameters of the PT beam analysis (continued)

Numerical model	Original test specimen	Average tensile stress of tendon	Dist. type	C.O.V. (%)	Standard deviation (MPa)	Remarks
RB1-LN25-HPR	RB1 (Bonded tendon)	$0.67f_{pu}$ (=1,296 MPa)	Normal dist.	25	324.0	
RB1-LN20-Eq				20	259.2	Equivalent tendon model
RU1 (Section 5.1)	RU1 (Unbonded tendon)	$0.65f_{pu}$ (=1,262 MPa)	-	0	0	Original numerical model
RU1-L0			-	0	0	
RU1-LN1.0			Normal dist.	1.0	12.6	
RU1-LN2.5				2.5	31.6	
RU1-LN5.0				5.0	63.1	
RU1-LN10				10	126.2	
RU1-LN15				15	189.3	
RU1-LN20				20	252.4	
RU1-LN30				30	378.6	
RU1-LU5.0			Uniform dist.	5.0	63.1	
RU1-LU10				10	126.2	
RU1-LU20				20	252.4	
RU1-LU30				30	378.6	
RU1-LP5.0			Polarized dist.	5.0	63.1	
RU1-LP10				10	126.2	
RU1-LP20				20	252.4	
RU1-LP30				30	378.6	
RU1-LP40				40	504.8	
RU1-H0		$0.8f_{pu}$ (=1,544 MPa)	-	0	0	
RU1-HN1.0			Normal dist.	1.0	15.4	
RU1-HN2.5				2.5	38.6	
RU1-HN5.0				5.0	77.2	
RU1-HN10				10	154.4	
RU1-HN12.5				12.5	193.0	
RU1-HU5.0			Uniform dist.	5.0	77.2	
RU1-HU10				10	154.4	
RU1-HU15				15	231.6	
RU1-HP5.0			Polarized dist.	5.0	77.2	
RU1-HP10				10	154.4	
RU1-HP15				15	231.6	

Table 4-9 Analysis parameters of the PT beam analysis (continued)

Numerical model	Original test specimen	Average tensile stress of tendon	Dist. type	C.O.V. (%)	Standard deviation (MPa)	Remarks
RU1-LN0-HPR	RU1 (Unbonded tendon)	$0.65f_{pu}$ (=1,262 MPa)	Normal dist.	0	0	
RU1-LN5.0-HPR				5.0	63.1	
RU1-LN10-HPR				10	126.2	
RU1-LN20-HPR				20	252.4	
RU1-LN30-HPR				30	378.6	
RU1-LN5.0-Eq				5.0	63.1	Equivalent tendon model

4.2.3 Analysis results: effects on the ultimate capacities

From the analysis with aforementioned parameters, the load-midspan deflection curves of the PT beams subjected to 4 equal point loads can be obtained. From the load-deflection curves, the influence of individual strand force deviations on the ultimate flexural capacity of PT beams is analyzed. The load-deflection curves obtained from each analysis series are shown in **Figures 4-17 ~ 30**. The ultimate load ($P_{u,FEA}$), ultimate bending moment ($M_{u,FEA}$), and percentage of strength reduction compared to the analysis models with no tensile force deviations (RB1-L0, RB1-H0, RU1-L0, RU1-H0, RB1-L0-HPR and RU1-L0-HPR) are summarized in **Table 4-10**.

Table 4-10 Effects on the ultimate capacities

Series	Effects on the ultimate capacities								
RB1-LN	C.O.V. (%)	0	1.0	2.5	5.0	10	15	20	25
	Ultimate load, $P_{u,FEA}$ (kN)	43.45	43.45	44.09	43.83	43.77	43.36	43.18	43.03
	Ultimate bending moment, $M_{u,FEA}$ (kN-m)	90.37	90.36	91.39	90.98	90.88	90.21	89.94	89.70
	Strength reduction (%)	0	0.02	-1.13	-0.67	-0.56	0.17	0.48	0.74
RB1-LU	C.O.V. (%)	0	5.0	10	20	30			
	Ultimate load, $P_{u,FEA}$ (kN)	43.45	43.87	43.67	43.13	42.80			
	Ultimate bending moment, $M_{u,FEA}$ (kN-m)	90.37	91.04	90.71	89.85	89.33			
	Strength reduction (%)	0	-0.74	-0.38	0.58	1.16			
RB1-LP	C.O.V. (%)	0	5.0	10	20	30			
	Ultimate load, $P_{u,FEA}$ (kN)	43.45	43.87	43.85	43.15	42.59			
	Ultimate bending moment, $M_{u,FEA}$ (kN-m)	90.37	91.03	91.00	89.89	89.00			
	Strength reduction (%)	0	-0.73	-0.70	0.53	1.52			
RB1-HN	C.O.V. (%)	0	1.0	2.5	5.0	10	12.5		
	Ultimate load, $P_{u,FEA}$ (kN)	45.67	45.75	45.69	45.76	45.06	45.67		
	Ultimate bending moment, $M_{u,FEA}$ (kN-m)	93.91	94.05	93.95	94.06	92.94	93.92		
	Strength reduction (%)	0	-0.14	-0.04	-0.16	1.04	-0.01		
RB1-HU	C.O.V. (%)	0	5.0	10	15				
	Ultimate load, $P_{u,FEA}$ (kN)	45.67	45.76	44.73	45.66				
	Ultimate bending moment, $M_{u,FEA}$ (kN-m)	93.91	94.06	92.41	93.91				
	Strength reduction (%)	0	-0.16	1.60	0.00				
RB1-HP	C.O.V. (%)	0	5.0	10	15				
	Ultimate load, $P_{u,FEA}$ (kN)	45.67	45.76	42.62	45.54				
	Ultimate bending moment, $M_{u,FEA}$ (kN-m)	93.91	94.06	93.83	93.71				
	Strength reduction (%)	0	-0.16	0.09	0.21				

Table 4-10 Effects on the ultimate capacities (continued)

Series	Effects on the ultimate capacities								
RU1-LN	C.O.V. (%)	0	1.0	2.5	5.0	10	15	20	30
	Ultimate load, $P_{u,FEA}$ (kN)	36.59	36.62	36.60	36.55	36.21	36.05	35.91	35.19
	Ultimate bending moment, $M_{u,FEA}$ (kN-m)	79.38	79.43	79.40	79.32	78.78	78.52	78.31	77.14
	Strength reduction (%)	0	-0.06	-0.01	0.08	0.76	1.09	1.36	2.82
RU1-LU	C.O.V. (%)	0	5.0	10	20	30			
	Ultimate load, $P_{u,FEA}$ (kN)	36.59	35.94	36.21	36.06	35.46			
	Ultimate bending moment, $M_{u,FEA}$ (kN-m)	79.38	78.34	78.79	78.54	77.58			
	Strength reduction (%)	0	1.31	0.75	1.06	2.28			
RU1-LP	C.O.V. (%)	0	5.0	10	20	30	40		
	Ultimate load, $P_{u,FEA}$ (kN)	36.59	36.09	36.23	36.05	35.62	34.94		
	Ultimate bending moment, $M_{u,FEA}$ (kN-m)	79.38	78.59	78.81	78.52	77.83	76.75		
	Strength reduction (%)	0	1.00	0.73	1.09	1.95	3.32		
RU1-HN	C.O.V. (%)	0	1.0	2.5	5.0	10	12.5		
	Ultimate load, $P_{u,FEA}$ (kN)	40.68	40.70	40.65	40.62	40.12	40.21		
	Ultimate bending moment, $M_{u,FEA}$ (kN-m)	85.93	85.96	85.89	85.84	85.04	85.18		
	Strength reduction (%)	0	-0.03	0.05	0.10	1.04	0.87		
RU1-HU	C.O.V. (%)	0	5.0	10	15				
	Ultimate load, $P_{u,FEA}$ (kN)	40.68	40.61	40.08	40.08				
	Ultimate bending moment, $M_{u,FEA}$ (kN-m)	85.93	85.83	84.97	84.97				
	Strength reduction (%)	0	0.12	1.12	1.12				
RU1-HP	C.O.V. (%)	0	5.0	10	15				
	Ultimate load, $P_{u,FEA}$ (kN)	40.68	40.60	40.00	40.05				
	Ultimate bending moment, $M_{u,FEA}$ (kN-m)	85.93	85.81	84.84	84.92				
	Strength reduction (%)	0	0.14	1.27	1.18				

Table 4-10 Effects on the ultimate capacities (continued)

Series	Effects on the ultimate capacities						
RB1-LN-HPR	C.O.V. (%)	0	5.0	10	20	25	
	Ultimate load, $P_{u,FEA}$ (kN)	55.05	55.05	53.75	55.15	53.33	
	Ultimate bending moment, $M_{u,FEA}$ (kN-m)	108.93	108.93	106.84	109.09	106.18	
	Strength reduction (%)	0	-0.01	1.91	-0.15	2.53	
RU1-LN-HPR	C.O.V. (%)	0	5.0	10	20	30	
	Ultimate load, $P_{u,FEA}$ (kN)	52.23	52.28	51.96	51.90	51.81	
	Ultimate bending moment, $M_{u,FEA}$ (kN-m)	104.41	104.49	103.99	103.88	103.74	
	Strength reduction (%)	0	-0.07	0.41	0.51	0.65	

Note: The ultimate bending moment ($M_{u,FEA}$) is calculated with consideration of beam self-weight; strength reduction is calculated based on the ratio of ultimate bending moment.

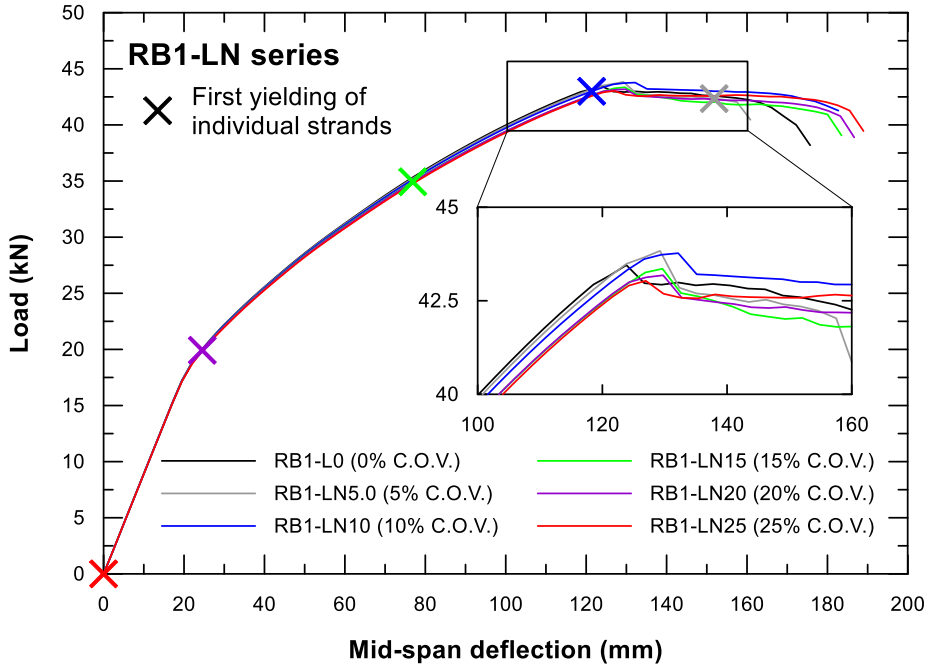

Figure 4-17 Load-deflection curves for the RB1-LN series

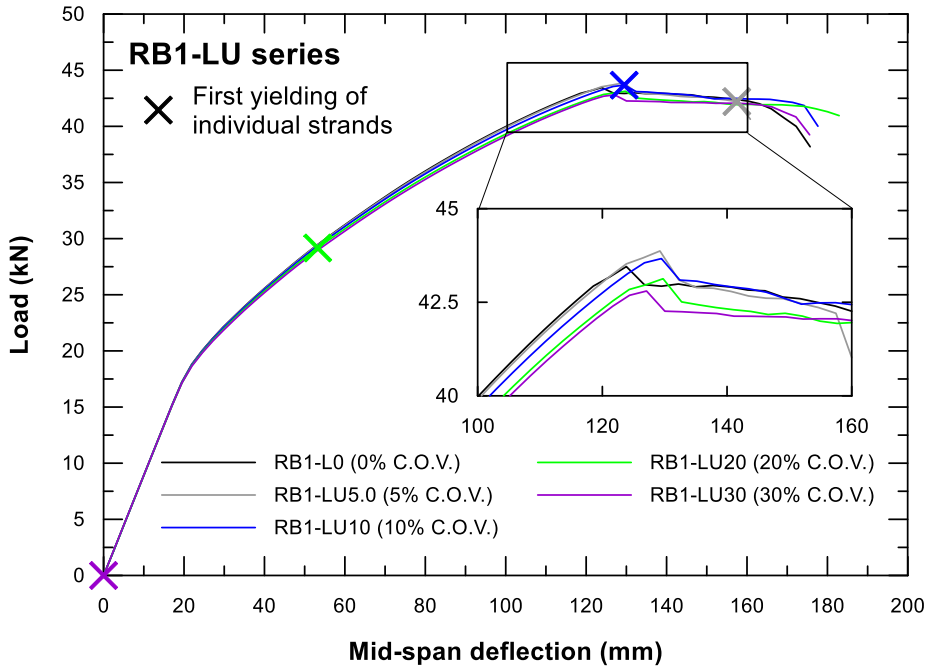

Figure 4-18 Load-deflection curves for the RB1-LU series

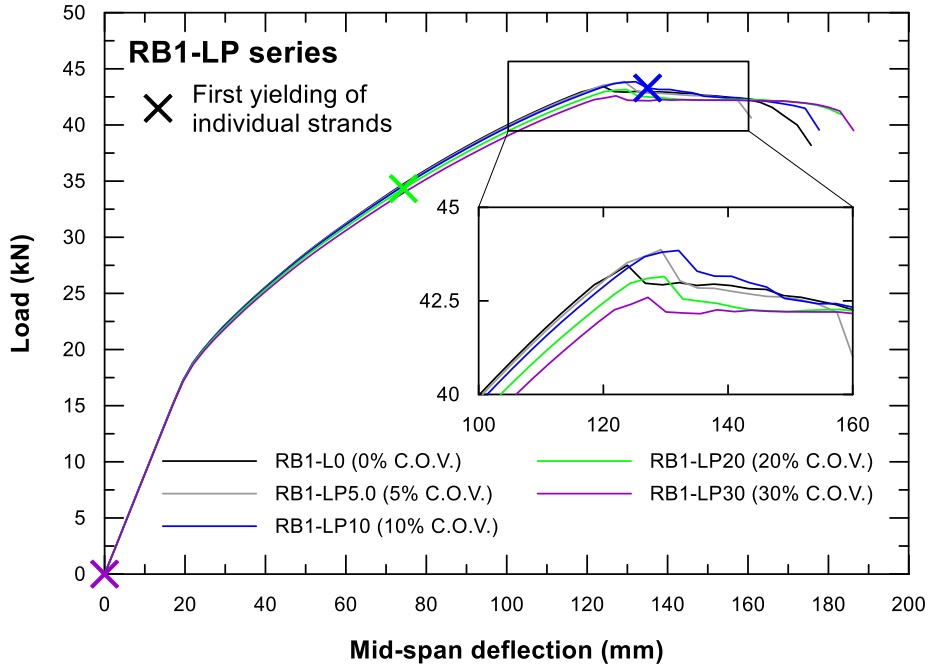

Figure 4-19 Load-deflection curves for the RB1-LP series

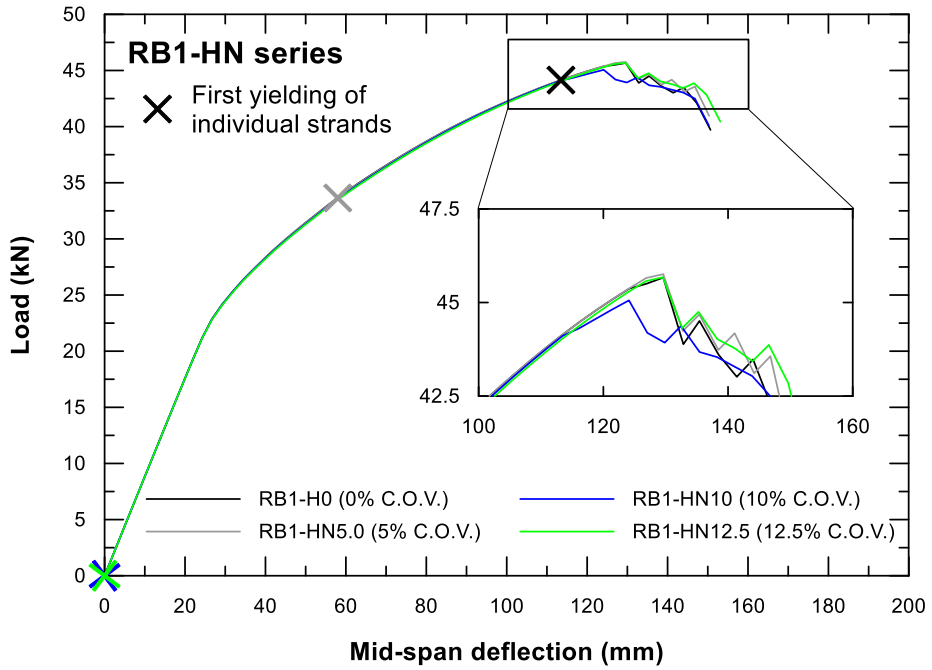

Figure 4-20 Load-deflection curves for the RB1-HN series

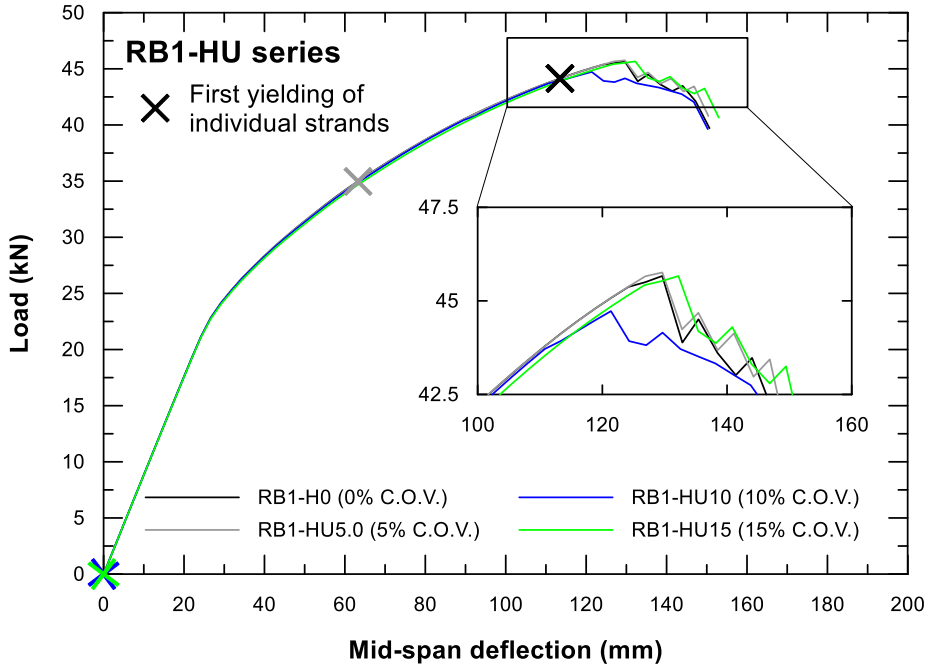

Figure 4-21 Load-deflection curves for the RB1-HU series

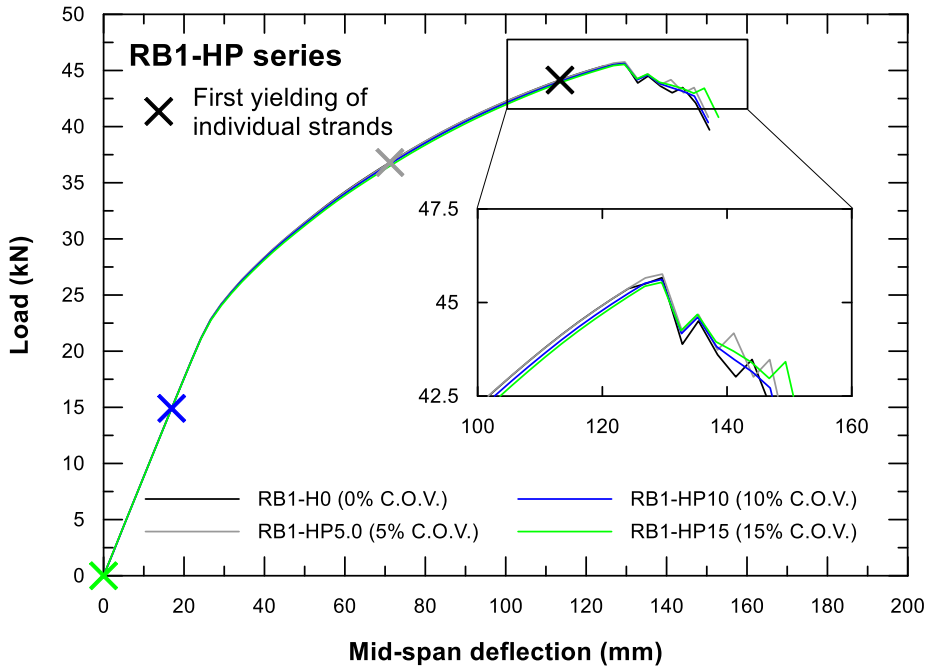

Figure 4-22 Load-deflection curves for the RB1-HP series

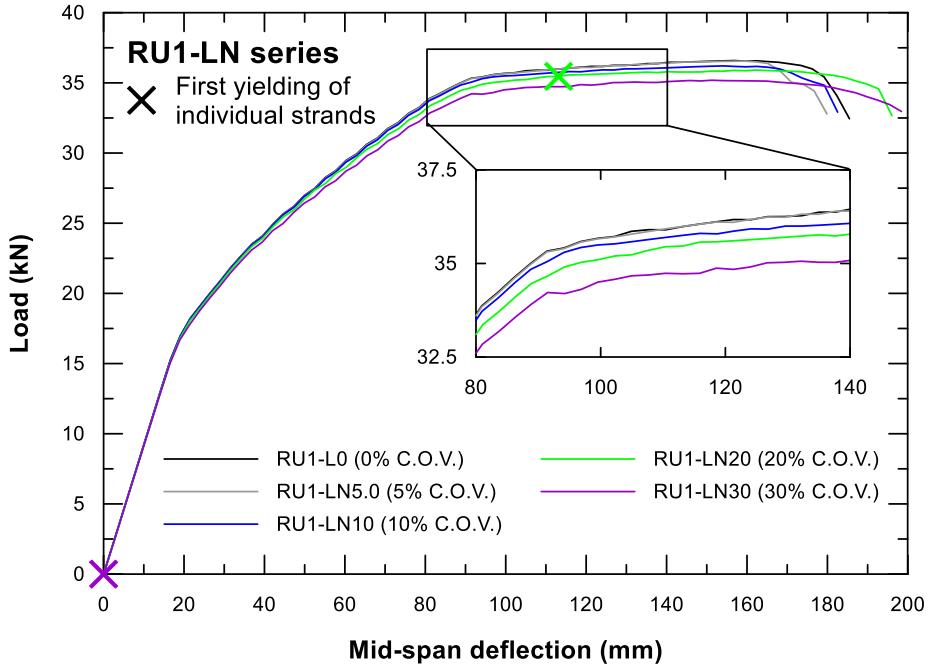

Figure 4-23 Load-deflection curves for the RU1-LN series

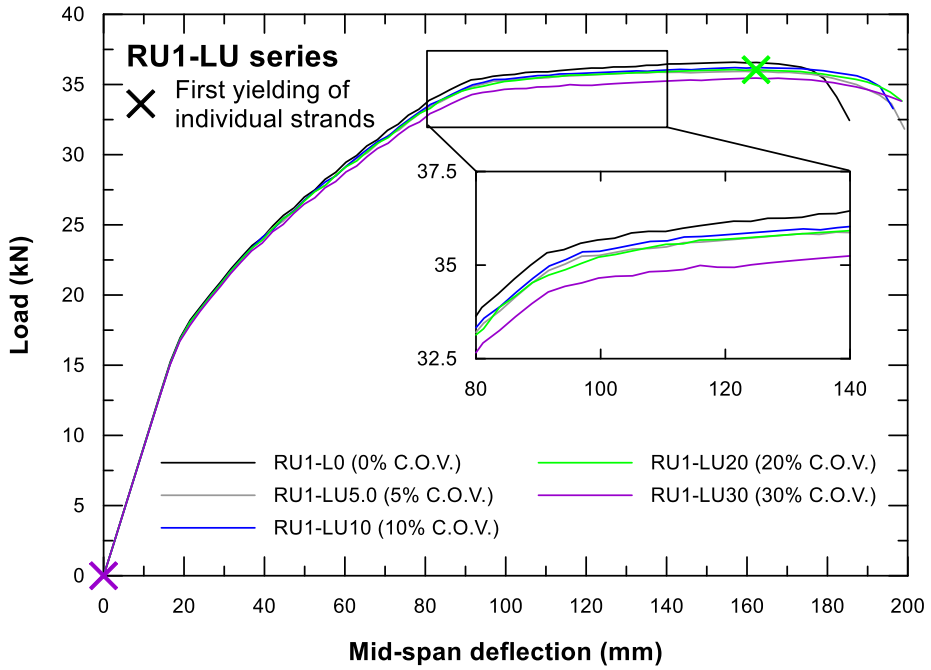

Figure 4-24 Load-deflection curves for the RU1-LU series

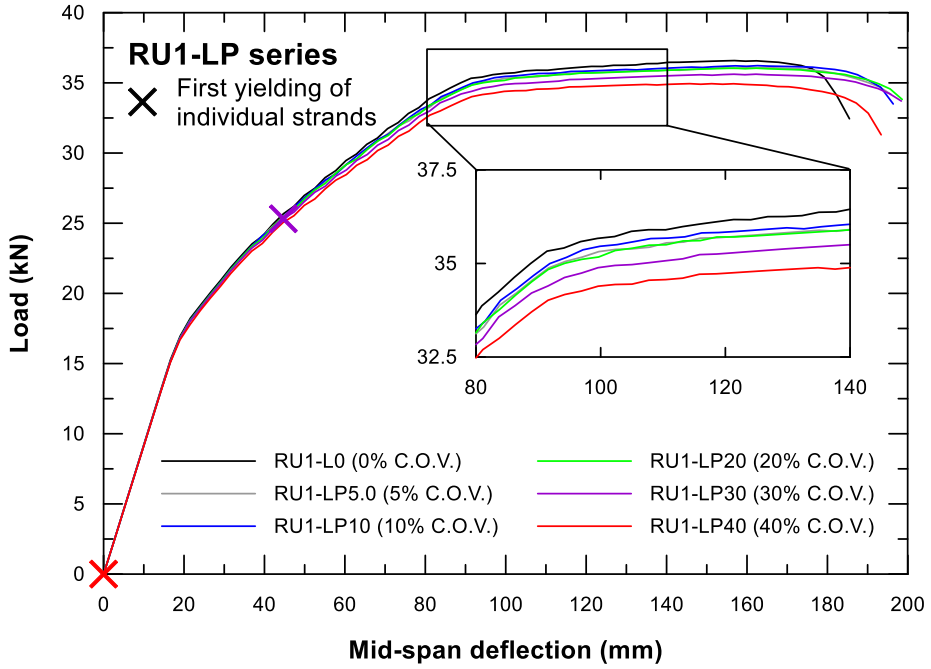

Figure 4-25 Load-deflection curves for the RU1-LP series

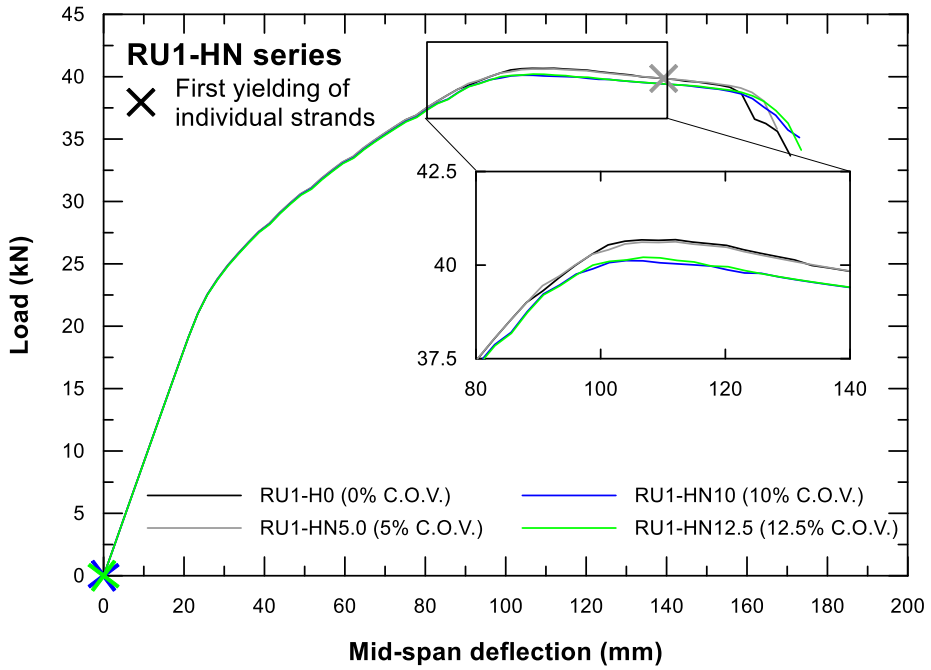

Figure 4-26 Load-deflection curves for the RU1-HN series

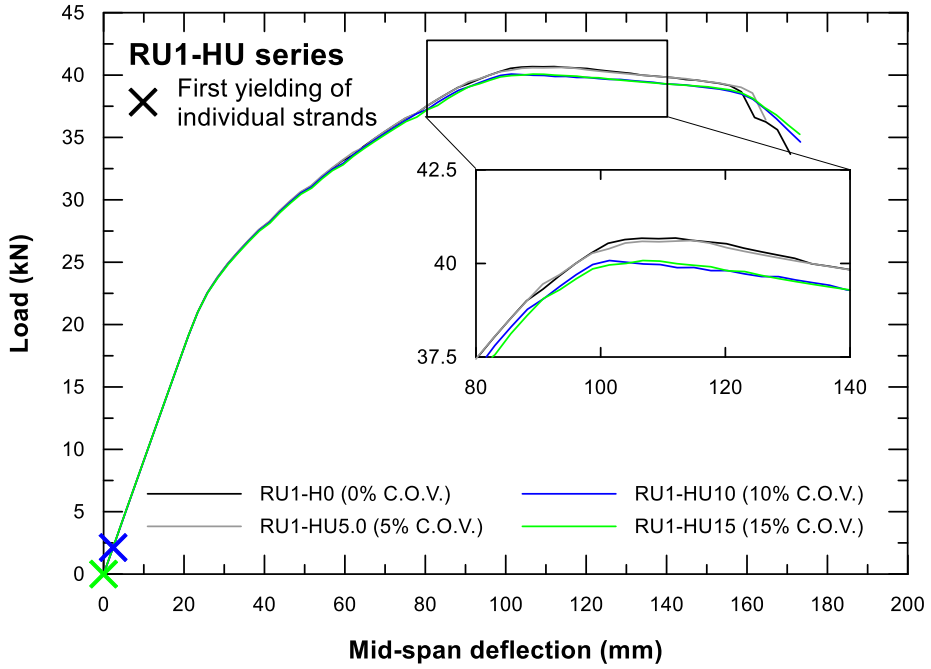

Figure 4-27 Load-deflection curves for the RU1-HU series

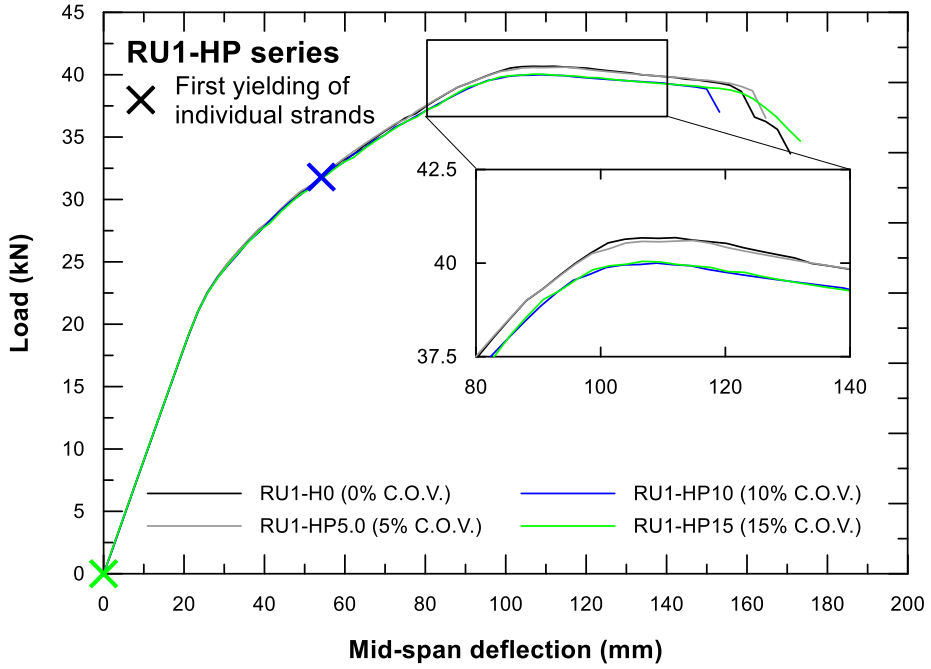

Figure 4-28 Load-deflection curves for the RU1-HP series

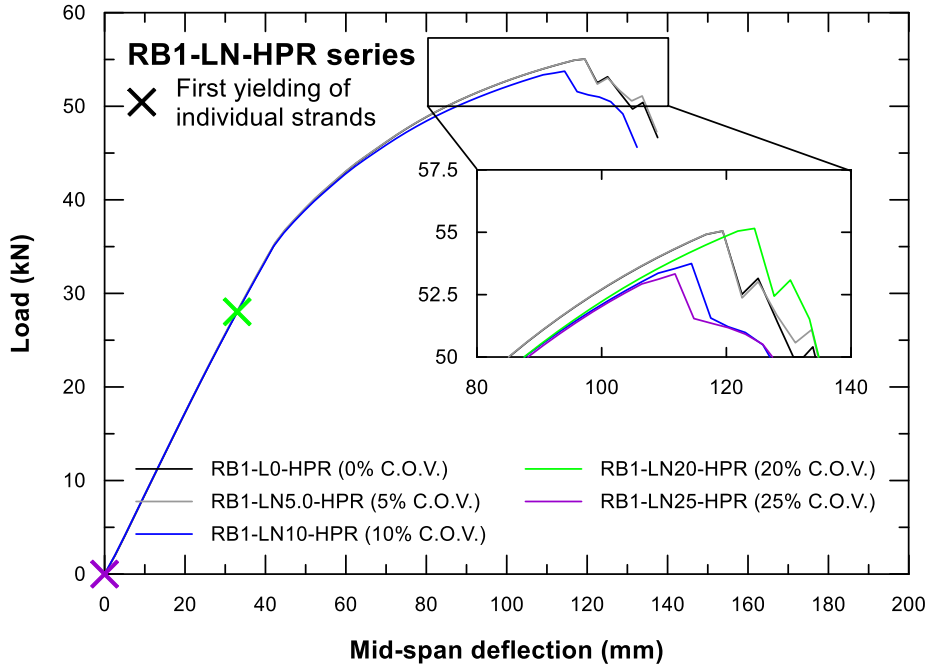

Figure 4-29 Load-deflection curves for the RB1-LN-HPR series

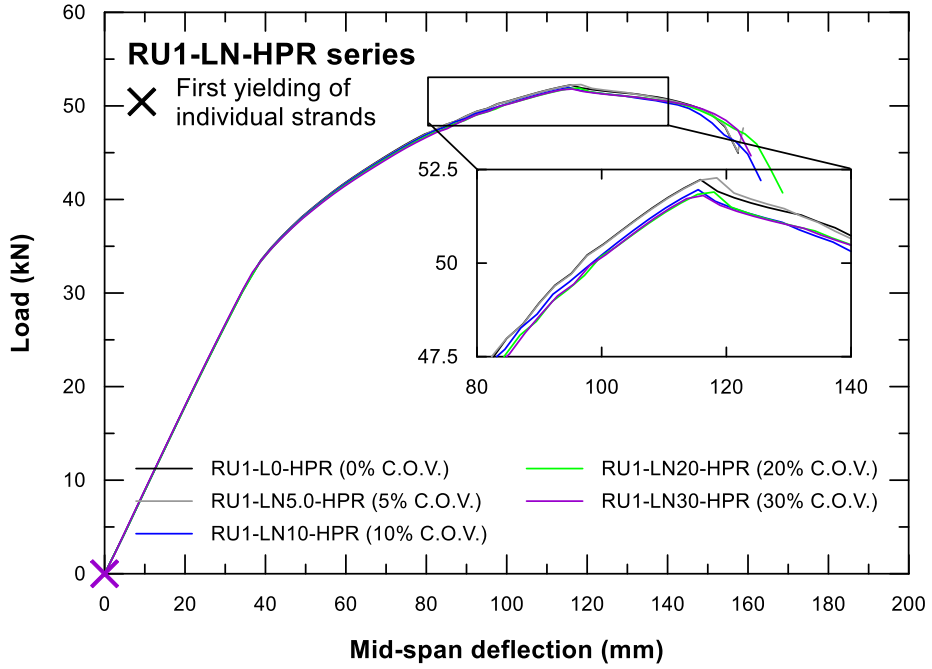

Figure 4-30 Load-deflection curves for the RU1-LN-HPR series

From the analysis, it can be seen that the ultimate strength of PT beams tends to decrease slightly, as the tensile force deviation (C.O.V.) increases. Also, the increment of tensile force deviation reduces the flexural stiffness of PT beams after concrete cracking. But the effect of tensile force deviation on ultimate capacity is found to be slightly different between RB1 series (bonded tendon) and RU1 series (unbonded tendon).

The RB1 series analysis models showed slight decrease in ultimate strength with increasing tensile force deviation, but the strength reduction effect is not significant. The RB1-LP30 analysis model has the highest strength reduction, with an ultimate load reduction of 1.52%. Whereas in the realistic range of tensile force deviations (0 ~ 5% C.O.V.), the strength is slightly increased, unexpectedly. Overall, the increment of ultimate capacity is too small to be neglected; thus, it can be concluded that small tensile force deviation (0 ~ 5% C.O.V.) in the PT beam has little effect on the globally structural behavior.

In the case of the RU1 series analysis models, it can be seen that the ultimate strengths are slightly decreased with increasing tensile force deviations, and the strength reduction effect is more evident than the RB1 series. The highest strength reduction is shown in the RU1-LP40 analysis model, which has the largest tensile force deviation among the analyzed models, with an ultimate load reduction of 3.32%. Likewise the RB1 series, there is negligible strength reduction effect at the realistic level of tensile force deviations (0 ~ 5% C.O.V.).

Comparing the bonded tendon and unbonded tendon with the same average tensile force, C.O.V. of individual tensile forces, and distribution type, the reduction of ultimate capacity is more prominent in the RU1 series with unbonded tendons, even though all other conditions are the same. This is due to the difference of tensile stress increment in bonded and unbonded tendons. **Figures 4-32 ~ 36** and **Tables 4-11** discussed in **Section 4.2.4** show that the average tensile stress increments of tendon (strands) in the RB1 series and

RU1 series are significantly different. For bonded tendons (RB1 series), the tensile stress increment is concentrated in the middle span so that the bonded tendons have larger stress increment, whereas the unbonded tendon shows relatively small increment of tensile stresses. This means that the large increment of tensile stress does not necessarily result in a greater reduction of ultimate capacity.

As can be inferred from **Figures 3-4** and **3-5** (equivalent tendon stress-strain relationship), assuming that no strand failures before the failure of a member, there is no strength reduction effect by tensile force deviation in the elastic range of tendon stress at ultimate (f_{ps}). If the final tensile stress (f_{ps}) is in the post-yield range (over 1,800 MPa in **Figures 3-4** and **3-5**), the flexural stiffness in the load-deflection curve can be affected by tensile force deviation, but the ultimate strength of a beam is not significantly affected. This is because the resulting tensile stresses (f_{ps}) are the same regardless of tensile force deviations. On the other hand, if the resulting tensile stress (f_{ps}) is near the yield strength (f_{py}), there is a reduction of f_{ps} due to tensile force deviations. As the tensile force deviation becomes larger, the f_{ps} decreases. It means that the decrease in f_{ps} depends on the tendon strain at the ultimate state (ε_{ps}).

In other words, the reduction of ultimate capacity is highly affected by the tensile force deviation, when the tensile stress of tendon at ultimate state (f_{ps}) is near or slightly below the yield stress (f_{py}). **Figure 4-31** shows the corresponding equivalent tendon material models for the RB1-LN, RB1-HN, RU1-LN, and RU1-HN series, and the difference of tensile stress of the tendon due to the tensile force deviation is shown for the given tendon strain. The tendon stress and strain at ultimate state (f_{ps} and ε_{ps}) are marked in the graphs (**Figure 4-31**).

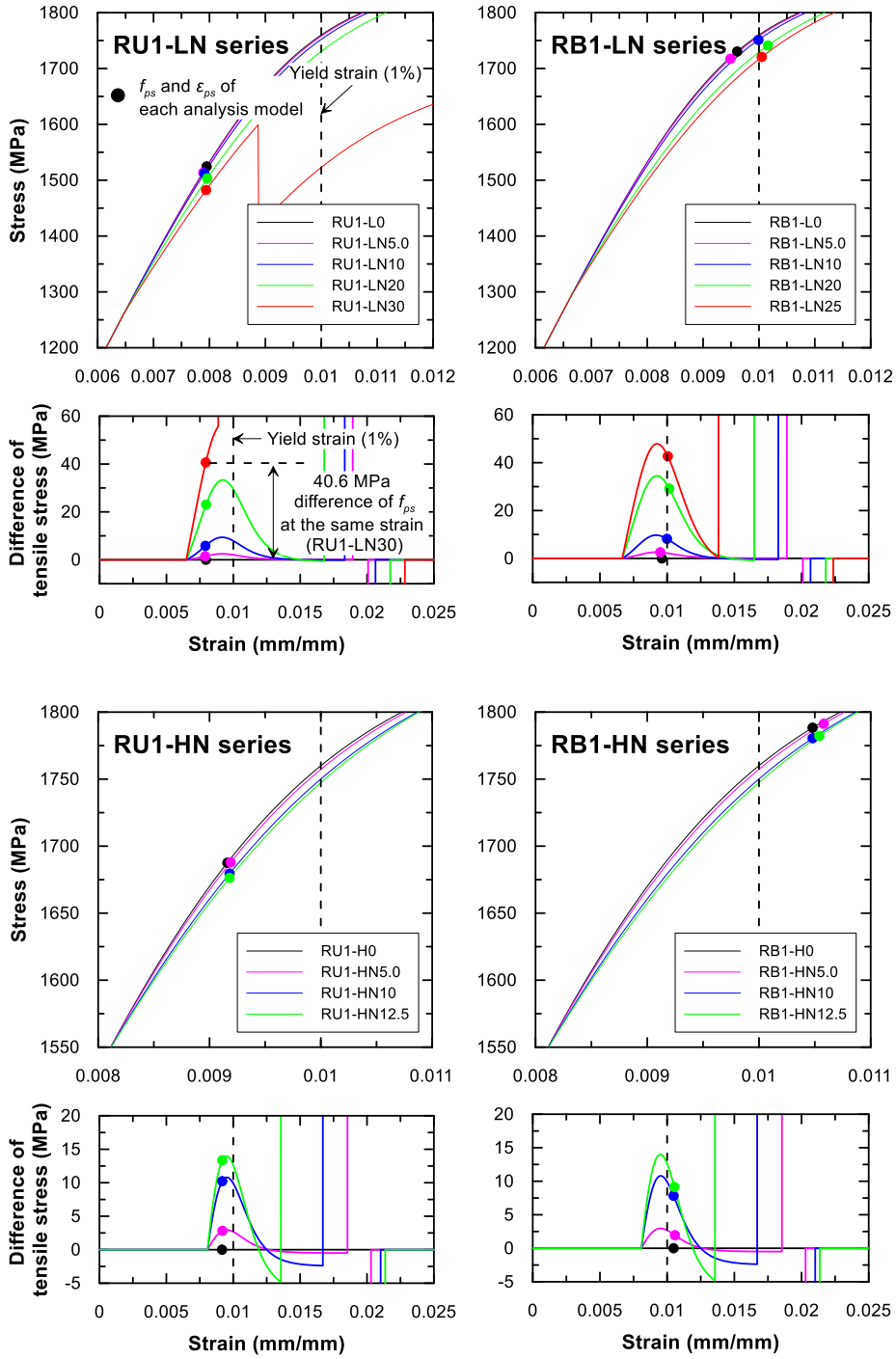

Figure 4-31 Equivalent tendon material models and the tendon stress and strain at ultimate state (f_{ps} and ε_{ps})

As can be seen in **Figure 4-31**, the RU1 series show that the strains at ultimate state (ε_{ps}) are not much different according to the tensile force deviation. Because the tensile stress at ultimate state (f_{ps}) decreased, the tendency of strength reduction effects due to the tensile force deviation can be noticed more clearly compared to the RB1 series. On the other hand, in the case of the RB1 series, there is a slight difference between the ε_{ps} values. This may be due to the nature of the bonded tendon where the stress increment is concenterated in the mid-span of the beam. Because of the slightly different ε_{ps}, it can be analyzed that the difference in f_{ps} is not clearly noticed compared to the RU1 series.

In the same manner, the results of RB1-LN-HPR series and RU1-LN-HPR series (**Figure 4-29** and **4-30**), which have high prestressing ratio (0.70%), can be analyzed. From the results, it can be seen that the strength reduction due to tensile force deviation is not proportional to the prestressing ratio. As summarized in **Table 4-11**, smaller values of f_{ps} are observed, as the prestressing ratio increases under the same conditions. In the case of RB1-LN-HPR series, the f_{ps} is around 1,600 MPa, which is about 120 MPa smaller than the RB1-LN series. But, it is still close to the yield stress. The ε_{ps} of RB1-LN-HPR series is around 1% elongation, which is sensitive to the tensile force deviation. Since the area ratio of tendon is larger than RB1-LN series (0.43%), the strength reduction due to the tensile force deviation is more prominent. On the other hand, in the case of RU1-LN-HPR series, the f_{ps} is around 1,400 MPa. The effect of strength reduction by the tensile force deviation is relatively small. Therefore, the strength reduction due to tensile force deviation is not prominent compared to RU1-LN series.

In **Figures 4-17 ~ 30**, the first strand yielding occurs earlier as the tensile force deviation increases. There is no strand failure until reaching the ultimate strength because no deformation of PT beams is excessive, and no yielding of a strand occurs with lower tensile force deviations. However, when the tensile force deviation is relatively large, the increase of the tensile stress exceeds the

yield strength of the strand, leading to the premature yielding of the first strand. The yielding of a strand makes no adverse effects on the ultimate capacity of a PT beam under monotonic loading, but can affect its hysteresis behavior under cyclic loading and long-term behavior of PT beam. Therefore, the yielding of strands should not occur prematurely.

4.2.4 Analysis results: tensile stress increment

In this analysis, the behavior of seven equivalent strands can be analyzed individually, since the seven equivalent strands are individually modeled as **Figure 4-13**. The average tensile stress increments due to the increase of 4 equal point loads applied to the PT beam are summarized in **Table 4-11**. **Figures 4-32 ~ 36** show the individual and average tensile stress increments of 7 individual strands in a tendon.

Table 4-11 Effects on the average tensile stress increment of the tendons

Series	Initial stress	Effects on the average tensile stress increment at the mid-span								
RB1-LN	1,296 MPa	C.O.V. (%)	0	1.0	2.5	5.0	10	15	20	25
		Average tensile stress at ultimate load (MPa)	1,730	1,728	1,718	1,717	1,751	1,734	1,741	1,720
		Average tensile stress increment (MPa)	411	409	399	399	432	417	425	407
		Reduction of tensile stress increment (%)	0	0.3	2.7	2.9	-5.3	-1.5	-3.5	0.9
RB1-LU	1,296 MPa	C.O.V. (%)	0	5.0	10	20	30			
		Average tensile stress at ultimate load (MPa)	1,730	1,716	1,733	1,723	1,684			
		Average tensile stress increment (MPa)	411	397	414	408	374			
		Reduction of tensile stress increment (%)	0	3.2	-0.8	0.6	9.0			
RB1-LP	1,296 MPa	C.O.V. (%)	0	5.0	10	20	30			
		Average tensile stress at ultimate load (MPa)	1,730	1,708	1,731	1,731	1,691			
		Average tensile stress increment (MPa)	411	390	412	414	380			
		Reduction of tensile stress increment (%)	0	5.0	-0.4	-1.0	7.4			
RB1-HN	1,544 MPa	C.O.V. (%)	0	1.0	2.5	5.0	10	12.5		
		Average tensile stress at ultimate load (MPa)	1,788	1,789	1,790	1,791	1,780	1,782		
		Average tensile stress increment (MPa)	230	231	231	233	224	229		
		Reduction of tensile stress increment (%)	0	-0.3	-0.4	-1.2	2.8	0.6		
RB1-HU	1,544 MPa	C.O.V. (%)	0	5.0	10	15				
		Average tensile stress at ultimate load (MPa)	1,788	1,789	1,780	1,774				
		Average tensile stress increment (MPa)	230	230	224	222				
		Reduction of tensile stress increment (%)	0	0.1	2.6	3.5				
RB1-HP	1,544 MPa	C.O.V. (%)	0	5.0	10	15				
		Average tensile stress at ultimate load (MPa)	1,788	1,794	1,780	1,776				
		Average tensile stress increment (MPa)	230	235	224	225				
		Reduction of tensile stress increment (%)	0	-2.1	2.8	2.0				

Table 4-11 Effects on the average tensile stress increment of the tendons (continued)

Series	Initial stress	Effects on the average tensile stress increment at the mid-span								
RU1-LN	1,262 MPa	C.O.V. (%)	0	1.0	2.5	5.0	10	15	20	30
		Average tensile stress at ultimate load (MPa)	1,524	1,521	1,512	1,512	1,512	1,506	1,503	1,482
		Average tensile stress increment (MPa)	260	258	249	248	249	243	241	221
		Reduction of tensile stress increment (%)	0	0.6	4.3	4.4	4.0	6.4	7.2	15.0
RU1-LU	1,262 MPa	C.O.V. (%)	0	5.0	10	20	30			
		Average tensile stress at ultimate load (MPa)	1,524	1,516	1,520	1,504	1,482			
		Average tensile stress increment (MPa)	260	252	256	241	222			
		Reduction of tensile stress increment (%)	0	2.9	1.4	7.1	14.3			
RU1-LP	1,262 MPa	C.O.V. (%)	0	5.0	10	20	30	40		
		Average tensile stress at ultimate load (MPa)	1,524	1,519	1,519	1,505	1,481	1,444		
		Average tensile stress increment (MPa)	260	255	255	243	220	189		
		Reduction of tensile stress increment (%)	0	1.8	1.8	6.5	15.3	27.3		
RU1-HN	1,544 MPa	C.O.V. (%)	0	1.0	2.5	5.0	10	12.5		
		Average tensile stress at ultimate load (MPa)	1,687	1,690	1,690	1,688	1,679	1,676		
		Average tensile stress increment (MPa)	148	150	150	149	142	140		
		Reduction of tensile stress increment (%)	0	-0.8	-1.1	-0.2	4.6	5.6		
RU1-HU	1,544 MPa	C.O.V. (%)	0	5.0	10	15				
		Average tensile stress at ultimate load (MPa)	1,687	1,688	1,678	1,669				
		Average tensile stress increment (MPa)	148	149	140	135				
		Reduction of tensile stress increment (%)	0	-0.4	5.4	9.0				
RU1-HP	1,544 MPa	C.O.V. (%)	0	5.0	10	15				
		Average tensile stress at ultimate load (MPa)	1,687	1,689	1,691	1,689				
		Average tensile stress increment (MPa)	148	149	151	150				
		Reduction of tensile stress increment (%)	0	-0.6	-1.7	-0.9				

Table 4-11 Effects on the average tensile stress increment of the tendons (continued)

Series	Initial stress	Effects on the average tensile stress increment at the mid-span						
RB1-LN-HPR	1,262 MPa	C.O.V. (%)	0	5.0	10	20	25	
		Average tensile stress at ultimate load (MPa)	1,611	1,610	1,593	1,590	1,565	
		Average tensile stress increment (MPa)	287	285	270	269	246	
		Reduction of tensile stress increment (%)	0	0.6	6.0	6.1	14.3	
RU1-LN-HPR	1,262 MPa	C.O.V. (%)	0	5.0	10	20	30	
		Average tensile stress at ultimate load (MPa)	1,424	1,423	1,417	1,411	1,399	
		Average tensile stress increment (MPa)	158	157	154	148	141	
		Reduction of tensile stress increment (%)	0	0.5	3.0	6.6	11.0	

Note: Reduction of tensile stress increment is calculated based on the ratio of average tensile stress increment.

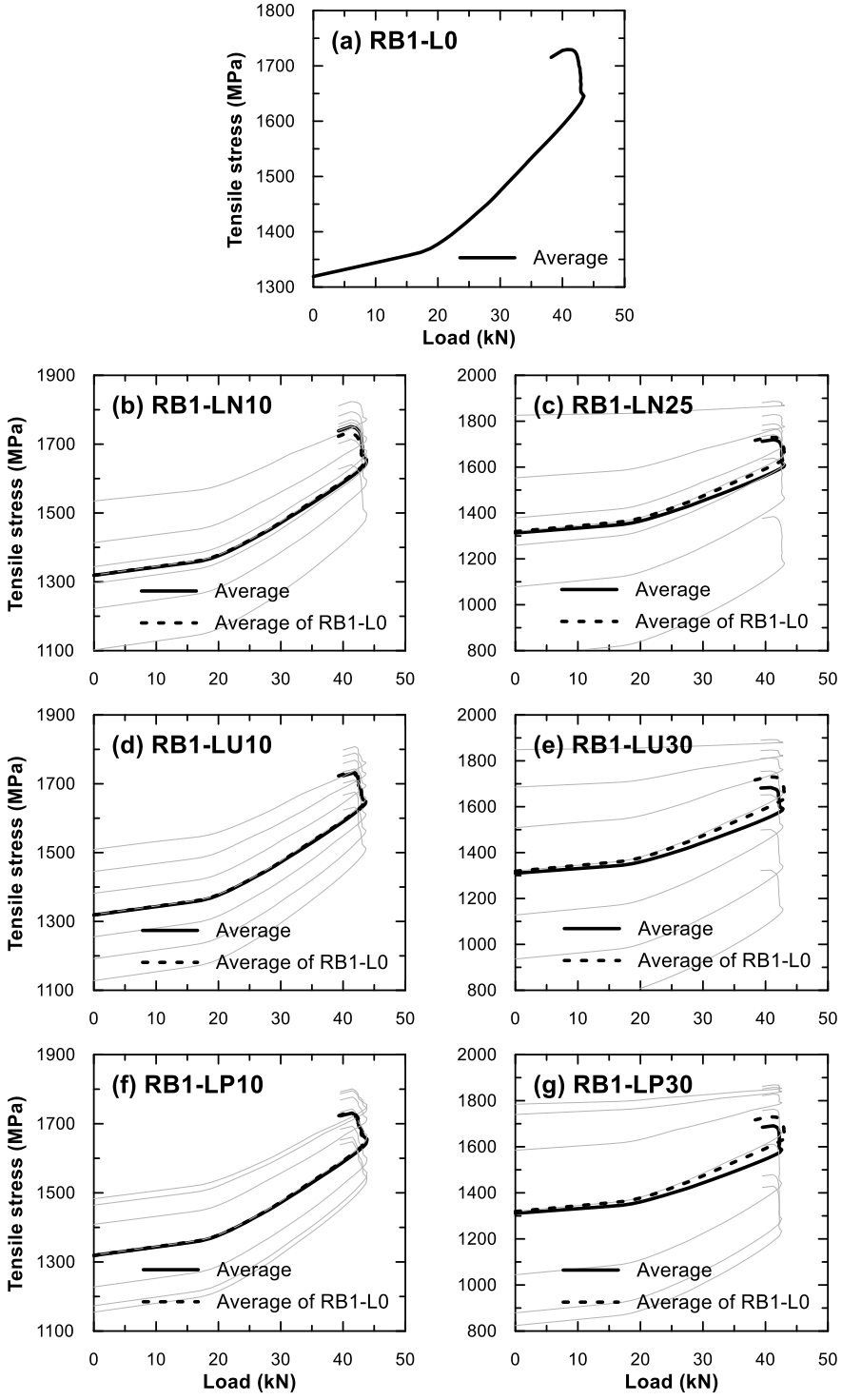

Figure 4-32 Tensile stress increment curves for the RB1-L series

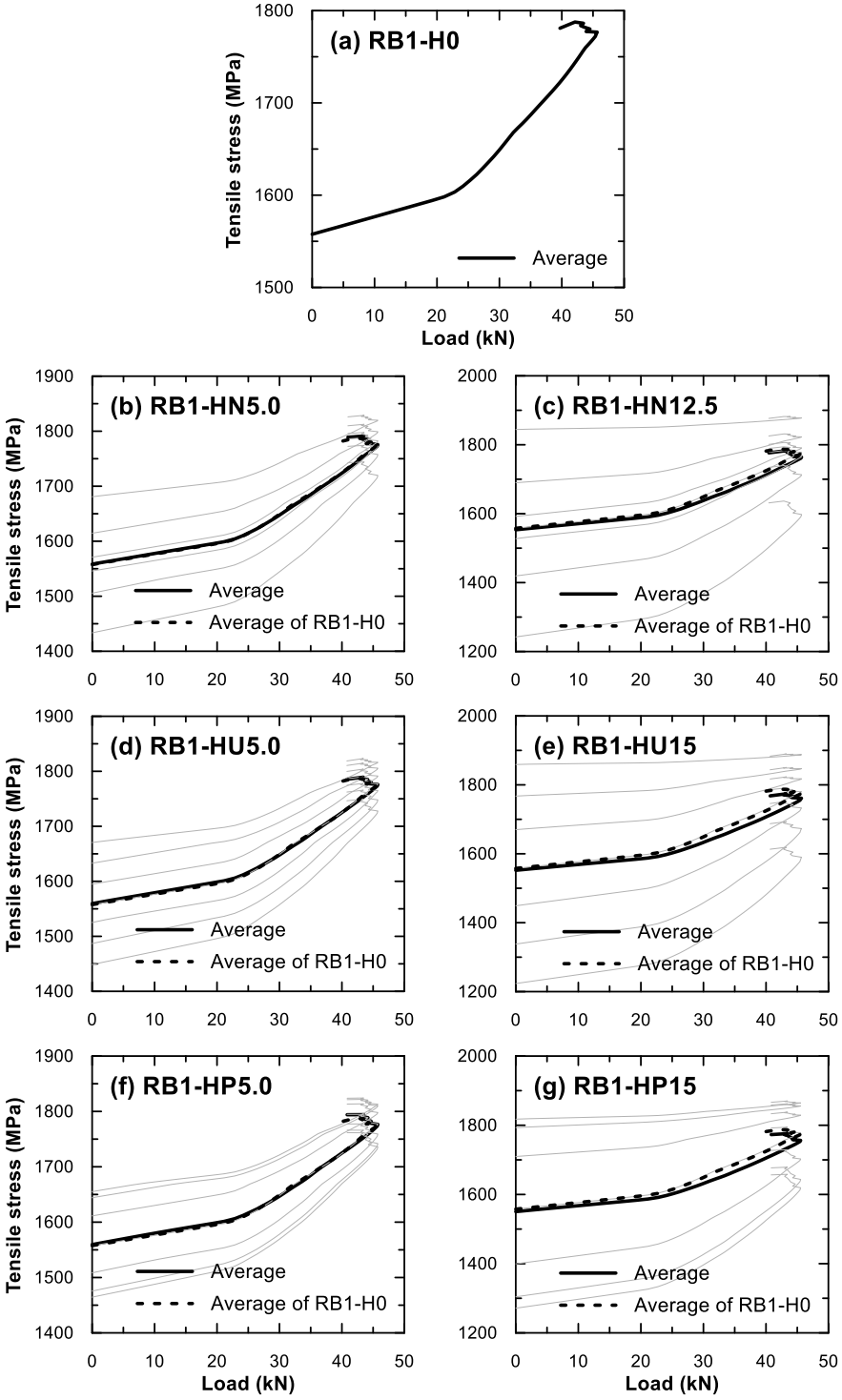

Figure 4-33 Tensile stress increment curves for the RB1-H series

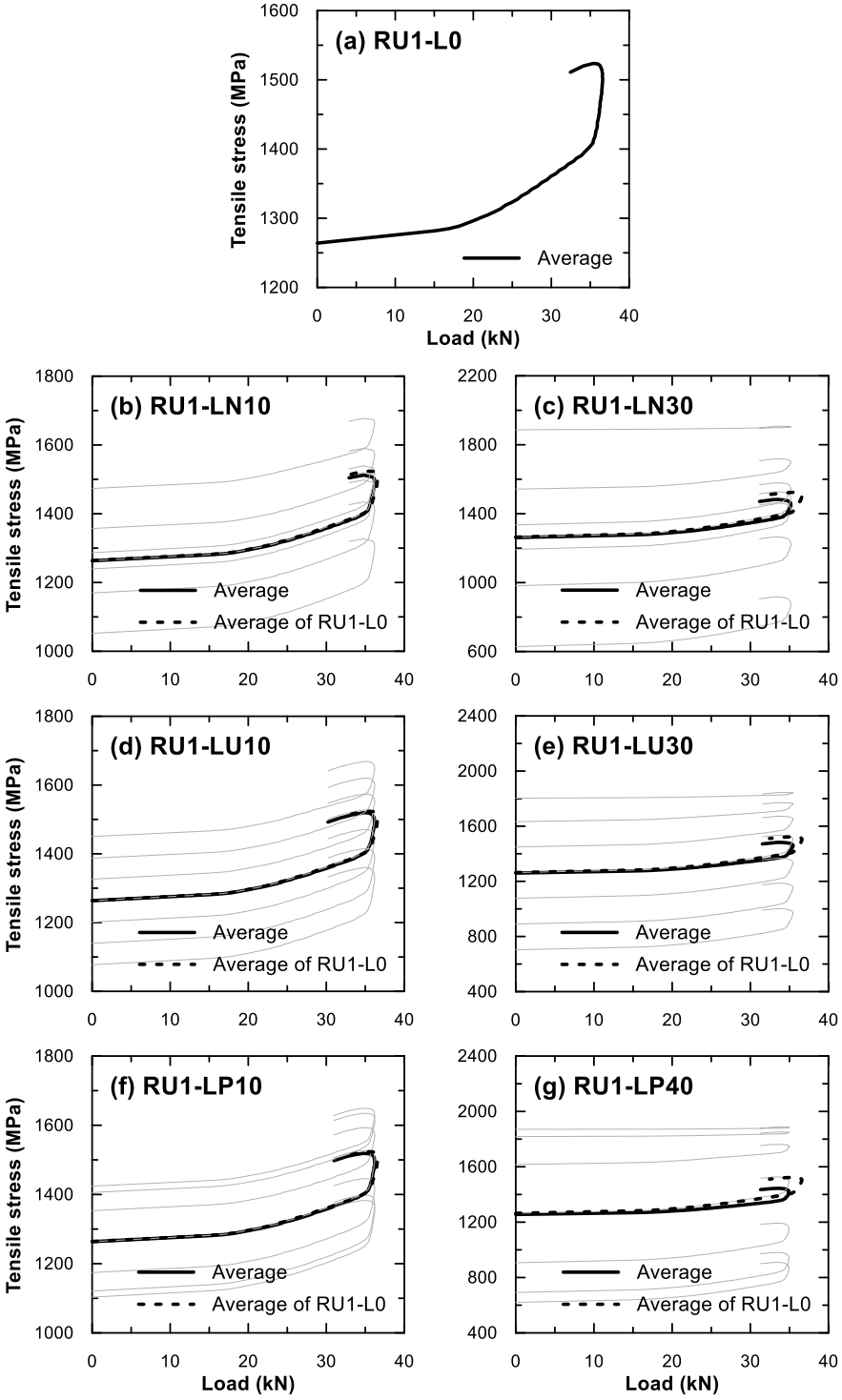

Figure 4-34 Tensile stress increment curves for the RU1-L series

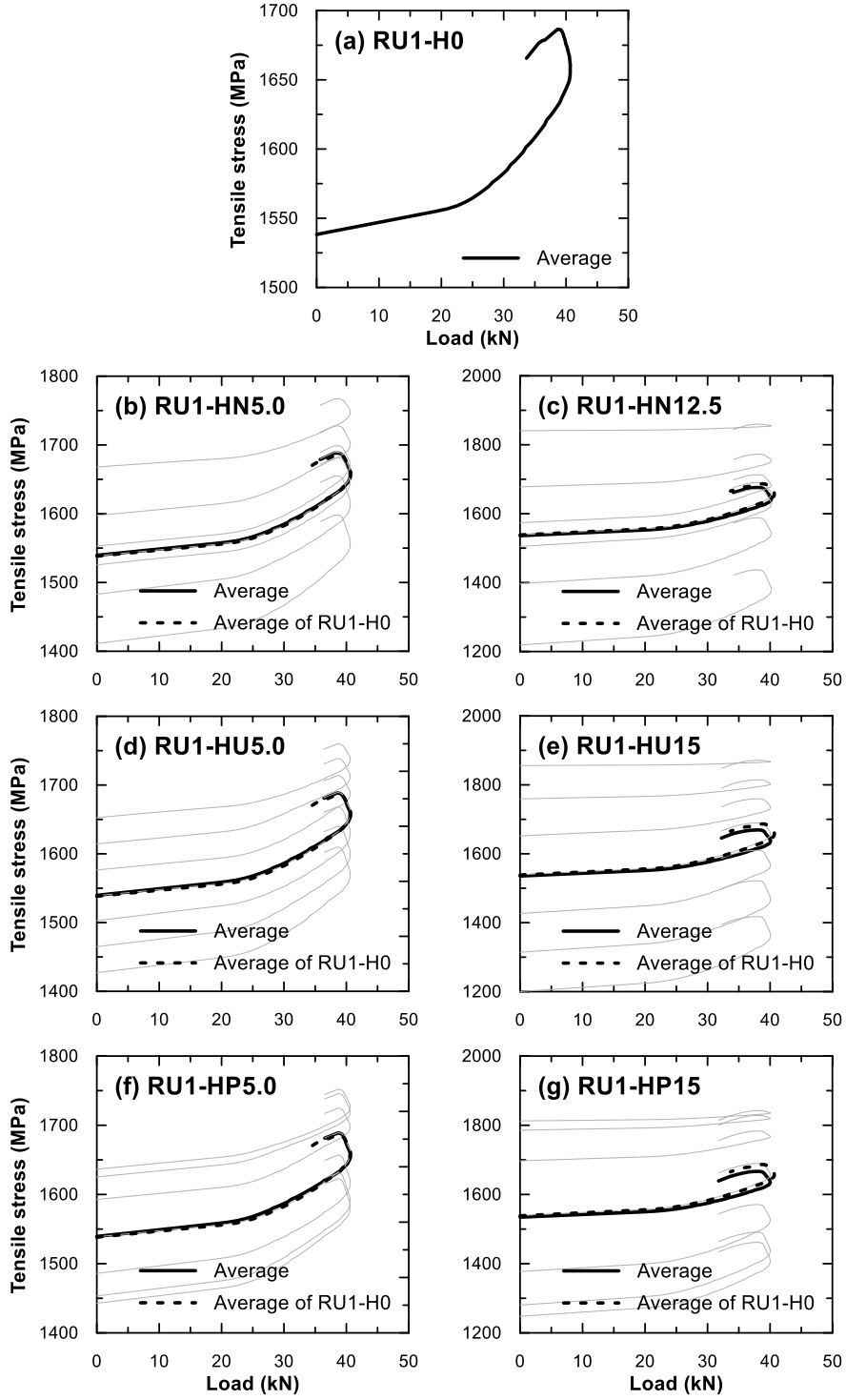

Figure 4-35 Tensile stress increment curves for the RU1-H series

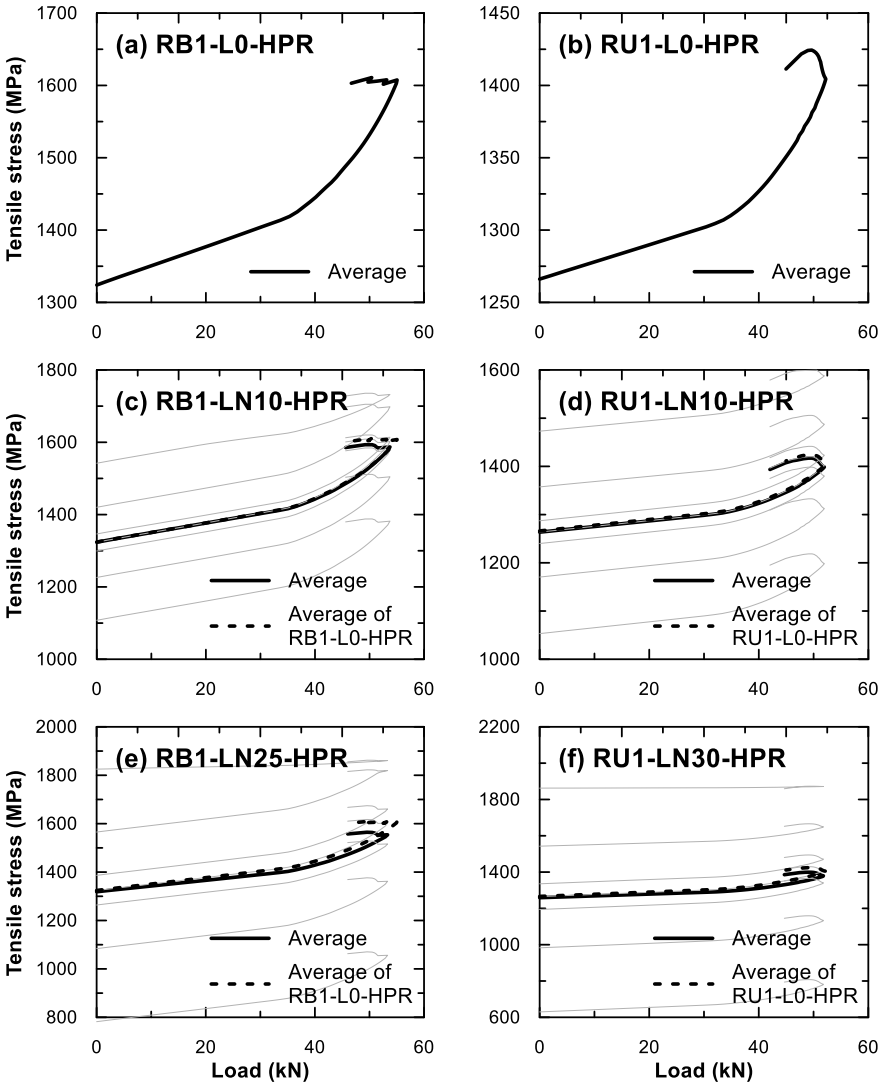

Figure 4-36 Tensile stress increment curves for the RB1-LN-HPR series and RU1-LN-HPR series

In the previous section, the influence of individual strand force deviation on the ultimate strength of PT beam is found to be not significant. However, the influence on the tensile stress of tendon is relatively significant. From the analysis, it is found that large deviation of individual strand tensile forces makes average tensile stress at the ultimate stage (average f_{ps} of individual strands) become smaller. In RB1 series (bonded tendon), RB1-LP30 analysis model has the largest reduction of f_{ps}, which is about 46 MPa in reference to the f_{ps} of RB1-L0 (0% C.O.V.) model. In RU1 series (unbonded tendon). RU1-LP40 analysis model has the largest reduction of f_{ps}, which is about 80 MPa in reference to the f_{ps} of RU1-L0 (0% C.O.V.) model.

The deviation in individual strand tensile forces reduces the average f_{ps} of tendon (**Figure 4-31**), which results the reduction of ultimate flexural strength of PT beam. The ultimate flexural strength of PT beam is highly dependent on the tensile stress at ultimate stage (f_{ps}). However, in this analysis model, since the prestressing reinforcement ratio is not very large (0.43%), the effect on ultimate strength of PT beam is not significant.

In the analysis models with large C.O.V. of individual strand tensile forces greater than 10%, there were perceptible reductions in tensile stress at ultimate stage (f_{ps}). While no significant reductions in f_{ps} are observed in the realistic range of tensile force deviation (less than 5% C.O.V.). In small deviations, there is no significant change in the equivalent tendon stress-strain relationship from the case of 0% C.O.V. Therefore, there is no significant effect on the ultimate strength of PT beam in low deviation of individual tensile forces.

Figures 4-32 ~ 36 show how much average tensile force of tendon decreases by the deviation of individual tensile forces at each loading stage. The gray lines indicate tensile stresses of seven individual strands. In the linear region of load-deflection curves (**Figures 4-17 ~ 30**), the deflection of PT beam is very small and there is no significant change in the strain of tendon. In the

linear region, there is negligible difference in the average tensile stress of tendon due to deviation of individual tensile forces. Also, there is no significant difference in the equivalent tendon stress-strain relationship at the low level of tensile stress.

After cracks occur in concrete, tensile stresses of individual strands rapidly increase, since the flexural stiffness decreases. Then, when the tensile stress of individual strand tensioned with the highest tensile force reaches near the yield strength of strand, average tensile force of tendon starts to decrease compared to the case of no tensile force deviation (0% C.O.V.). As a result, in the ultimate stage, the average tensile stress of tendon decrease significantly.

4.2.5 Verification of equivalent tendon material model

RB1-LN20 and RU1-LN5.0 analysis models (original models) were used to verify the equivalent tendon material model proposed in **Section 3.1**. The equivalent tendon material model is applied to RB1-LN20-Eq and RU1-LN5.0-Eq analysis models (verification models), and one strand per one tendon is modeled as the same as RB1 and RU1 analysis models (original models discussed in **Section 4.1**), whereas RB1-LN20 and RU1-LN5.0 models were modeled with seven equivalent strands per one tendon. For the verification models, the individual strand tensile force deviation is considered in the equivalent tendon stress-strain relationship. Except this concept, there is no difference between the original models and verification models.

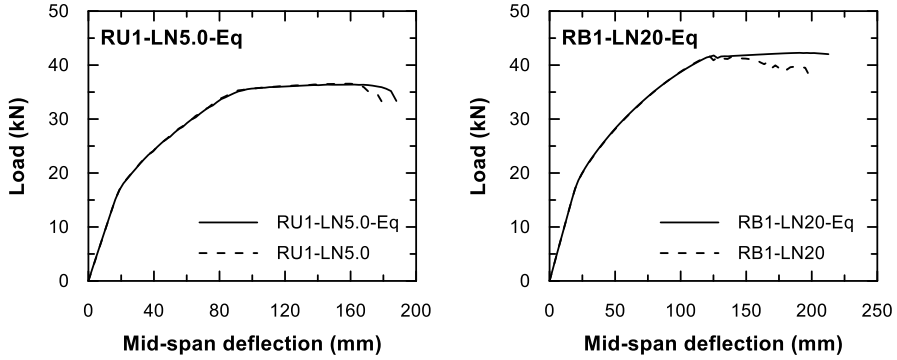

Figure 4-37 Verification of equivalent tendon material model: Load-deflection curves

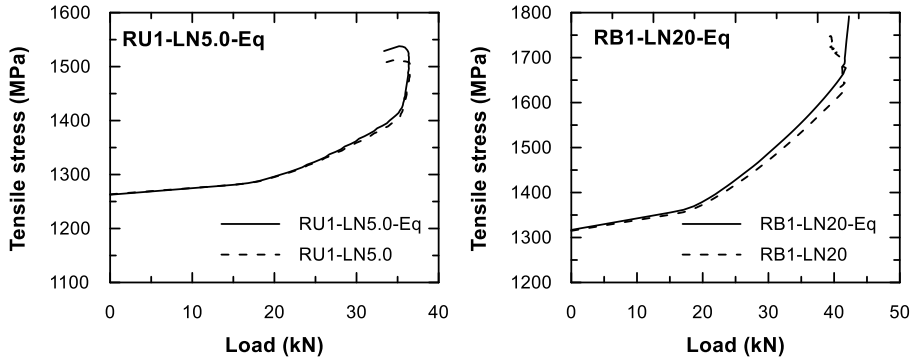

Figure 4-38 Verification of equivalent tendon material model: Tensile stress increment curves

4.3 Effects of tensile force deviation of the individual strands on the structural behavior of partial model of nuclear containment building

4.3.1 Numerical modeling concepts for the partial model of nuclear containment

In this section, numerical analysis is conducted to investigate the effect of the tensile force deviation of individual strands on the structural performance of nuclear containment structures. As discussed in **Chapter 3**, the tensile force deviation can reduce the equivalent yield strength of the entire tendon. It can cause premature cracks on the concrete wall, and reduction of ultimate capacity in extreme inner pressure conditions.

Most of the post-tensioning systems in the containment buildings of pressurized water reactor type (PWR) is composed of horizontal (circumferential) tendons and vertical (inverted-U) tendons. Theoretically, in the vertical tendons, there are very little tensile force deviations due to initial slack effects. As shown in **Figure 4-39**, vertical tendons typically have uniformly distributed arrangement without irregular local curvatures by gravity. Even before tensioning or initial arrangement operation, the strands are concentrated inward in the duct (i.e., at the bottom of the duct at the dome part). The initial slack effects shown in **Figure 3-1** may not be found from the vertical tendons. Because the tensile force deviation due to initial slack is dominant in the horizontal tendons, the numerical analysis is conducted with a focus on the effect of the initial slack on the horizontal ring-shaped partial model of a nuclear containment building (**Figure 4-40**).

The geometry of the analytical model, arrangement of reinforcement and tendons, and material properties are based on the ‘Overpressurization test of a 1:4 scale prestressed concrete containment vessel model’ (**Figure 4-41**) conducted by Sandia National Laboratory (Hessheimer et al., 2003). Because the experiment was carried out on a 1:4 scale, the cross-sectional area and

arrangement of the reinforcement and tendons are also arranged to 1:4 scale in the numerical model.

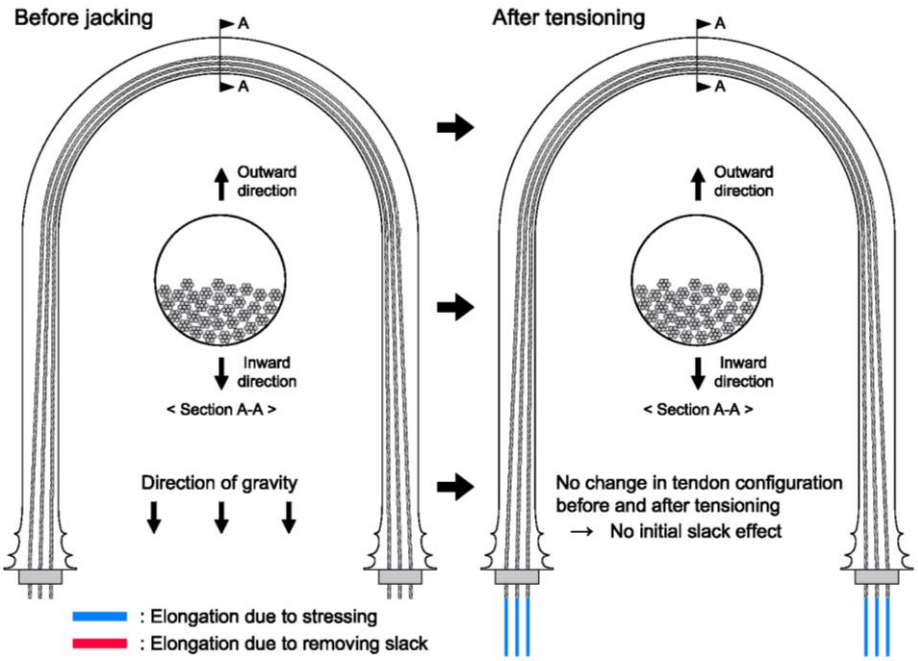

Figure 4-39 Initial slack effects in the vertical tendons of the nuclear containments

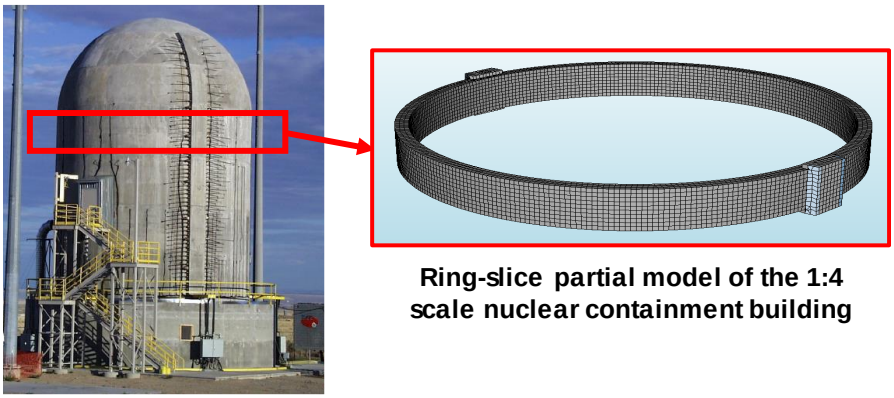

Figure 4-40 The numerical analysis model: ring-slice partial model of the 1:4 scale nuclear containment building (the picture was taken from Hessheimer et al. (2003))

(a) Tendon arrangement (b) After construction (c) After structural failure mode test (SFMT)

Figure 4-41 Overpressurization test of a 1:4 scale prestressed concrete containment vessel model conducted by Sandia National Laboratory (Hessheimer et al., 2003)

The original nuclear containment building, which is the base model of the experiment (Hessheimer et al., 2003), had unbonded bare-strand tendons as a post-tensioning system. A tendon had 48 bare-strands. For the 1:4 scale experiment, the cross-sectional area of the tendon was reduced to 1/16 and the number of strands in a tendon was reduced to 3 strands in the experiment. Since the main parameter of this analysis is the tensile force deviation in the individual strands in this analysis, it is assumed that 48 equivalent strands are installed in the 1:4 scale-model. Each equivalent strand has 1/16 cross-sectional area of the strand used in the experiment. The differential tensile forces applied to the 48 equivalent strands are considered by the equivalent tendon material model proposed in **Chapter 3**. The 48 strands in the tendon are modeled as one large equivalent strand in the analysis model. In other words, the deviations of individual tensile forces are reflected in the stress-strain relationship of the equivalent strand (tendon). To analyze the effects of bonded vs. unbonded condition of tendons, both of the analysis models with unbonded tendons (same as the experiment) and bonded tendons are modeled.

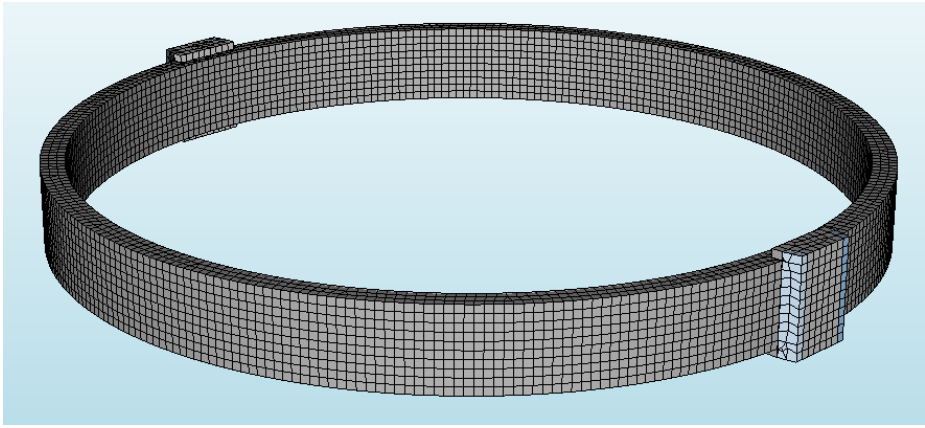

(a) Concrete wall, liner plate and buttress

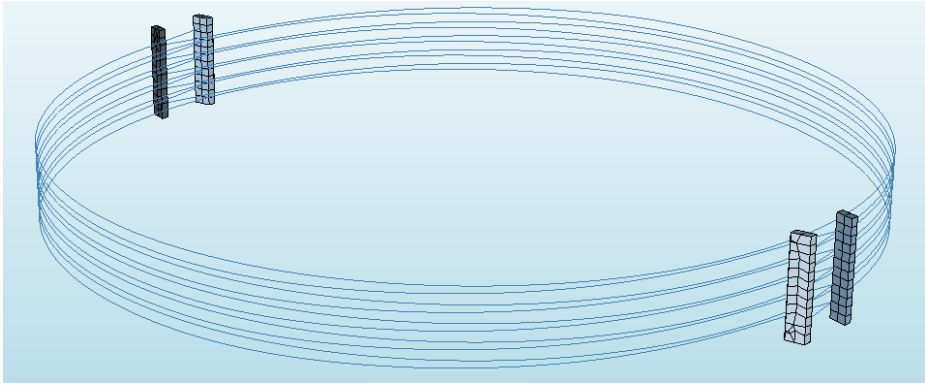

(b) Tendon and anchorage block

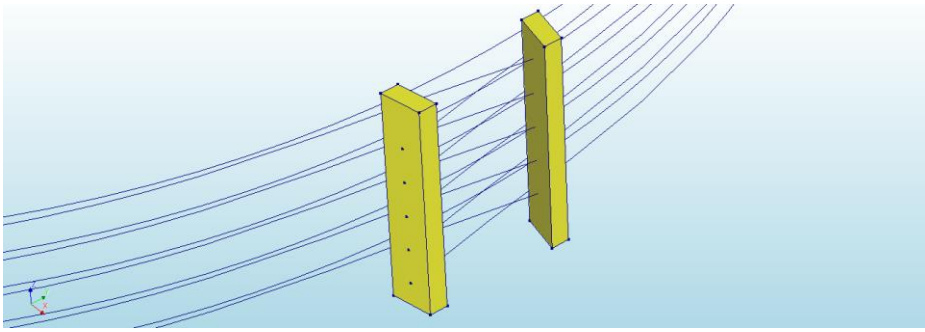

(c) Tendon and anchorage block

Figure 4-42 Numerical analysis model in DIANA FEA for ring-slice partial model of 1:4 scale nuclear containment building

Geometrical properties

The geometrical properties of the analysis model are as follows (**Figure 4-42**): The inner and outer radii of the wall are 5,375 mm and 5,700 mm, respectively. The thickness and height of the wall are 325 mm and 1,125 mm, respectively. Ten, 360° circular tendons are arranged at an interval of 112.5 mm. Five tendons are anchored at the first buttress (0°) and the other five tendons are anchored at the second buttress (180°). The radius of the tendon is 5,610 mm. The cross-sectional area of a tendon is 339.3 mm^2 (In the experiment, it consists of three 13.7 mm seven-wire strands with a cross-sectional area of 113.1 mm^2). The analysis focuses on the inner pressure resistance performance in the horizontal radial direction. No vertical tendons are modeled.

Two buttresses are placed at the location of each end of a diameter of the wall (0° and 180° directions of the wall in **Figure 4-44**), with a width of 1,020 mm and a thickness of 550 mm (including the thickness of the wall). Non-prestressed D22 reinforcement (A_s = 380.13 mm^2) is placed in the longitudinal (circumferential) direction in two layers, inside and outside the tendons. Vertical and shear reinforcement is not modeled as it is expected to have negligible effects on the structural performance in the horizontal direction. A liner plate is modeled as a 1.8 mm thick steel plate inside the concrete wall.

Material properties

The material properties and material models applied to the analysis model are as follows (**Table 4-12**): Concrete used in the concrete wall has a 47.2 MPa compressive strength (f_c'). To define material properties of the concrete, the total strain based crack model (DIANA FEA, 2016) is used. Stress-strain relationship for compressive behavior is defined with the Thorenfeldt model, and tensile behavior is defined with the linear-ultimate crack strain model (**Figure 4-43**).

The yield strength (f_y) of the steel used in the liner plate is 375.7 MPa, and the tensile strength (f_u) is 499.3 MPa. For the liner plate, an elasto-plastic stress-strain relationship with strain hardening is applied (**Figure 4-43**). Non-prestressed D22 reinforcing bars have elasto-perfectly plastic stress-strain relationship with 459.0 MPa yield strength (f_y) (**Figure 4-43**). The prestressing steel is a 7-wire strand with a yield strength (f_{py}) of 1,680 MPa and a tensile strength (f_{pu}) of 1,857 MPa. For the prestressing steel, multi-linear stress-strain relationship based on the prestressing steel material model proposed by Mattock (1979) (**Eq. 3-2**) is applied (**Figure 4-43**).

Table 4-12 Material properties of the analysis model

Material	**Material properties**			
Concrete	f_c' (MPa)	f_t (MPa)	E_c (MPa)	-
	47.2	4.02	25,000	-
Liner plate	f_y (MPa)	f_u (MPa)	E_s (MPa)	ε_u (mm/mm)
	375.7	499.3	218,800	0.051
Non-prestressed rebar	f_y (MPa)	-	E_s (MPa)	-
	459.0	-	191,000	-
Prestressing steel	f_{py} (MPa)	f_{pu} (MPa)	E_p (MPa)	ε_{pu} (mm/mm)
	1,680	1,857	199,100	0.045

Note: f_c' is compressive strength of concrete; f_t is tensile strength of concrete; E_c is elastic modulus of concrete; f_y is yield strength of liner plate or non-prestressed rebar; f_u is tensile strength of liner plate; E_s is elastic modulus of liner plate or non-prestressed rebar; ε_u is ultimate strain of liner plate; f_{py} is yield strength of prestressing steel; f_{pu} is tensile strength of prestressing steel; E_p is elastic modulus of prestressing steel; and ε_{pu} is ultimate strain of prestressing steel.

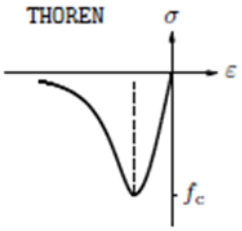

(c) Thorenfeldt

(a) Concrete compressive behavior: Thorenfeldt model (DIANA FEA, 2016)

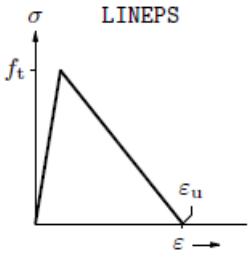

(d) linear, ultimate strain based

(b) Concrete tensile behavior: linear-ultimate crack strain model (DIANA FEA, 2016)

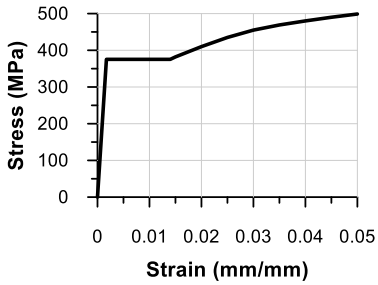

(c) Liner plate: elasto-plastic stress-strain relationship with strain hardening

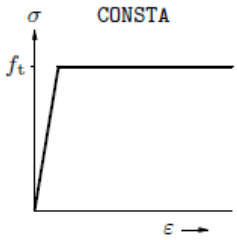

(b) ideal

(d) Non-prestressed reinforcement: elasto-perfectly plastic stress-strain relationship (DIANA FEA, 2016)

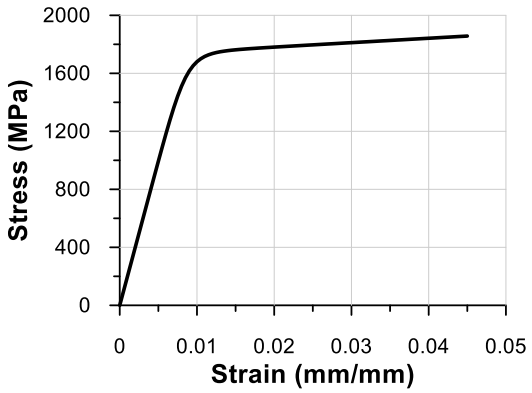

(e) Multi-linear stress-strain relationship of prestressing steel

Figure 4-43 Material models used in the analysis model

Finite element settings

In finite element analysis, 3D quadratic solid elements are used for the concrete wall, buttresses, and anchorages, and 2D quadratic shell elements are used for liner plate. 1D truss elements are used for prestressing steel, and embedded reinforcement grid elements are used for non-prestressing reinforcement. The default mesh size was set as 112.5 mm for all elements. For both bonded and unbonded tendons, alternative tendon modeling approaches using bond-slip reinforcement (Discussed in **Section 4.1**; DIANA FEA, 2016) are taken. For numerical iteration method, the Quasi-Newton (Secant) method is used.

The boundary condition for the analysis model is set as shown in **Figure 4-44**. Since the analysis focuses on the horizontal pressure resistance and deformation, the translation in the z-axis direction on the upper and lower surfaces of the concrete wall and buttresses is constrained, that is, no vertical deformation is allowed. In order to avoid unstable boundary condition, y-axis directional translation at nodal points corresponding to 0° and 180° of the concrete wall and buttresses is additionally restrained. Finally, x-axis directional translation at nodal points corresponding to 90° and 270° of the concrete wall is restrained.

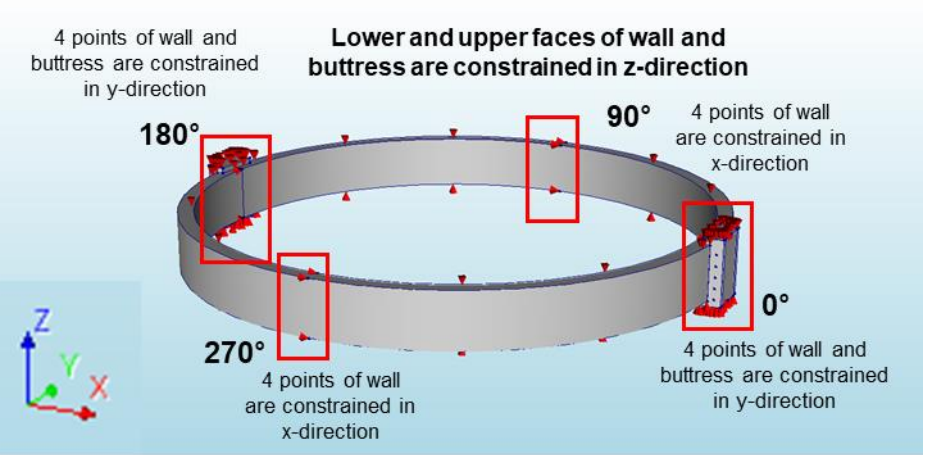

Figure 4-44 The boundary conditions in the analysis model

Tendon stress distribution along the length

As discussed in **Section 4.1**, for bonded or unbonded tendons, slip behavior and friction loss can be defined by setting the bond-slip parameters and the normal and shear stiffness moduli of bond-slip reinforcement (DIANA FEA, 2016). However, this alternative method cannot account for prestressing loss due to the wedge-slip of tendon. If the length of the tendon is short as shown in **Section 4.1**, tendon stress distribution can be modeled similarly to the theoretical distribution, by interchanging the fixed end and tensioning end and by applying the effective prestressing force calculated with consideration of the wedge-slip. However, in a long tendon, the M-shaped distribution (which can be seen in the theoretical tensile stress distribution after wedge-slip in both-end tensioning condition) cannot be described. The tensile stress distribution applied to this analysis model is different from the theoretical or measured stress distribution along the length.

Since the wedge-slip is not reflected in the model, the friction coefficients are modified in the analysis model to make average tensile stress be equal to the theoretical average tensile stress considering the wedge-slip. The tensile stress

distribution applied in the analytical model and theoretical distribution are shown in **Figure 4-45**. The applied friction coefficients and bond-slip reinforcement parameters are indicated in **Table 4-13**.

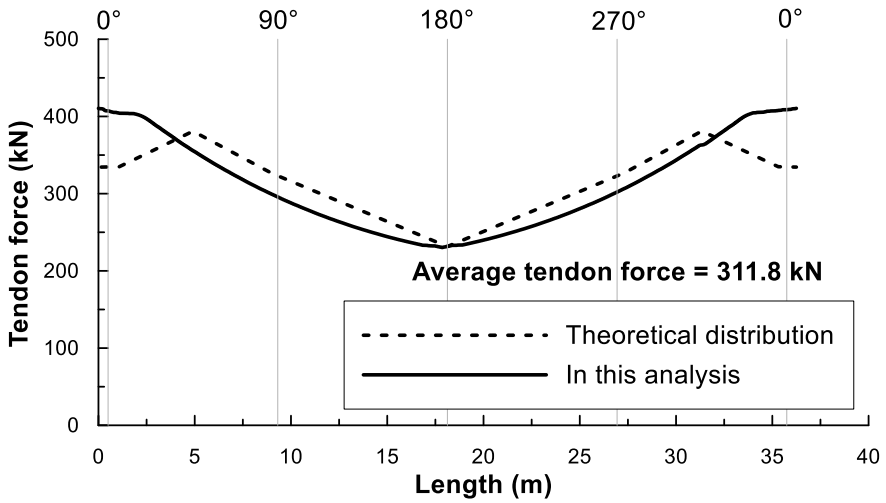

Figure 4-45 Tensile stress distribution applied in the analytical model and theoretical distribution

Table 4-13 Applied friction coefficients and bond-slip parameters in the numerical models

Type of the tendon		**Target friction coefficients in the analysis**		k_n, kN/m^3	k_t, kN/m^3	**Bond-slip parameters (Dörr, 1980)**	
		μ, /rad	k, /m			f_t, kN/m^2	dt^0, m
Unbonded tendon		0.18	0.001	2.15×10^7	-	1,640	1×10^{-7}
Bonded tendon	At jacking (unbonded state)	0.18	0.001	2.15×10^7	-	1,640	1×10^{-7}
	After grouting (bonded state)	-	-	2.15×10^7	2.15×10^7	-	-

Note: the measured curvature and wobble friction coefficients in the experiment (Hessheimer, 2003) were 0.21 and 0.001, respectively; μ is the target curvature friction coefficient; k is the target wobble friction coefficient; k_n is the normal stiffness modulus; k_t is the shear stiffness modulus; f_t is the bond-slip parameter; and dt^0 is the shear slip at start plateau in the bond slip model (Dörr, 1980).

4.3.2 Analysis parameters

To understand the effect of the tensile force deviation on the structural behavior of ring-shaped partial model of a nuclear containment building under inner pressure, three effective variables are considered. Each tendon is modeled as one large equivalent strand, which has stress-strain relationship defined by the equivalent tendon material model (**Section 3.1**). The analysis parameters are selected as follows:

- Bonded/unbonded condition of the tendon
- Average tensile stress of the tendon
- Standard deviation (C.O.V.) of the tensile stresses in the individual strands

In this analysis, only normal distribution is considered as a distribution type of individual tensile stresses. Distribution type is not considered as a variable. Also, the prestressing steel ratio and application of the equivalent tendon material model are not considered as a variable in this analysis.

A total of 20 analyses are conducted with the aforementioned parameters. The analysis parameters applied to each numerical model are summarized in **Table 4-14**. The naming rule is summarized in **Figure 4-46**. **Figure 4-47** shows the distribution of applied tensile stresses in the 'virtual' 48 individual strands in a tendon and corresponding equivalent tendon material models. The equivalent tendon material models suggested in **Figure 4-47** are applied to the numerical models, as a stress-strain relationship of the tendon.

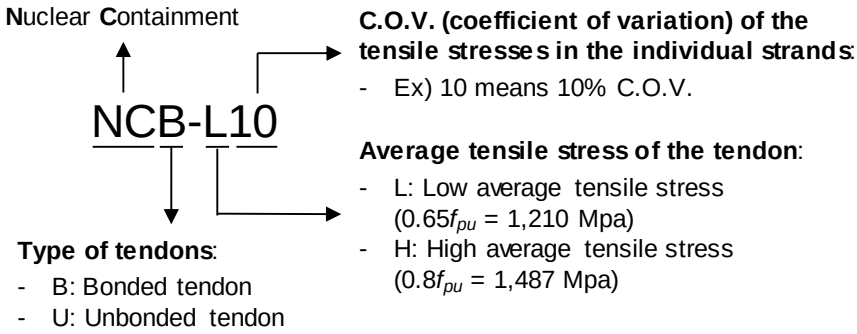

Figure 4-46 Naming rules for the nuclear containment numerical models

Table 4-14 Parameters used for the ring-shaped partial model analysis

Numerical model	Type of the tendons	Average tensile stress of tendon	C.O.V. (%)	Standard deviation (MPa)	Equivalent tendon material model		
					f_{py} (MPa)	f_{pu} (MPa)	ε_{pu} (%)
NCB-L0	Bonded tendon	$0.65f_{pu}$ (=1,210 MPa)	0	0	1,680	1,857	4.50
NCB-L5.0			2.5	30.3	1,679	1,855	4.47
NCB-L5.0			5.0	60.5	1,678	1,854	4.43
NCB-L10			10	121.0	1,675	1,852	4.35
NCB-L15			15	181.5	1,668	1,848	4.24
NCB-L25			25	302.5	1,625	1,800	3.43
NCB-H0		$0.8f_{pu}$ (=1,487 MPa)	0	0	1,680	1,857	4.50
NCB-H2.5			2.5	37.2	1,679	1,855	4.43
NCB-H5.0			5.0	74.4	1,678	1,852	4.34
NCB-H10			10	148.7	1,674	1,804	3.78
NCU-L0	Unbonded tendon	$0.65f_{pu}$ (=1,210 MPa)	0	0	1,680	1,857	4.50
NCU-L2.5			2.5	30.3	1,679	1,855	4.47
NCU-L5.0			5.0	60.5	1,678	1,854	4.43
NCU-L10			10	121.0	1,675	1,852	4.35
NCU-L15			15	181.5	1,668	1,848	4.24
NCU-L25			25	302.5	1,625	1,800	3.43
NCU-H0		$0.8f_{pu}$ (=1,487 MPa)	0	0	1,680	1,857	4.50
NCU-H2.5			2.5	37.2	1,679	1,855	4.43
NCU-H5.0			5.0	74.4	1,678	1,852	4.34
NCU-H10			10	148.7	1,674	1,804	3.78

Note: f_{py} is yield strength of equivalent tendon, which is defined as the stress at 1% elongation; f_{pu} is ultimate tensile strength of equivalent tendon; and ε_{pu} is elongation at ultimate tensile strength (f_{pu})

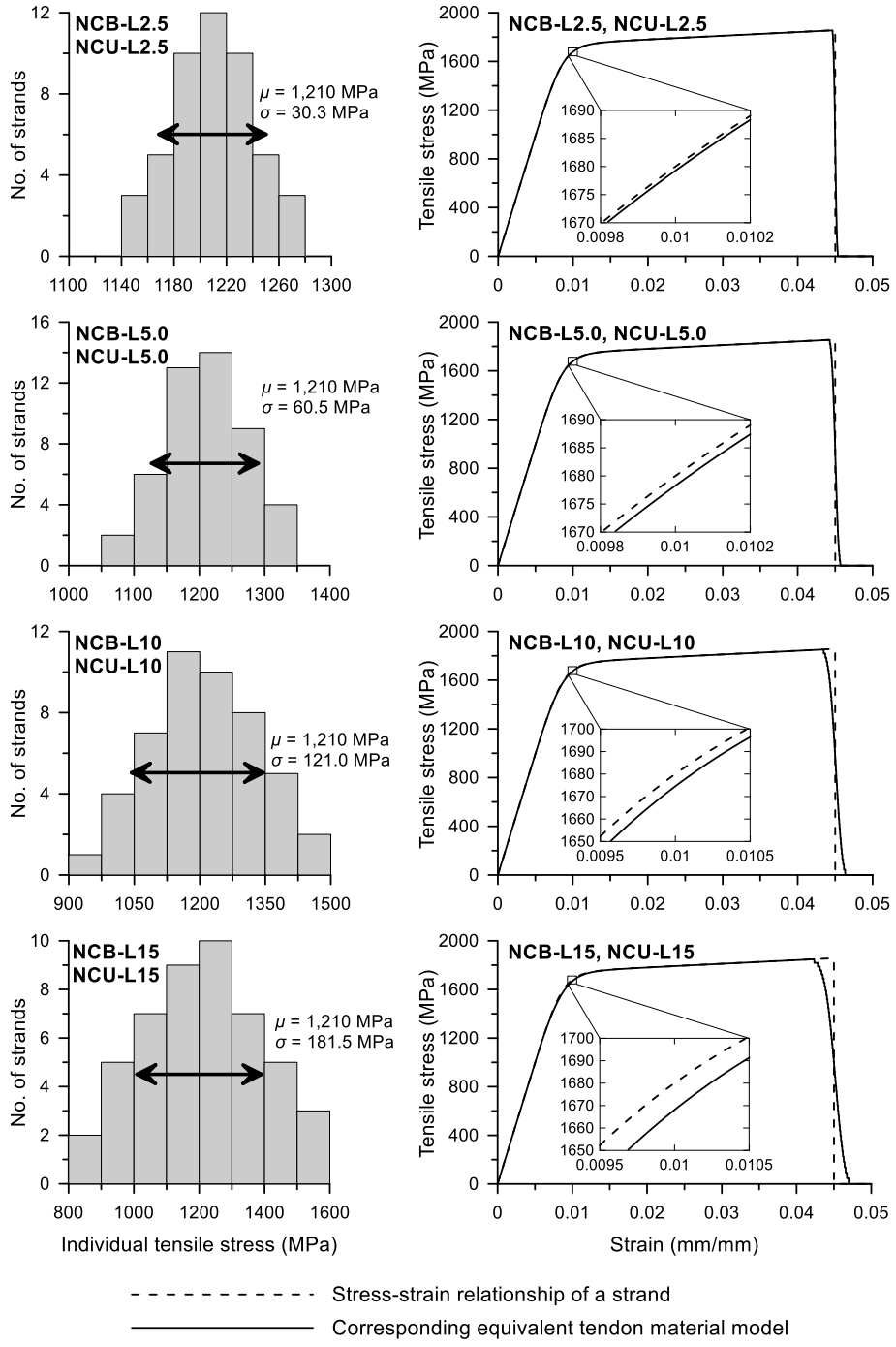

Figure 4-47 Distribution of individual tensile stresses and corresponding equivalent stress-strain relationship of a tendon

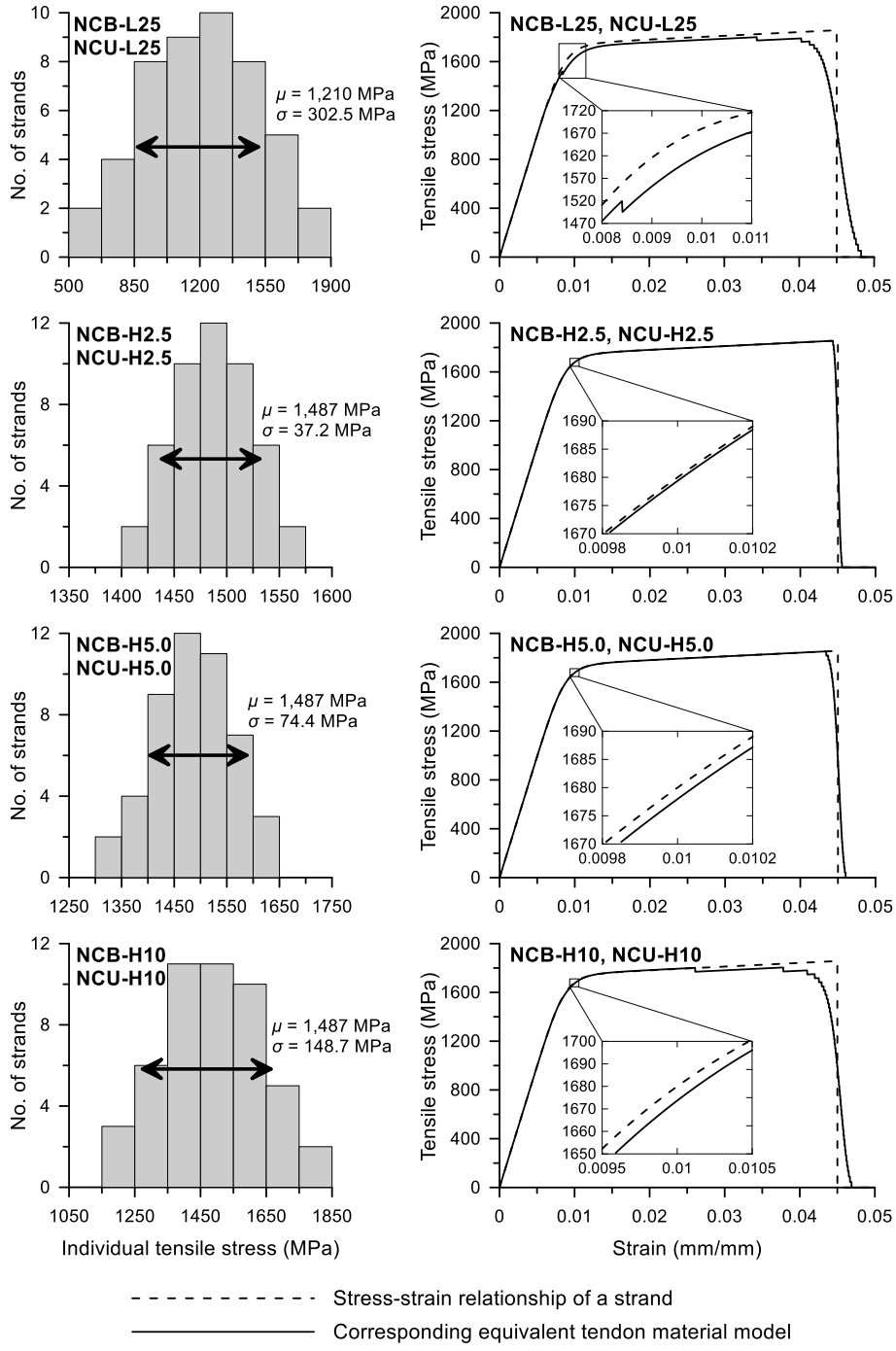

Figure 4-47 Distribution of individual tensile stresses and corresponding equivalent stress-strain relationship of a tendon (continued)

4.3.3 Analysis results: ultimate capacity for inner pressure

From the analysis with aforementioned parameters, the pressure-displacement curves for the ring-slice partial models of nuclear containments subjected to inner pressure can be obtained. The pressure-displacement curves obtained from each analysis series are shown in **Figures 4-48 ~ 55**. The ultimate inner pressure, inner pressure at cracking, and percentage of inner pressure capacity reduction in reference to the analysis models with no tensile force deviations (NCB-L0, NCB-H0, NCU-L0, and NCU-H0) are summarized in **Table 4-15**.

Table 4-15 Effects on the ultimate inner pressure capacities

Series	**Effects on the ultimate inner pressure capacities**						
NCB-L	C.O.V. (%)	0	2.5	5.0	10	15	25
	Ultimate inner pressure (MPa)	0.9496	0.9496	0.9495	0.9534	0.9568	0.9445
	Pressure at cracking (MPa)	0.8665	0.8664	0.8664	0.8664	0.8663	0.8646
	Strength reduction (%)	0	-0.002	0.008	-0.401	-0.768	0.535
NCB-H	C.O.V. (%)	0	2.5	5.0	10		
	Ultimate inner pressure (MPa)	1.0853	1.0854	1.0856	1.0883		
	Pressure at cracking (MPa)	0.9947	0.9947	0.9946	0.9946		
	Strength reduction (%)	0	-0.009	-0.033	-0.278		
NCU-L	C.O.V. (%)	0	2.5	5.0	10	15	25
	Ultimate inner pressure (MPa)	0.9353	0.9353	0.9352	0.9386	0.9340	0.9378
	Pressure at cracking (MPa)	0.8648	0.8648	0.8648	0.8647	0.8646	0.8643
	Strength reduction (%)	0	0.003	0.008	-0.354	0.142	-0.269
NCU-H	C.O.V. (%)	0	2.5	5.0	10		
	Ultimate inner pressure (MPa)	1.0622	1.0623	1.0622	1.0617		
	Pressure at cracking (MPa)	0.9720	0.9720	0.9720	0.9718		
	Strength reduction (%)	0	-0.006	0.008	0.051		

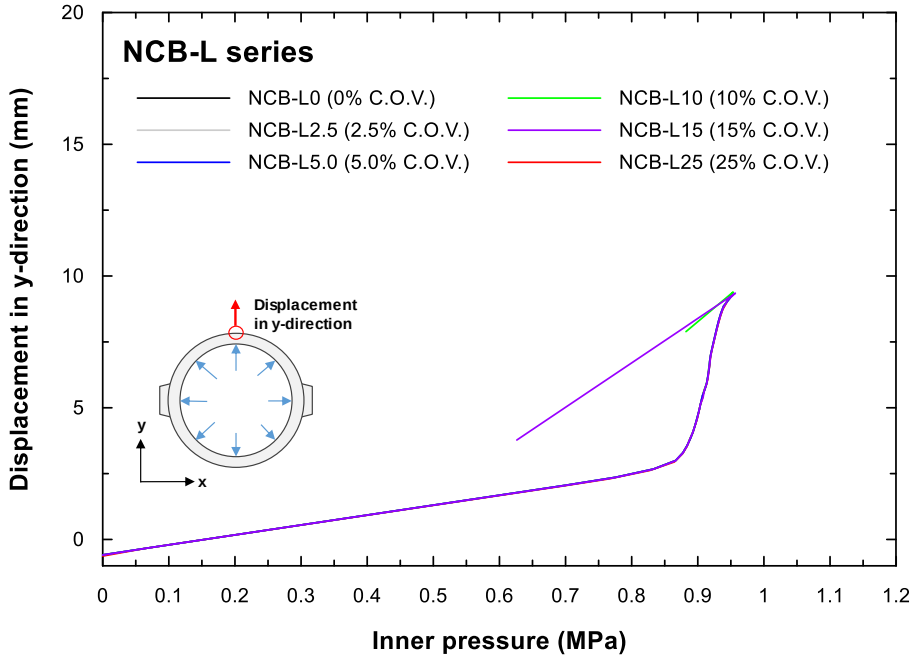

Figure 4-48 Pressure-displacement curves for the NCB-L series (90° azimuth)

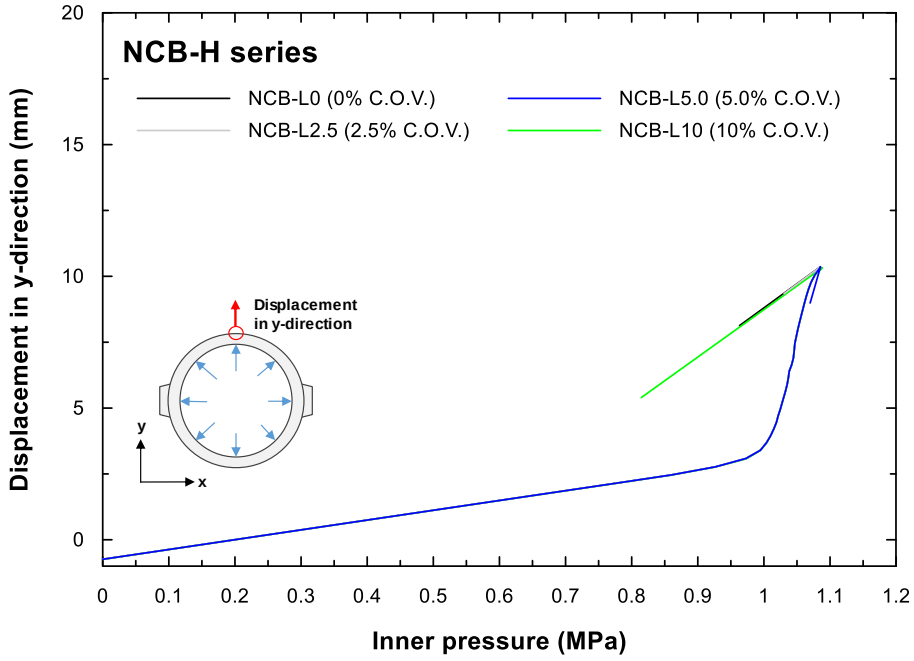

Figure 4-49 Pressure-displacement curves for the NCB-H series (90° azimuth)

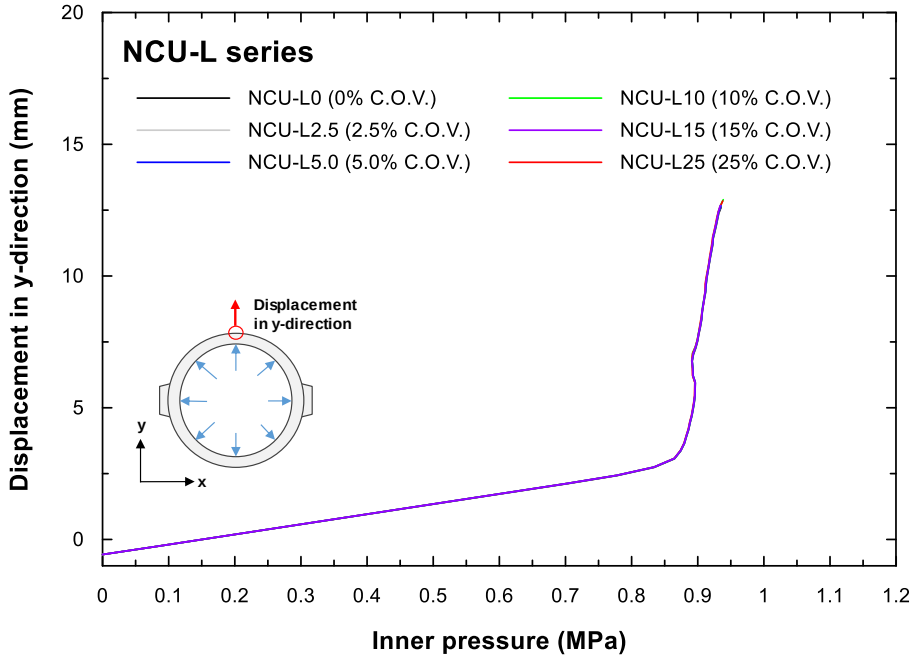

Figure 4-50 Pressure-displacement curves for the NCU-L series (90° azimuth)

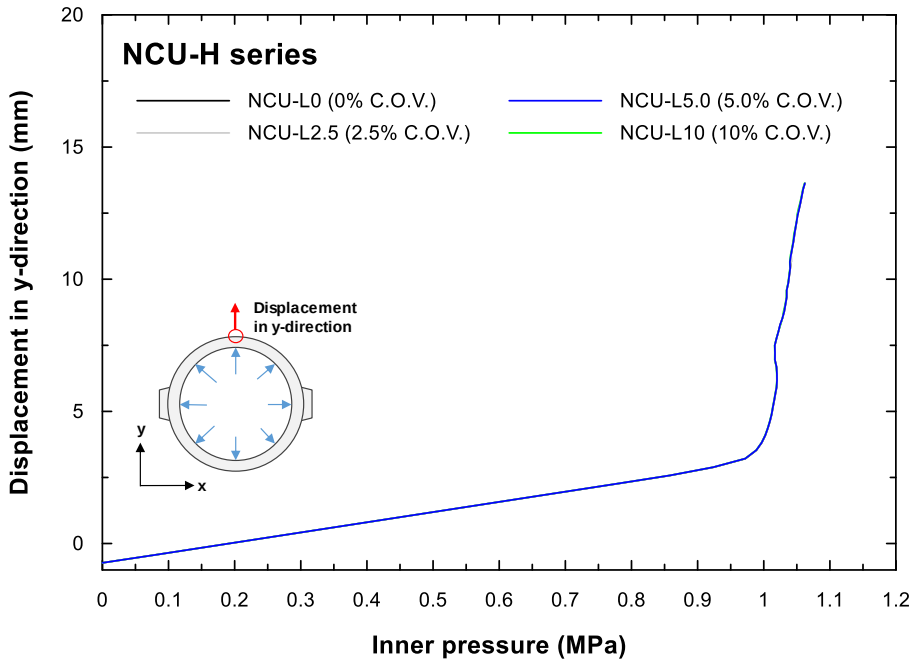

Figure 4-51 Pressure-displacement curves for the NCU-H series (90° azimuth)

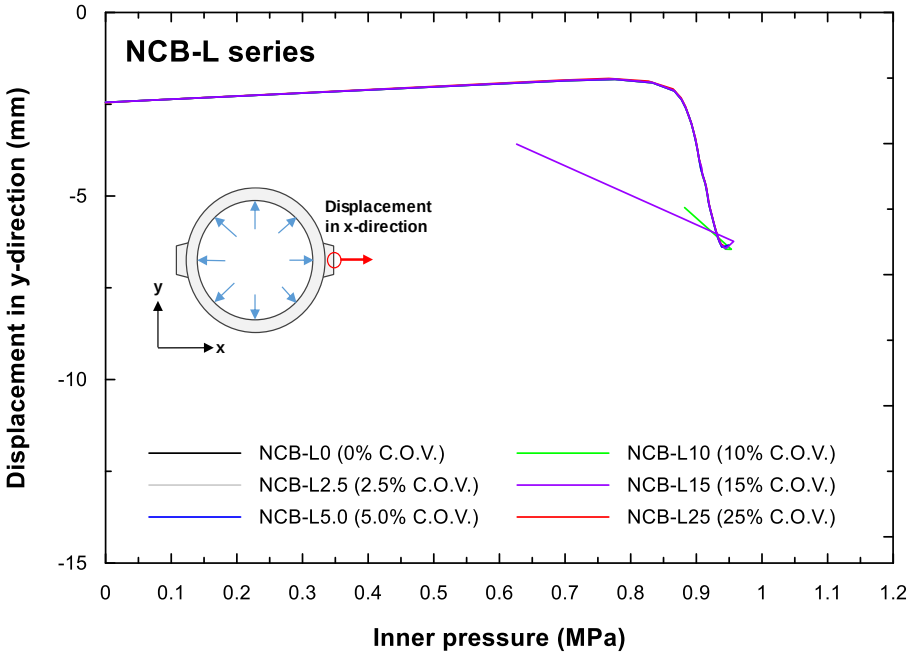

Figure 4-52 Pressure-displacement curves for the NCB-L series (0° azimuth)

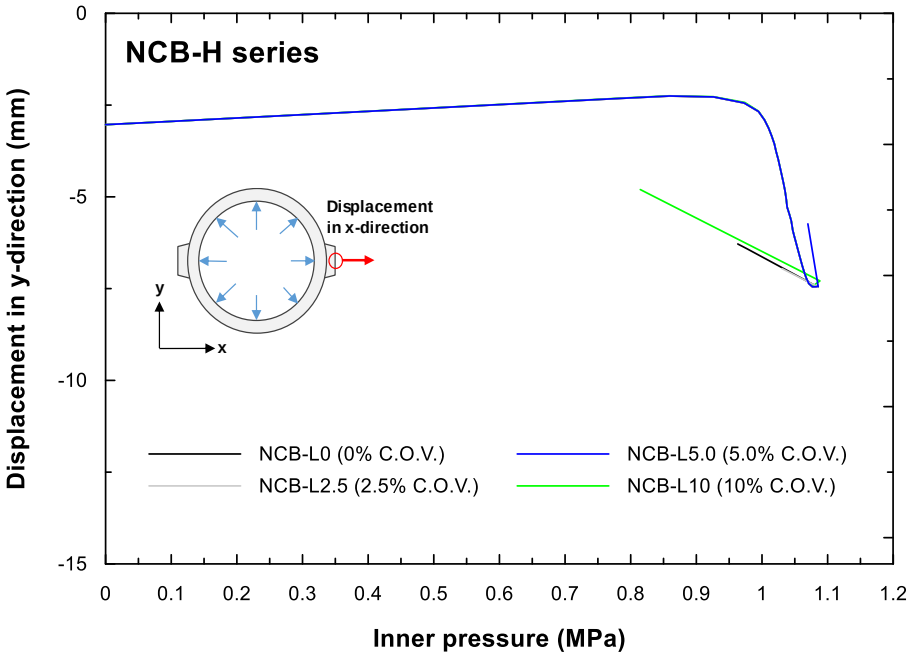

Figure 4-53 Pressure-displacement curves for the NCB-H series (0° azimuth)

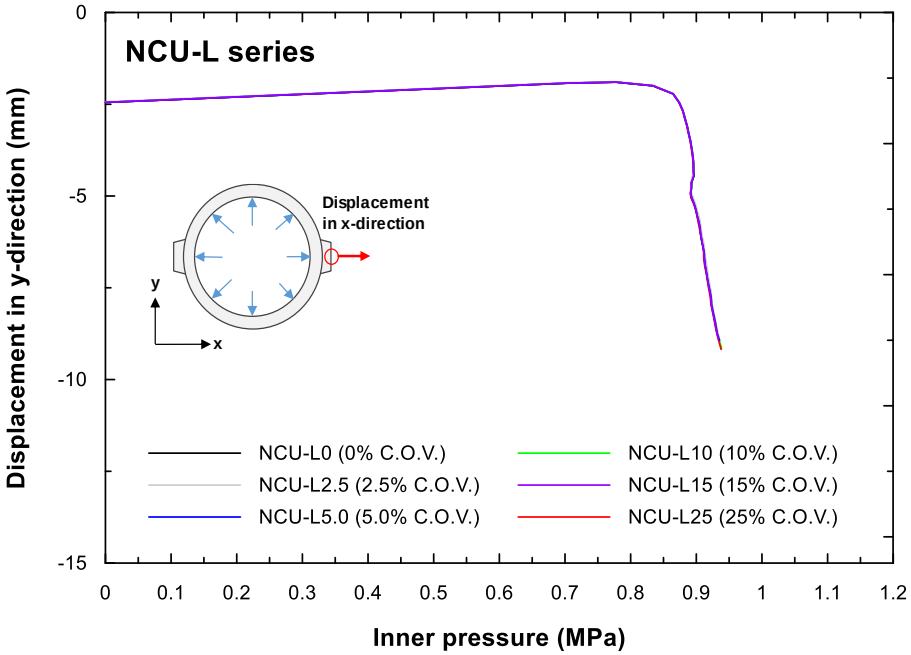

Figure 4-54 Pressure-displacement curves for the NCU-L series (0° azimuth)

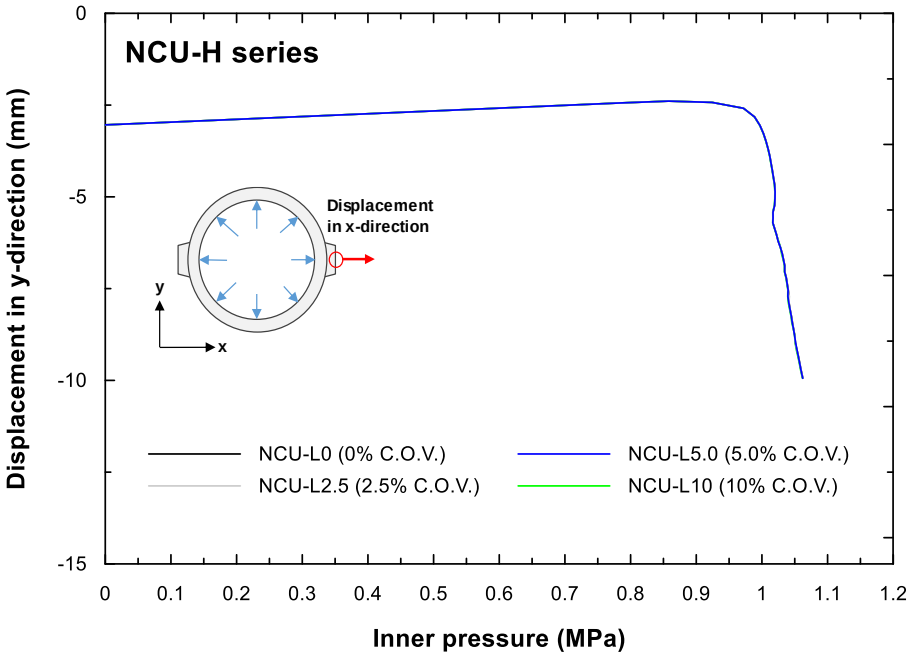

Figure 4-55 Pressure-displacement curves for the NCU-H series (0° azimuth)

The analysis results show that the individual tensile stress deviation has negligible effect on the ultimate inner pressure capacity of ring-shaped partial model. In the realistic level of tensile force deviations under 5% C.O.V., the reduction of ultimate inner pressure is under 0.03%. Considering the error due to the analysis settings such as load step size and/or convergence criteria, it can be concluded that there is 'negligible' or 'no' strength reduction effect due to the individual strand tensile force deviation. Even though there is large tensile force deviation around 25% C.O.V., the decrease of ultimate inner pressure is less than 0.5%.

Figure 4-56 shows the corresponding equivalent tendon material models for the NCB-L, NCB-H, NCU-L, and NCU-H series, and difference of tensile stress of the tendon due to the tensile force deviation is shown for the given tendon strain. The tendon stress and strain at ultimate stages (f_{ps} and ε_{ps}) are marked in the graphs (**Figure 4-56**). The marked f_{ps} and ε_{ps} are calculated in the tendon elements located at jacking ends.

Figures 4-56 ~ 58 show that the calculated f_{ps} is much smaller than the yield stress of strand, even under ultimate pressure. Considering that the decrease of tensile stress due to individual strand force deviation is significant near the equivalent yield stress of tendon, it can be concluded that the effect of tensile force deviation on the equivalent tendon stress-strain relationship is not significant in this analysis.

Also, the marked f_{ps} and ε_{ps} in **Figure 4-56** are calculated at the jacking ends (near buttresses), where tensile stress of tendon has the highest value. In the remained region except the buttress, tensile stress is smaller than that in the buttress region (**Figures 4-45**, **57**, and **58**). It means that the effect on equivalent tendon stress-strain relationship is less than the buttress region.

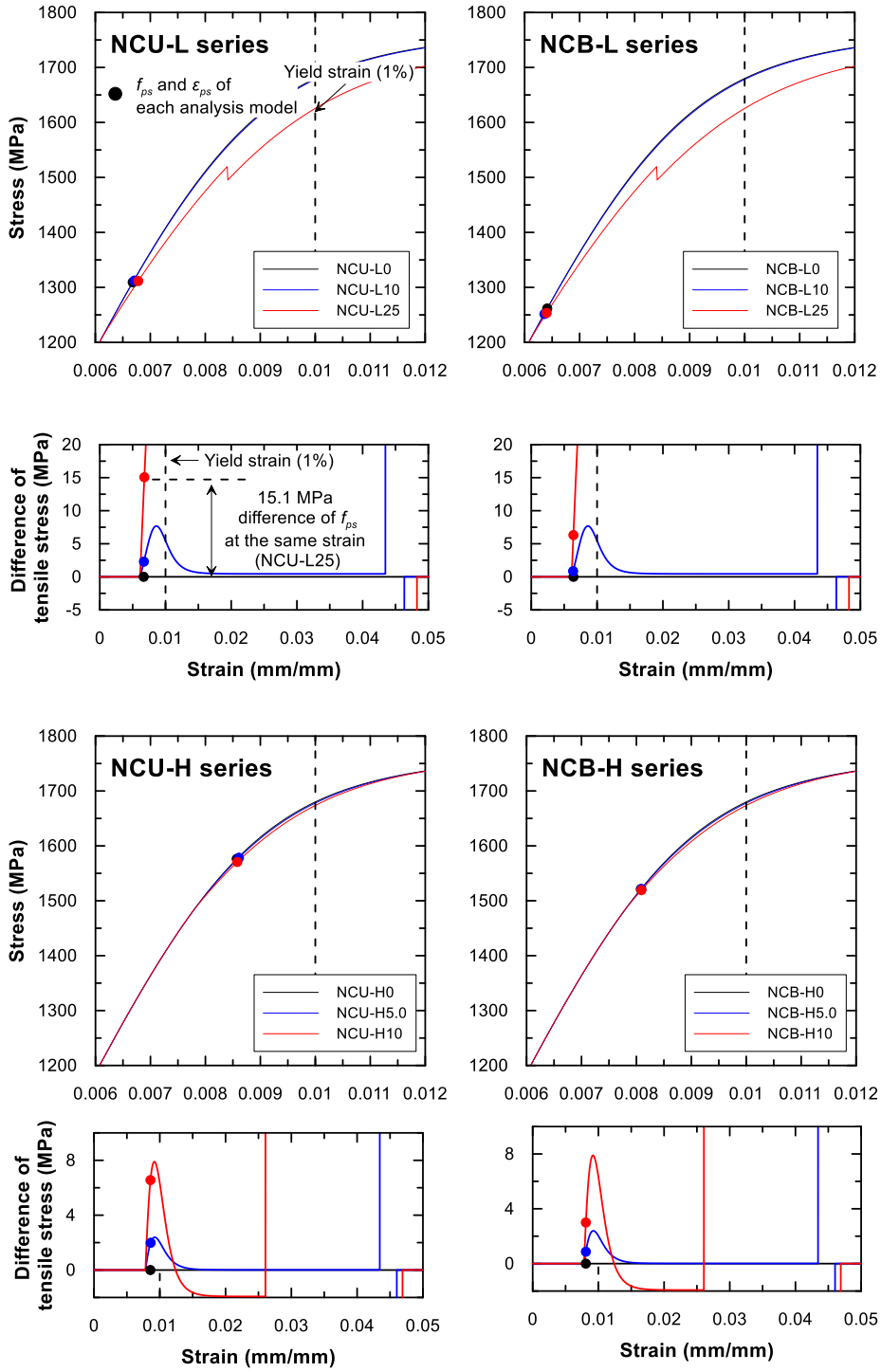

Figure 4-56 Equivalent tendon material models and the tendon stress and strain at ultimate state (f_{ps} and ε_{ps})

As shown in **Figure 4-56**, when the equivalent tendon material model is constructed using the individual strand tensile force distribution of jacking ends ($0.65f_{pu}$ for NCB-L and NCU-L series; $0.8f_{pu}$ for NCB-H and NCU-H series), the individual strand tensile force deviation does not affect the equivalent tendon stress-strain relationship under $0.65f_{pu}$ and $0.8f_{pu}$, respectively.

As a result, in this analysis, the difference of equivalent tendon stress-strain relationship due to tensile force deviation is perceptible only in the vicinity of jacking ends (near buttresses), where the tensile stress is the highest. Whereas the difference of equivalent tendon stress-strain relationship can be neglected in other regions. In fact, although the decrease of tensile stress due to tensile force deviation can occur in other regions except the buttresses, the tensile stress decrement effect is negligible because the tensile stress in those regions is much smaller than the yield stress.

4.3.4 Analysis results: tensile stress increment

In **Section 4.2**, the tendons of PT beams were modeled as 7 individual strands; therefore, the tensile stress increment could be analyzed for individual strands (**Figures 4-32 ~ 36**). Whereas, in the numerical analysis of this section, the tendons are modeled using the equivalent tendon material model, the tensile stress increment of individual strands cannot be analyzed. **Figures 4-57** and **58** show the tensile stress increment due to increasing load (inner pressure) for both NCB series (bonded tendon) and NCU series (unbonded tendon). The tendon at the middle height of analysis model (**Figure 4-42**) is monitored. Due to the long length and large cumulative angle change of tendon, the friction loss along the length is significant. The tensile stress increment is analyzed for three regions corresponding to the jacking end, 1/4 length, and 1/2 length.

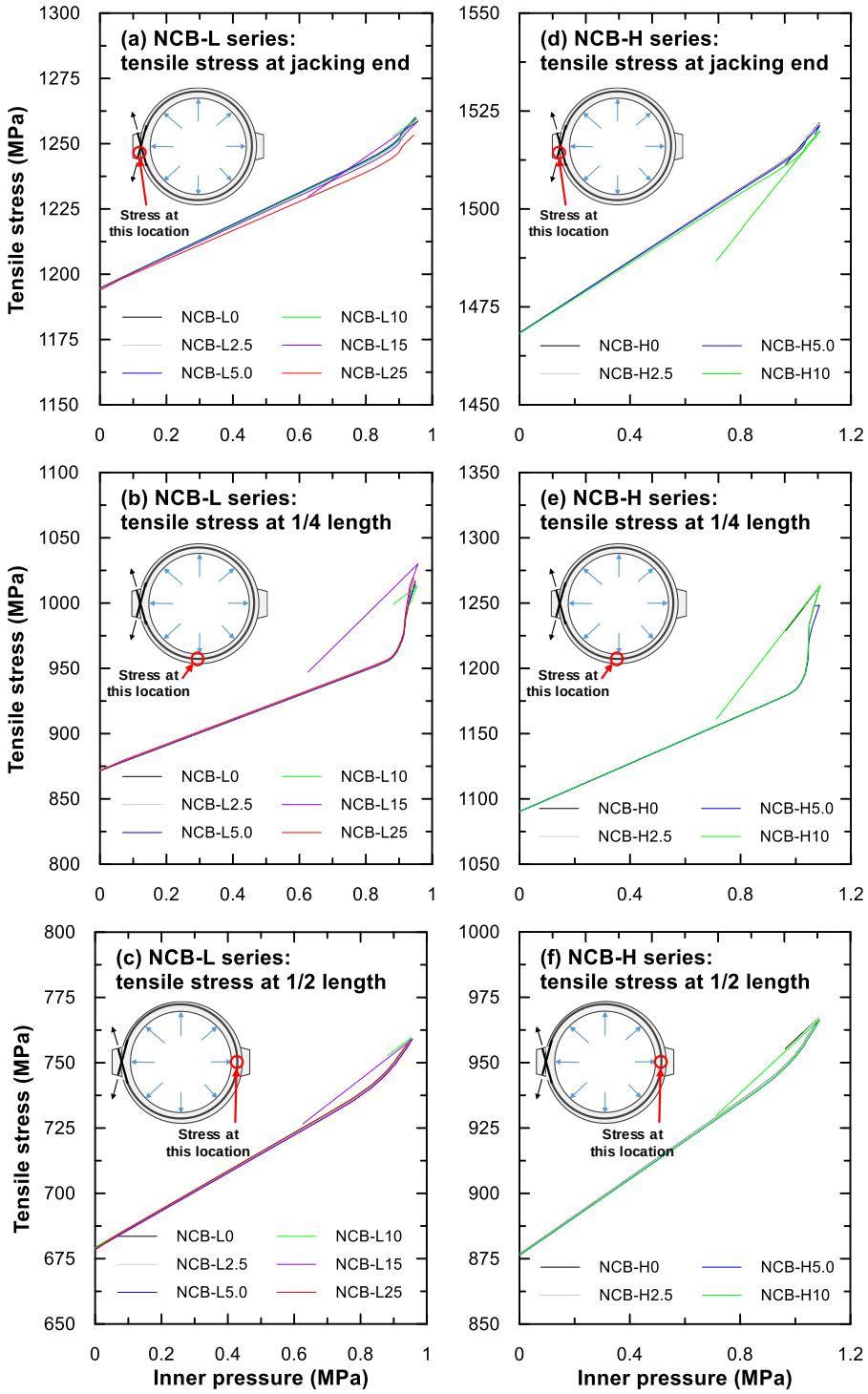

Figure 4-57 Tensile stress increment curves for the NCB series (bonded tendons)

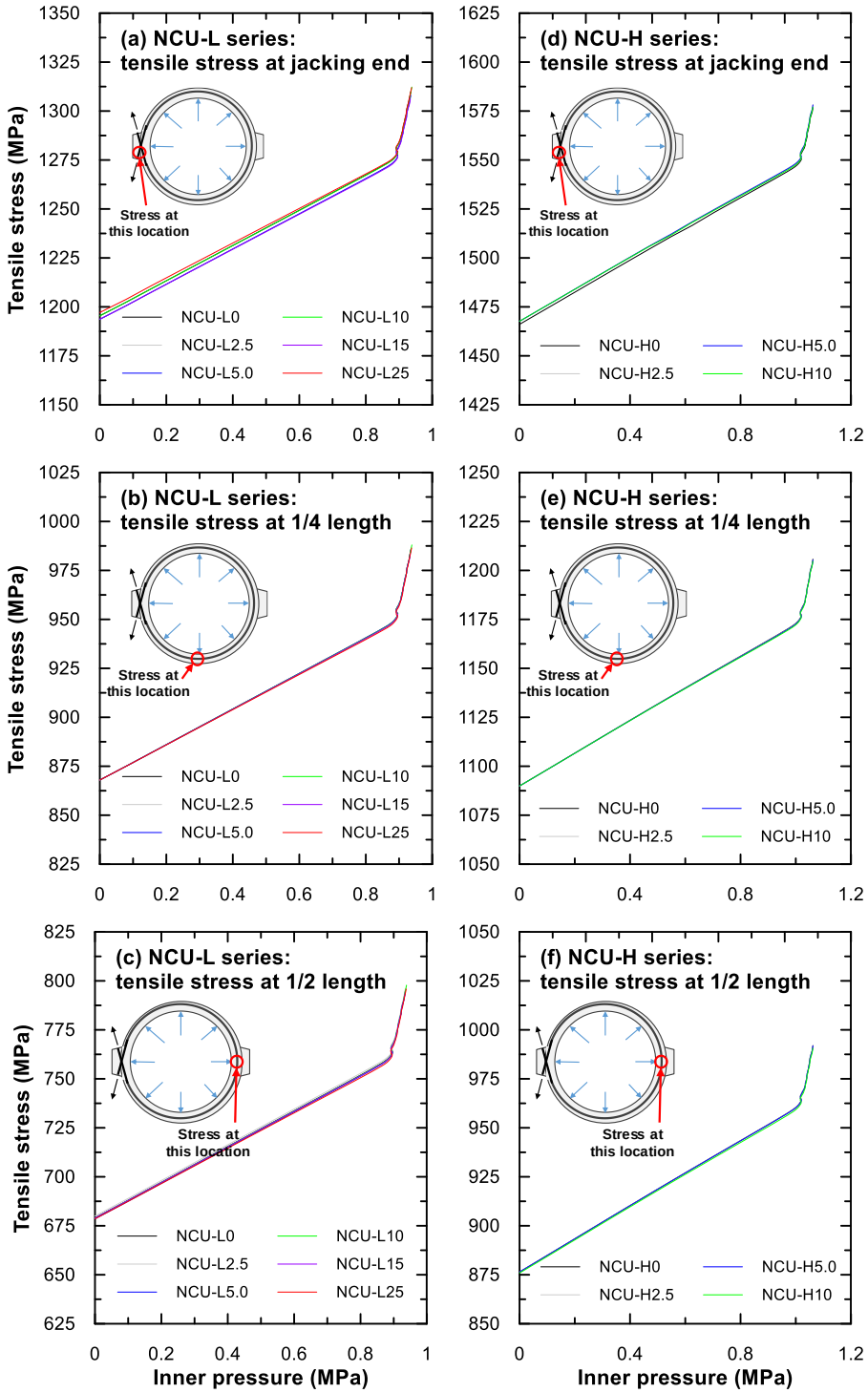

Figure 4-58 Tensile stress increment curves for the NCU series (unbonded tendons)

Comparing the results between **Figures 4-57** and **58**, it can be noticed that the characteristics of the bonded and unbonded tendons are properly reflected in the corresponding numerical model. In the bonded tendon (**Figure 4-57**), there is a difference in the tensile stress increment in each monitored region, which is consistent with the fact that the strain compatibility with the concrete wall exists. Near the buttress (Jacking end and 1/2 length of monitored tendon) where the deformation is relatively small, tensile stress increment of around 75 MPa is observed between the initial and ultimate states. However, near the 1/4 length region where the deformation is relatively large, tensile stress increment of around 150 MPa is observed. On the other hand, in the unbonded tendon (**Figure 4-58**), consistent tensile stress increment of around 100 MPa is observed in each monitored region. These results are consistent with the characteristics of unbonded tendon, that is, tensile strain is almost equally distributed along the length.

As mentioned in the previous section, tensile stress at the ultimate state (f_{ps}) is in linear region of equivalent stress-strain relationship. Tensile stress is low except the jacking end region due to large friction loss. This means that in the analysis using the equivalent tendon material model, except for the region with high tensile stress near the jacking end, the effect of individual strand force deviation on the tensile stress reduction is close to zero, even though the standard deviation of individual tensile forces is large.

The material properties of equivalent tendon and structural behavior can be changed by individual strand force deviation only near the buttress (jacking end). However, as can be seen in **Figures 4-57** and **58**, f_{ps} does not increase significantly at the jacking end, even though tensile stress is the highest. This is because the concrete under tensile stress caused by inner pressure is fractured prematurely, the failure of the whole structure precedes yielding of the tendon. As mentioned in **Section 3.1**, tensile stress reduction due to the tensile force deviation is large when the f_{ps} reaches near the equivalent yield strength (f_{py}). The difference in structural behavior due to the tensile force

deviation is not clearly distinguished in this analysis.

In conclusion, due to the combined effect of the relatively low tensile stress associated with large friction loss and the fact that shell structures subjected to internal pressure do not significantly increase the f_{ps}, the strength reduction effect is not clearly observed as shown in **Figures 4-48 ~ 55**.

4.4 Discussion

In this chapter, an alternative modeling approach for unbonded and bonded post-tensioning tendons using the Bond-slip reinforcement (DIANA FEA, 2016) is verified and compared with the previous experimental data (Mattock et al., 1971). Based on the modeling method, a series of numerical analyses of unbonded and bonded PT beams and ring-shaped partial models of nuclear containment structures subjected to individual strand force deviation are performed.

As discussed in **Section 4.1**, the modeling method using the Bond-slip reinforcement (DIANA FEA, 2016) depicts the friction-slip behavior between prestressing steel and concrete quite well. Also, the tensile stress increment with increasing external load can be adequately described. It could be a useful alternative method to model the interaction between tendon and concrete. However, since the Bond-slip reinforcement (DIANA FEA, 2016) is not specialized for post-tensioning tendon, it is difficult to precisely define wobble and curvature friction coefficients or anchor set loss. There is a limitation to accurately describe the characteristics of post-tensioning tendons.

In **Section 4.2**, the influence of individual strand force deviation on the flexural strength reduction of PT beams is analyzed. In general, there is a tendency that the flexural strength decreases, as the deviation increases. This

is due to the phenomenon that the tensile stress of equivalent tendon decreases at the same strain due to the increased tensile force deviation. However, considering the results that the analysis model with the largest flexural strength reduction shows 3.3% reduction, and the models with realistic ranges of tensile force deviation (under 10% C.O.V.) show negligible reduction in strength, it can be concluded that the effect of tensile force deviation on the structural behavior is limited.

In **Section 4.3**, the effect of individual strand force deviation on the ultimate inner pressure capacity of ring-shaped partial models of nuclear containment structure is analyzed. The difference among the analysis results is not perceptible and the influence on the structural behavior is close to be zero. This is due to the combined effect of relatively low average tensile stress due to large friction loss and relatively small tensile stress at ultimate state (f_{ps}).

In common, the difference in structural behavior due to the individual strand force deviation depends on the change of equivalent tendon stress-strain relationship due to the deviation. Also, it is found that the degree of strength reduction depends on the tensile stress at ultimate state (f_{ps}). If the f_{ps} has a value close to the equivalent tendon yield strength (f_{py}), strength reduction appears to be noticeable, when the standard deviation of individual tensile forces is excessively large. In conclusion, in order to determine the effect of strand force deviation on the structural behavior, it is necessary to consider the value of f_{ps} based on the equivalent tendon material model.

Chapter 5. Conclusion

In this study, the effect of individual strand tensile force deviation on the stress-strain relationship of equivalent tendon was investigated by proposing 'equivalent tendon material model'. The effects on the ultimate strength of post-tensioned structures (PT beam and ring-shaped partial model of nuclear containment) are analyzed through the series of numerical analysis. The results can be summarized as follows:

1) From the review of current code and specification (**Section 2.1**), it is found that there are no acceptance criteria for individual strand force deviation in a post-tensioning tendon. As reported from previous studies (**Section 2.2**), bare-strand tendons had C.O.V. of individual strand force deviations of approximately 5 ~ 10% near the average tensile stress of $0.6f_{pu}$. Furthermore, larger deviation could occur in horizontal circumferential tendons unless initial arrangement jack is utilized. In case that the deviation adversely affects structural performance, certain acceptance criteria for individual strand force deviation need to be provided in the code or specification.

2) To provide a theoretical basis on the material properties of tendon affected by individual strand force deviation due to initial slack effect, the equivalent tendon material model is proposed. Based on the application of the equivalent tendon material model, it is found that the deviation in individual tensile forces can slightly reduce the equivalent yield stress of the entire tendon, and significantly reduce the tensile strength and ultimate strain. However, since the tendon stress at ultimate state (f_{ps}) typically does not reach to the tensile strength of prestressing steel in unbonded PT structures, the decrease of equivalent tensile

strength has no significant effect on the overall structural behavior of PT systems. On the other hand, the reduction in equivalent yield stress has some degree of effects on the behavior of PT structures and needs to be considered.

3) Due to the quadratic relationship between the initial stress of prestressing steel (f_{pi}) and relaxation loss, there is difference in the average relaxation loss depending on the level of tensile force deviation, even though the tendons have the same average initial tensile stress. However, the additional relaxation loss due to tensile force deviation can be neglected in the realistic level of tensile force deviation (under 10% C.O.V.).

4) Alternative modeling approach using the bond-slip reinforcement (DIANA FEA, 2016) is applied to the models with both bonded and unbonded tendons in PT structures. Using the previous experimental data (Mattock et al., 1971), it is verified that the modeling approach can be a viable alternative to describe the overall flexural and concrete-to-prestressing steel interactive behavior of PT structures.

5) From the series of numerical analysis of PT beams, it is found that there are strength reduction effects due to the individual strand force deviation. If the increased average strand force deviation is near the yield strain of the tendon (around 1% strain), the strength can be reduced perceptibly with large tensile force deviation (over 10% C.O.V.). However, in the realistic range of tensile force deviation (under 10% C.O.V.), the strength reduction effects are not significant and therefore neglected. The reduction in ultimate flexural strength is dependent on the decrease of tensile stress at ultimate state (f_{ps}) due to tensile force deviations. When the deviation is large, the decrease of f_{ps} is perceptible because of the decreased equivalent yield stress.

6) From the series of numerical analysis of the ring-shaped partial models

of a nuclear containment, it is found that the strength reduction effects can be negligible, even though the individual tensile force deviation is large. The reason is that tensile stress increment and f_{ps} are relatively small compared to those in PT beams, because the entire section of concrete wall is subjected to tensile stress under inner pressure, which results in premature failure of concrete. Another reason is that the f_{ps} reaches near the yield stress only in the region of the buttress, whereas other parts have relatively small f_{ps}, where the tensile stress reduction effects can be neglected.

In conclusion, the individual strand tensile force deviations would have limited effects on the ultimate capacity of PT structures. Based on this study, an acceptance criteria for the standard deviations of individual tensile forces may not be needed in terms of ultimate capacity of both bonded and unbonded PT structures. However, there is a need for more research on the effect of individual strand tensile force deviations on the durability and long-term behavior of PT structures.

References

1. ACI Committee 318 (2014), "Building Code Requirements for Structural Concrete and Commentary (ACI 318-14)," American Concrete Istitute, Farmington Hills, MI.

2. AASHTO (2012), "AASHTO LRFD Bridge Design Specifications, 6th Ed.," American Association of State Highway Transportation Officials, Washington D.C., USA.

3. AASHTO (2010), "AASHTO LRFD Bridge Construction Specifications, 3rd Ed.," American Association of State Highway Transportation Officials, Washington D.C., USA.

4. AFCEN (2012), "ETC-C EPR Technical Code for Civil Works," AFCEN, Courbevoie, France.

5. Chandoga, M., and Jarosevic, A. (2005), "Rehabilitation and Monitored Prestressing of Corroded Tendons," *Proceedings of the fib symposium: Structural Concrete and Time*, La Plata, Argentina.

6. Cho, K., Park, S. Y., Cho, J.-R., Kim, S. T., and Park, Y.-H. (2015), "Estimation of Prestress Force Distribution in the Multi-Strand System of Prestressed Concrete Structures," *Sensors*, V. 15, No. 6.

7. Cho, K., Cho, J.-R., Kim, S. T., Park, S. Y., Kim, Y.-J., and Park, Y.-H. (2016), "Estimation of Prestress Force Distribution in Multi-Strand System of Prestressed Concrete Structures Using Field Data Measured by Electromagnetic Sensor," *Sensors*, V. 16, No. 8.

8. DIANA FEA (2016), "DIANA User's Manual – Concrete and Masonry Analysis, Release 10.1," DIANA FEA BV, Delft, Netherlands.

9. Domage, J.-B., Elias, S., and Laurens, J.-M. (2010), "State of the Art Post-Tensioning for Nuclear Containments," *Proceedings of the 3rd fib International Congress*, Washington, D.C., USA.

10. Dörr, K. (1980), "Ein Beitrag zur Berechnung von Stahlbetonscheiben unter besonderer Berücksichtigung des Verbundverhaltens," PhD thesis, University of Darmstadt, Darmstadt, Germany.

11. Hessheimer, M. F., Klamerus, E. W., Lambert, L. D., Rightley, G. S., and Dameron, R. A. (2003), "Overpressurization Test of a 1:4-Scale Prestressed Concrete Containment Vessel Model," Sandia National Laboratories, NUREG/CR-6810, SAND2003-0840P, Albuquerque, NM.

12. Joint ACI-ASME Committee 359 (2015), “2015 ASME Boiler and Pressure Vessel Code, Section III. Rules for Construction of Nuclear Facility Components, Division 2. Code for Concrete Containments,” The American Society of Mechanical Engineers, New York, NY.

13. Kang, T. H.-K., Huang, Y., Shin, M., Lee, J. D., and Cho, A. S. (2015), “Experimental and Numerical Assessment of Bonded and Unbonded Post-Tensioned Concrete Members,” *ACI Structural Journal*, V. 112, No. 6.

14. Kang, T. H.-K., and Park, J.-H. (2016), “Full-Scale Mock-Up Tests of Nuclear Containment with HDPE-Coated Unbonded Tendons,” Presentation, Joint ACI Committee 349, Concrete Nuclear Structures, Working Group B, Nuclear Structures-Design, ACI Fall 2016 Convention, Philadelphia, PA.

15. KICT (2015), “Development of Smart Prestressing System and Grouting Technology for Prestressed Concrete Bridges,” Korea Institute of Construction Technology, Goyang, Korea. (in Korean)

16. Mattock, A. H., Yamazaki, J., and Kattula, B. T. (1971), “Comparative Study of Prestressed Concrete Beams, with and without Bond,” *ACI Journal Prodeedings*, V. 68, No. 2.

17. Mattock, A. (1979), “Flexural Strength of Prestressed Concrete Sections by Programmable Calculator,” *PCI Journal*, V. 24, No. 1.

18. Namman, A. E. (2004), “Prestressed Concrete Analysis and Design: Fundamentals, 2nd Ed.,” Techno Press 3000, Ann Arbor, MI.

19. Park, J., and Hong, J. (2009), “Present Status of Nuclear Containments and ISI in Korea,” *Progress in Nuclear Energy*, V. 51, No. 8.

20. PTI (2006), “Post-Tensioning Manual, 6th Ed.,” Post-Tensioning Institute, Farmington Hills, MI.

21. PTI/ASBI (2012), “PTI/ASBI M50.3-12 Guide Specification for Grouted Post-Tensioning,” Post-Tensioning Institute, Farmington Hills, MI.

22. SETRA (2006), “European Technical Approval No. ETA-06/0006,” SETRA, Bagneux Cedex, France.

23. Shin, H., and Kang, T. (2017), “Nonlinear Finite Element Analysis of Unbonded Post-Tensioned Concrete Members,” *The 8th Asia and Pacific Young Researchers and Graduates Symposium (YRGS 2017)*, Tokyo, Japan.

24. VSL (2015), “VSL Strand Post-Tensioning Systems,” VSL International Ltd., Köniz, Switzerland.

Appendix A : The code requirements for the tendon installation methods

A.1 The code requirements for the tendon elongation methods

ASME (2015)	**CC-4432.5 Twisting and Coiling**: (a) Prestressing tendons comprised of multiple elements shall be twisted, as necessary, to minimize differential length of the individual prestressing steel elements. Twisting is mandatory for all horizontal circumferential tendons comprised of multiple elements stressed simultaneously as a group. The amount of twist shall be specified in the construction·procedure. However, intentional twisting of tendons comprised of multiple elements stressed simultaneously as a group may be waived for horizontal circumferential tendons as well as other configurations of tendons meeting all other requirements of CC-4430 provided the following additional conditions are met: (1) Tendons shall be 1/2 in. (13 mm) strand (ASTM A416) that are prefabricated and pulled into the duct at one time (complete tendon). All strands shall be the same hand lay. (2) Provisions shall be made to keep strands in the tendon bundle parallel as the tendon is pulled into the duct. (3) The uncoiler shall allow individual strands to move against each other as the tendon is pulled in. The tendon shall be pulled from a cage versus being pre-tied and pulled in from a rotating table (lazy susan).
PTI/ASBI (2012)	**11.2 – Strand:** Inspect strand reels and packs for broken wires. Remove and discard lengths of strand containing broken wires. Push or pull strands through the ducts to make up tendons using methods that will not cause strands to snag on lips or joints in the ducts. Strands that are pushed shall have rounded-off ends or be fitted with smooth protective caps. Alternatively, strands may be assembled into complete tendons, which are pulled through the ducts using a special steel wire sock or other suitable pulling attachment such as a welded or brazed end lug. The tendon ends shall be rounded for smooth passage through the ducts. Strand shall not be intentionally rotated during installation. ~ (The latter part is omitted)
AASHTO (2010)	**10.4.2.2-Placement for Post-Tensioning:** All prestressing steel preassembled in ducts and installed prior to the placement of concrete shall be accurately placed and held in position during concrete placement. When the prestressing steel is installed after the concrete has been placed, the Contractor shall demonstrate to the satisfaction of the Engineer that the ducts are free of water and debris immediately prior to installation of the steel. The total number of

	strands in an individual tendon may be pulled into the duct as a unit, or the individual strand may be pulled or pushed through the duct.
AFCEN (2012) (ETC-C)	**2.5.3.3 TENDON INSTALLATION:** Generally, tendon installation shall take place by pushing the strands. ~ (The latter part is omitted) **2.5.3.4.1 Execution:** Initial simultaneous tensioning of each strand of a tendon, with individual displacements of each strand inducing a load between 10 and 15 kN for each strand at the anchorage, ~ (The latter part is omitted)
SETRA (2006) (VSL construction specification)	**2.4 INSTALLATION OF DUCTS AND STRANDS:** ~ (The former part is omitted) - Strand bundles fabricated in a mobile workshop located adjacent to the worksite and then drawn either before or after concreting into the ducts installed in the passive reinforcement; - Tendons composed by pushing through strand by strand before or after concreting into the ducts installed in the passive reinforcement.

Appendix B : MATLAB code to constitute equivalent tendon material model

B.1 MATLAB code to constitute equivalent tendon material model

```
% MATLAB code to constitute equivalent tendon material model
% Made by Hyeongyeop Shin

clear all; close all;

-----------------------------------------------------------------------------------------------
%% Tendon Input

Input_type=3 ;      % Input_type=1 : Individual tensile stresses follow direct input,
                    % Input_type=2 : Individual tensile stresses follow normal
                       distribution
                    % Input_type=3 : Individual tensile stresses follow uniform
                       distribution
n=7 ;               % Number of strands in the tendon

fpu=1930 ;                      % Tensile strength of prestressing steel
fpy=1760 ;                      % Yield strength of prestressing steel
Es=195470 ;                     % Elastic modulus of prestressing steel
strain=[0:0.00001:0.025] ;      % Considered range of tendon strain
fs=zeros(1,size(strain,2)) ;

if Input_type==1                                % Direct input
    Sheet=xlsread('TensileForces_Ch.5.2.xlsx') ;
    TP=Sheet(1,8:14) ;                          % Direct input using EXCEL sheet
    % TP=[1125 1250 1375 1500 1625 1750 1875] ;  % Direct input in MATLAB
                                                    script
    Avg_TP=mean(TP) ;               % Average value of individual tensile forces
    Cov_TP=std(TP)/mean(TP) ;       % C.O.V. of individual tensile forces
else
    Avg_TP=0.8*fpu ;                % Target mean value of individual tensile forces
    Cov_TP=0.05 ;                   % Target C.O.V. of individual tensile forces
    Std_TP=Cov_TP*Avg_TP ;          % Target standard deviation of individual tensile
                                       forces
    TP_seed=zeros(1,n) ;
    for i=1:n
        TP_seed(1,i)=(i/(n+1)) ;
    end ;
    if Input_type==2
        TP_prior=norminv(TP_seed,Avg_TP,Std_TP) ;
        Avg_TP_prior=mean(TP_prior) ;
        Std_TP_prior=std(TP_prior) ;
        Std_TP_posterior=Std_TP*(Std_TP/Std_TP_prior) ;
        TP=norminv(TP_seed,Avg_TP,Std_TP_posterior) ;
    elseif Input_type==3
        TP_prior=zeros(1,n) ;
        TP=zeros(1,n) ;
```

```
            for i=1:n
                TP_prior(1,i)=Avg_TP+(TP_seed(1,i)-0.5)*Std_TP ;
            end ;
            Avg_TP_prior=mean(TP_prior) ;
            Std_TP_prior=std(TP_prior) ;
            Std_TP_posterior=Std_TP*(Std_TP/Std_TP_prior) ;
            for i=1:n
                TP(1,i)=Avg_TP+(TP_seed(1,i)-0.5)*Std_TP_posterior ;
            end ;
      else ;
      end ;
end ;

-----------------------------------------------------------------------------------------------
%% Original tendon material model: Mattock (1979)

eps_pu=0.0195 ;
K=1.04 ;
Q=(fpu-K*fpy)/(eps_pu*Es-K*fpy) ;
syms RR ;
RRR=solve(fpy==0.01*Es*[Q+(1-Q)/((1+(0.01*Es/K/fpy)^RR)^(1/RR))],RR) ;
R=double(RRR) ;

for j=1:size(strain')
      fs(j)=strain(j)*Es*(Q+(1-Q)/((1+(strain(j)*Es/K/fpy)^R)^(1/R))) ;
      if fs(j)<=fpu
      else
            fs(j)=0 ;
      end ;
end ;

TPP=[TP Avg_TP] ;
eps_fs_TPP=zeros(n+1,2) ;
for i=1:n+1
      ii=1 ;
      while fs(ii)-TPP(i)<0
            ii=ii+1 ;
      end ;
      eps_fs_TPP(i,1)=strain(ii);
      eps_fs_TPP(i,2)=fs(ii) ;
end ;

-----------------------------------------------------------------------------------------------
%% Constitute equivalent tendon material model

fss=zeros(n,size(strain,2)) ;

for i=1:n
      for j=1:size(strain')
```

```
            if strain(j)*Es*(Q+(1-Q)/((1+(strain(j)*Es/K/fpy)^R)^(1/R)))<=Avg_TP
                  fss(i,j)=strain(j)*Es*(Q+(1-Q)/((1+(strain(j)*Es/K/fpy)^R)^(1/R))) ;
                  if fss(i,j)>=0
                  else
                        fss(i,j)=0 ;
                  end ;
            else
                  fss(i,j)=(strain(j)-eps_fs_TPP(n+1,1)+eps_fs_TPP(i,1))*Es*(Q+(1-
Q)/((1+((strain(j)-
eps_fs_TPP(n+1,1)+eps_fs_TPP(i,1))*Es/K/fpy)^R)^(1/R)))+(eps_fs_TPP(n+1,2)-
eps_fs_TPP(i,2)) ;
                  if fss(i,j)<=fpu+eps_fs_TPP(n+1,2)-eps_fs_TPP(i,2)
                  else
                        fss(i,j)=0 ;
                  end ;
            end ;
      end ;
end ;

for i=1:size(strain')
avg_fss(i)=mean(fss(:,i)) ;
end ;

---------------------------------------------------------------------------------------------------
%% Output: Equivalent tendon matarial model defined by multi-linear stress-strain
relationship

eqten=[strain; fs; avg_fss]';                % Output: Equivalent tendon material model
eqten_reduced=zeros(99,2) ;
for i=1:99
eqten_reduced(i,:)=eqten(25*(i-1)+1,[1 3]) ;    % Output: Equivalent tendon material
                                                      model for DIANA FEA input (99-
                                                      linear stress-strain relationship)
end ;
```

국 문 초 록

멀티스트랜드 텐던의 개별강연선 긴장력 편차가 포스트텐션 구조 거동에 미치는 영향

멀티스트랜드 포스트텐션 텐던은 주로 빌딩, 교량, 원전 격납건물 등 대규모 건축물과 토목구조물에 이용되는데, 강연선의 설치 방법과 긴장 방법 등의 시공적 요인에 따라 텐던의 개별 강연선에 가해지는 긴장력의 편차가 일상적으로 발생한다. 그러나, 현재까지 개별 강연선의 긴장력 편차를 측정한 연구는 있었으나, 이러한 편차가 포스트텐션 구조물의 거동에 미치는 영향에 대한 연구는 이루어지지 않았다. ASME (2015), PTI/ASBI (2012) 등 관련 코드와 시방서에서도 마찬가지로 일관성있는 긴장력 편차 관리 기준과 긴장력 편차를 줄일 수 있는 강연선 설치 방법을 제시하고 있지 않다. 현행 기준의 개선을 위해, 우선 개별 강연선 긴장력 편차가 포스트텐션 구조물의 내력에 미치는 영향을 정량적으로 파악할 필요가 있다. 따라서, 본 연구에서는 Initial slack 현상에 의해 발생하는 개별 강연선 긴장력 편차가 포스트텐션 구조물의 극한 내력에 미치는 영향을 이론적 연구와 수치해석을 통해 분석하였다.

Initial slack 현상에 의해 발생하는 개별 강연선 긴장력 편차가 텐던의 응력-변형률 관계에 미치는 영향을 분석하고 이를 수치해석에 적용하기 위해 등가 텐던 재료모델을 제안하였으며, 이를 통해 개별 강연선 긴장력 편차가 증가하면 텐던의 등가 항복강도가 약간 감소하며 인장강도가 크게 감소하는 경향이 있음을 알 수 있었다. 또한, 개별 강연선 긴장력 편차는 텐던의 평균적인 릴랙세이션 손실을 증가시킬 수 있다는 것을 이론적으로 확인하였으며, 추후 포스트텐션 구조물의 장기 거동에 미치는 영향을 연구할 필요성을 제시하였다.

개별강연선 긴장력 편차가 과도할 경우 포스트텐션 보의 휨 강도가 감소할 수 있다는 것을 비선형 유한요소해석으로 확인할 수 있었다. 하지만, 강도 감소에 미치는 영향은 제한적이었으며, 현실적인 범위의 긴장력 편차 수준(변동계수 10% 이하)에서는 무시할만한 정도의 강도 감소를 보였다. 반면, 원전 격납건물 부분모형은 모든 범위의 긴장력 편차 수준에서 무시할만한 내압성능의 감소가 있었다. 이로부터, 개별 강연선 긴장력 편차에 의한 포스트텐션 구조물의 강도 감소는 극한상태에서의 텐던 응력(f_{ps})이 긴장력 편차에 의해 얼마나 감소하는지와 관련있다는 것을 알 수 있었으며, 극한상태에서의 텐던 응력(f_{ps})이 텐던의 등가 항복강도(f_{py})와 가까울수록 구조물의 강도 감소가 두드러진다는 결론이 도출되었다.

본 연구는 멀티스트랜드 텐던의 개별강연선 긴장력 편차가 포스트텐션 구조물의 강도 감소에 미치는 영향을 분석하고 평가할 수 있는 방법을 제안하였다는 것에 의의가 있다. 본 연구의 결과 및

결론은 향후 멀티스트랜드 포스트텐션 텐던의 긴장력 관리 기준을 보다 합리적으로 개선하는데 있어 기초 연구자료로 활용될 수 있을 것이며, 개별 강연선 긴장력 편차의 허용 기준의 제정 및 개정에 있어 유용한 자료가 될 것으로 기대된다.

핵심용어: 멀티스트랜드 텐던, 개별 강연선 긴장력 편차, 초기 슬랙, 등가 텐던 재료모델, 유한요소해석, 포스트텐션 보, 원전 격납건물
학번: 2016-21074